THE ROLE OF THE INTEGRATED STRESS RESPONSE KINASE GCN2 IN CELL CYCLE REGULATION AND TUMORIGENESIS

Stacey L. Lehman

A DISSERTATION

in

Cell and Molecular Biology

Presented to the Faculties of the University of Pennsylvania

in

Partial Fulfillment of the Requirements for the

Degree of Doctor of Philosophy

2015

Supervisor of Dissertation

_____

Constantinos Koumenis, Ph.D., Professor of Radiation Oncology

Graduate Group Chairperson

_____

Daniel S. Kessler, Ph.D., Associate Professor of Cell and Developmental Biology

Dissertation Committee

Sandra Ryeom, Ph.D., Assistant Professor of Cancer Biology

James C. Alwine, Ph.D., Professor of Cancer Biology

Serge Y. Fuchs, M.D., Ph.D., Associate Professor of Animal Biology

Anil K. Rustgi, M.D., T. Grier Miller Professor of Medicine

THE ROLE OF THE INTEGRATED STRESS RESPONSE KINASE GCN2 IN CELL CYCLE

REGULATION AND TUMORIGENESIS

ACKNOWLEDGMENT

First, I would like to acknowledge all the Koumenis lab members I worked with, past and present, including Steve Tuttle, Lori Hart, Carly Sayers, Jiangbin Ye, Souvik Dey, Vladimir Popov, John Verginadis, Natalie Daurio, Feven Tameire, Lauren Brady, Tatini Datta, Huayi Liu, Anna Mesina, David Guttmann, Yi Cheng, Cindy Bi, Alexandra Monroy, and Shire Beach. Thank you for your technical assistance, feedback, support, and, most importantly, friendship during my time in lab. You have become my second family, and I will miss working with all of you! I would especially like to thank George Cerniglia from the Maity lab for his help with the metabolic labeling experiments and Gregg Johannes from Drexel University College of Medicine for his assistance with the polysome extractions. Your help with these technically challenging experiments is greatly appreciated.

Thank you to my advisor, Costas Koumenis, for your support and mentorship. I have learned so much in your lab over the past five years, and I feel that I have truly grown into an independent scientist. I really appreciate that you gave me the opportunity to attend so many conferences as a graduate student to present my work to researchers from all over the world. Under your guidance, I developed the skills, confidence, and diligence to become a successful scientist, and for that, I will always be grateful.

Next, I would like to thank my thesis committee, Sandra Ryeom, Jim Alwine, Serge Fuchs, and Anil Rustgi, for their thoughtful comments and advice during the course of my dissertation research. You helped to strengthen my work and encouraged my growth as a scientist throughout my training.

I would also like to acknowledge my CAMB friends, especially Christie, Jonathan, and Keeley. From our Cell 600 study group to our culinary adventures in West Philly, I have so many fond memories from our time at Penn. Thank you for your friendship!

To my boyfriend, Mike: thank you for your never-ending love and support throughout my time as a grad student. I know I can always count on you to be there for me, during the happy

times and the stressful times. You have been an incredible source of strength and assurance. I am excited to reciprocate and be by your side as you start graduate school in the fall!

And finally, to my parents: thank you for your 27 years and counting of love and encouragement. Growing up, you always told me that I could do anything I put my mind to and gave me the confidence to follow my dreams. Thank you for supporting my all educational endeavors from preschool all the way to graduate school. I never would have been able to make it this far without you!

ABSTRACT

THE ROLE OF THE INTEGRATED STRESS RESPONSE KINASE GCN2 IN CELL CYCLE REGULATION AND TUMORIGENESIS

Stacey L. Lehman

Constantinos Koumenis, Ph.D.

The tumor microenvironment is characterized by deficiencies in oxygen and nutrients, such as glucose and amino acids. Activation of the GCN2 arm of the Integrated Stress Response (ISR) in response to amino acid deprivation is one mechanism by which tumor cells cope with nutrient stress. GCN2 phosphorylates the alpha subunit of the eukaryotic translation initiation factor eIF2, leading to global downregulation of translation to conserve amino acids and initiation of a transcriptional program through the transcription factor ATF4 to promote recovery from nutrient deprivation. Loss of GCN2 results in decreased tumor cell survival *in vitro* under amino acid deprivation and attenuated tumor growth in xenograft models. However, the mechanisms by which GCN2 regulates cell survival and the role GCN2 plays in tumorigenesis are not clearly understood. Here, we demonstrate through ^{35}S labeling, luciferase reporter assays, and polysome profiling that activation of GCN2 selectively upregulates the translation of a $p21^{Cip1}$ transcript variant containing 5' upstream open reading frames (uORFs) through phosphorylation of eIF2α. Mutational analysis reveals that the uORFs suppress its translation under basal conditions, but promote its translation under stress. Functionally, ablation of p21 ameliorates G_1/S arrest and reduces cell survival in response to GCN2 activation. We also demonstrate in a genetically engineered mouse model of soft tissue sarcoma that loss of GCN2 has no major effect on the rate of tumor growth or animal survival. The sarcomas displayed compensatory activation of PERK or phospho-eIF2α independent upregulation of ATF4 in order to maintain ISR signaling, indicating that this pathway is critical for tumorigenesis. Together, these results demonstrate that GCN2 exerts its pro-survival effects partially through p21-induced cell cycle

arrest and that sarcomas adapt to loss of GCN2 by upregulating other components of the ISR in order to exploit the survival benefits of this signaling pathway.

TABLE OF CONTENTS

LIST OF TABLES

LIST OF FIGURES

CHAPTER I: GENERAL INTRODUCTION

Tumor cells must adapt to a variety of stressors in their microenvironment. These can include hypoxia, low pH, and deficiencies in nutrients, such as glucose and amino acids[1]. In order to survive these harsh conditions, tumor cells rely on pathways to sense and respond to stress. One such pathway is signaling through the serine/threonine kinase general control non-derepressible 2 (GCN2), which is activated in response to amino acid deprivation. GCN2 regulates a variety of processes to maintain sufficient levels of amino acids for cellular metabolism. The work herein elucidates the role GCN2 plays in suppressing cell proliferation to promote cell survival under nutrient stress and describes a genetically engineered mouse model of cancer in order to better understand the contribution of GCN2 to tumorigenesis.

GCN2: structure and function

GCN2 is a relatively large protein containing several functional domains (Figure I-1). When amino acids are in short supply, uncharged transfer RNAs (tRNAs) accumulate in cells. GCN2 senses amino acid deprivation by binding to uncharged tRNAs through its C-terminal histidyl-tRNA synthetase-like (HisRS-like) domain[2,3]. It has been demonstrated that individual uncharged tRNAs can compete away the interaction between GCN2 and total uncharged tRNA with similar efficiencies, suggesting that GCN2 can sense the deprivation of any amino acid because it binds to the various uncharged tRNAs with similar affinities.[4,5] The binding of uncharged tRNAs causes GCN2 to undergo a conformational change from its autoinhibitory state to its dimerized, catalytically active state. GCN2 homodimerizes through its C-terminal dimerization domain (DD)[6]. The HisRS-like domain also plays a role in dimerization[7]. GCN2's catalytic activity is carried out by its serine/threonine kinase domain, which is located within the middle of the protein[8]. Autophosphorylation on threonine residues within the kinase activation loop is required for maximum kinase activity[9]. GCN2 also contains a pseudokinase domain (YKD) N-terminal to the kinase domain. Although this domain is catalytically inactive, it interacts with and activates the kinase domain[10]. GCN2 interacts with GCN1 through its RING finger and WD repeat containing proteins and DEXDc-like helicases (RWD) domain at the N-terminus[11]. In yeast, this

interaction is required for GCN2 activation, although the exact mechanism of how GCN1 activates GCN2 is unclear. GCN2 directly interacts with translating ribosomes through its C-terminus[12], and it is thought that GCN1 facilitates the binding of uncharged tRNAs to GCN2 as they exit from the A site of the ribosome[11]. However, this interaction between GCN2 and ribosomes has not been observed in mammals[13], and therefore, it is not clear if the mammalian homologue of GCN1 activates GCN2 in a similar manner.

Figure I-1. GCN2 functional domains. GCN2 contains five functional domains: the RWD domain that binds to GCN1; the pseudokinase domain that activates GCN2 kinase activity; the serine/threonine kinase domain that phosphorylates eIF2α; the hisidyl-tRNA snythetase-like domain that binds uncharged tRNA; and the RB/DD domain that binds to ribosomes and is responsible for GCN2 homodimerization.

Upon activation, GCN2 phosphorylates the alpha subunit of eukaryotic translation initiation factor 2 (eIF2α) on serine 51[14]. GCN2 is a member of the signaling pathway known as the Integrated Stress Response (ISR), which consists of four kinases that phosphorylate eIF2α in response to a variety of stressors (Figure I-2). In addition to GCN2, these kinases include heme regulated inhibitor (HRI), PKR (protein kinase RNA-activated), and PERK (protein kinase RNA-activated-like endoplasmic reticulum kinase). HRI responds to heme deprivation, PKR to double-stranded RNA viral infections, and PERK to accumulation of unfolded proteins in the endoplasmic reticulum (ER)[15,16]. Phosphorylation of eIF2α by any of these four kinases leads to a general downregulation of translation. Paradoxically, eIF2α phosphorylation also leads to the enhanced translation of specific transcripts that contain upstream open reading frames (uORFs) in their 5' untranslated regions (UTRs)[16,17]. Both of these outcomes promote recovery from stress. However, if the stress is too prolonged or severe, continuous activation of the ISR can lead to apoptosis[15,16].

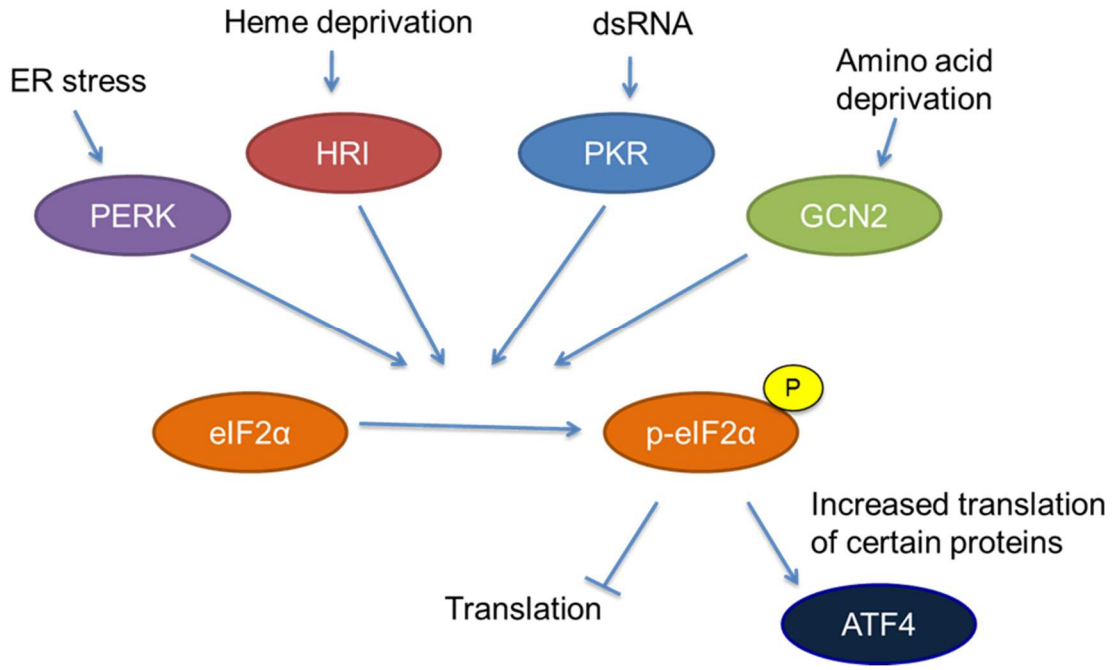

Figure I-2. The Integrated Stress Response signaling pathway. Four kinases in mammals phosphorylate eukaryotic translation initiation factor eIF2α in response to diverse stressors. Phosphorylation of eIF2α leads to translational suppression, but also translationally upregulates certain proteins, such as the transcription factor ATF4.

Consequences of GCN2 activation

Activation of GCN2 and subsequent phosphorylation of eIF2α generally lead to a global decrease in translation. In unstressed cells, eIF2 binds to the initiator methionyl tRNA, GTP, the small ribosomal subunit, and several other initiation factors to form the 43S preinitiation complex. The 43S preinitiation complex scans messenger RNAs (mRNAs) for start codons. Upon start codon recognition, the GTP bound to eIF2 is hydrolyzed to GDP to promote the association of the large ribosomal subunit with the initiation complex[18]. The guanine nucleotide exchange factor (GEF) eIF2B recycles the newly released eIF2-GDP back to eIF2-GTP so it can participate in another round of translation initiation. Under stressed conditions, phosphorylated eIF2α forms a stable complex with eIF2B, preventing its GEF activity and the recycling of eIF2 back to its active, GTP-bound form. This leads to translation inhibition[19].

Translational suppression under certain cellular stresses is beneficial for a number of reasons. First of all, translation is an extremely energetically costly process. Along with the

sodium potassium pump, translation is the highest ATP consuming process in the cell[20,21]. Downregulating translation helps to conserve ATP during unfavorable conditions. Additionally, translational regulation allows for rapid and efficient changes in gene expression in response to stress, as there is no time lag necessary to transcribe genes to mRNA first. In the context of GCN2 activation, translational suppression also helps to conserve amino acids when they are limiting by decreasing their incorporation into proteins.

GCN2 activation can also lead to the translational upregulation of specific transcripts through eIF2α phosphorylation. The most well-characterized of these is activating transcription factor 4 (ATF4)[22,23]. ATF4 is translationally upregulated under conditions of eIF2α phosphorylation due to the presence of uORFs in its 5' UTR (Figure I-3). Murine *Atf4* has two 5' uORFs. uORF1 is short and encodes for only three amino acids. uORF2 is longer and overlaps with the coding region for ATF4. Under normal conditions, translation initiates at uORF1. Since eIF2-GTP is in abundant supply, translation is able to rapidly reinitiate at uORF2. uORF2 is out of frame with respect to the ATF4 ORF, so no ATF4 protein is produced[22]. However, under stressed conditions when eIF2α is phosphorylated, recycling of eIF2-GDP to eIF2-GTP is greatly slowed. Thus, after translation of uORF1, translation reinitiation cannot occur rapidly enough for ribosomes to translate uORF2. Instead, ribosomes are much more likely to reinitiate translation at the actual ATF4 ORF, producing the ATF4 protein under stress[22]. Several other genes, such as growth arrest and DNA-damage-inducible 34 (GADD34)[24] and activating transcription factor 5 (ATF5)[25], are regulated by similar mechanisms.

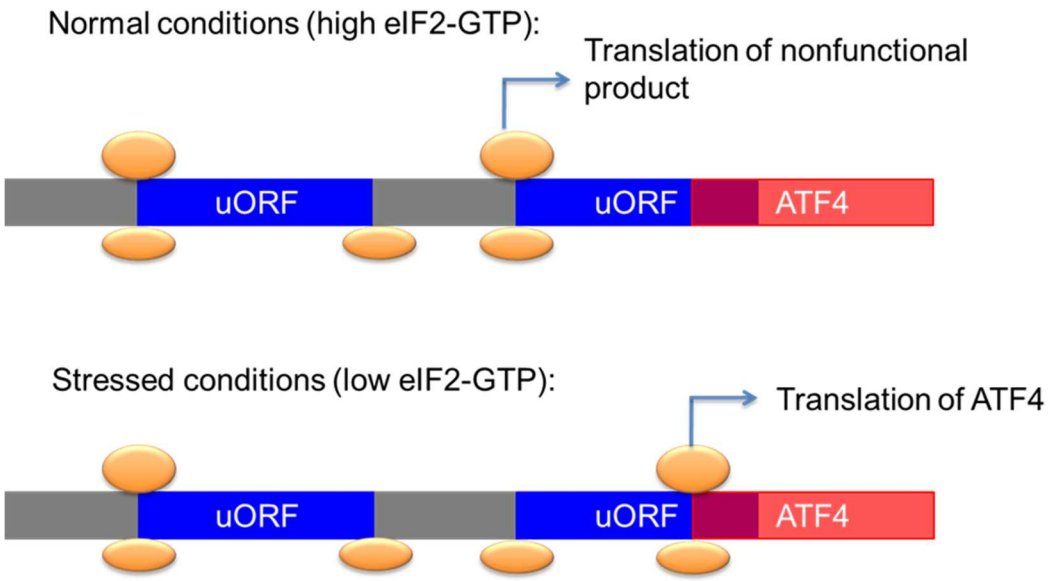

Figure I-3. Translational regulation of ATF4. Under normal conditions, ribosomes translate two uORFs in the ATF4 5' UTR, resulting in no ATF4 protein production. When eIF2α is phosphorylated under stress, translation reinitiation is delayed after translation of the first uORF, resulting in ribosomes translating the ATF4 ORF instead of the second uORF.

Translational upregulation of ATF4 initiates a transcriptional program that aids in stress recovery[26]. ATF4 regulates several categories of genes that are particularly important in the context of GCN2 activation, such as amino acid transporters, amino acid biosynthetic enzymes, aminoacyl tRNA synthetases, redox related genes, and autophagy related genes. Examples of these genes and their role in the GCN2-mediated stress response are discussed below. ATF4 also transcriptionally regulates additional transcription factors to amplify and provide specificity to the transcriptional response[26-28] and GADD34, a positive regulator of the eIF2α phosphatase, which provides negative feedback control to ISR activation[29].

Amino acid transporters and biosynthetic enzymes. ATF4 regulates the transcription of genes involved in regulating amino acid levels in order to increase their availability under stress. Two of the major categories of genes involved in these processes are amino acid transporters and amino acid biosynthetic enzymes. In regards to amino acid transporters, ATF4 has been demonstrated to regulate solute carrier family 7, member 5 (SLC7A5); solute carrier family 1,

member 5 (SLC1A5); and solute carrier family 3, member 2 (SLC3A2)[26]. All three transporters bring neutral amino acids, such as phenylalanine, tyrosine, leucine, arginine, and tryptophan, into the cell. ATF4 also regulates enzymes that synthesize amino acids. One of these is asparagine synthetase (ASNS), which produces asparagine from glutamine. A second is branched chain amino acid transaminase 1 (BCAT1), which synthesizes leucine, isoleucine, and valine from their alpha-keto acid forms[26].

Aminoacyl tRNA synthetases. ATF4 transcriptionally regulates a whole host of aminoacyl tRNA synthetases. These include alanyl-tRNA synthetase (AARS), asparaginyl-tRNA synthetase (NARS), tryptophanyl-tRNA synthetase (WARS), threonyl-tRNA synthetase (TARS), leucyl-tRNA synthetase (LARS), isoleucyl-tRNA synthetase (IARS), and tyrosyl-tRNA synthetase (YARS)[30]. As a whole, upregulation of aminoacyl tRNA synthetases promotes the charging of tRNAs, which would dampen GCN2 activation as the cells recover from amino acid starvation.

Antioxidant response. ATF4 is known to be a major regulator of antioxidant response genes under stress. In fact, ATF4$^{-/-}$ MEFs require supplementation with a reducing agent, such as β-mercaptoethanol, to grow in culture[26]. Although the ATF4-dependent induction of redox genes has not been widely studied in the context of GCN2, it has been demonstrated that GCN2$^{-/-}$ mice fed a leucine imbalanced diet exhibited increased oxidative damage in the liver[31]. ATF4-dependent regulation of redox response genes may be particularly important in the context of cysteine deprivation since it is required for cells to synthesize the antioxidant glutathione[32]. ATF4 has been shown to regulate the redox genes cytochrome b5 reductase 1 (CYB5R1), coproporphyrinogen oxidase (CPOX), ERO-1 like (ERO1L), FK506 binding protein 11 (FKBP11), and heme oxygenase 1 (HMOX1)[26].

Autophagy. Autophagy is a process in which double membrane structures engulf cytoplasmic material and fuse with lysosomes to degrade and recycle the contents. Autophagy has a variety of uses, including degrading nonfunctional or dysfunctional organelles and clearing the cytoplasm of misfolded or aggregated proteins[33]. In the context of GCN2 activation, autophagy acts as a starvation response by degrading cellular proteins and recycling the amino

acids as an energy source. It has been demonstrated that ATF4 regulates the transcription of several autophagy genes, including autophagy related 16-like 1 (ATG16L1), beclin 1 (BECN1), and autophagy related 12 (ATG12), in a GCN2-dependent manner under leucine starvation[34].

The ISR and cell cycle regulation

In response to stress, cells will often undergo cell cycle arrest to allow time for recovery before dividing. This can be achieved by induction of cell cycle inhibitors or suppression of cell cycle activators. The chief cell cycle activator proteins are the cyclins. As their name implies, cyclins are expressed in a periodic fashion as cells progress through the cell cycle. Cyclins form complexes with cyclin dependent kinases (CDKs) to activate their kinase activity; the complex then phosphorylates targets that are important for progression into the next phase of the cell cycle[35]. Typically, D cyclins are active in G_1 phase, E cyclins are active from late G_1 to early S, A cyclins are active from S phase into G_2, and B cyclins are active from G_2 into mitosis[35]. In mammalian cells, there are two major families of cell cycle inhibitors to counteract the effect of cyclins: the INK4 family and the CIP/KIP family. The INK4 family consists of $p15^{INK4B}$, $p16^{INK4A}$, $p18^{INK4C}$, and $p19^{INK4D}$. The CIP/KIP family consists of $p21^{CIP1}$, $p27^{KIP1}$, and $p57^{KIP2}$. Both groups of proteins form complexes with cyclin:CDK proteins to block their activity. The INK4 family proteins typically bind to CDK4 or CDK6 in complex with cyclin D, while the CIP/KIP family proteins typically bind CDK2 in complex with cyclin E or A[36].

There is mounting evidence that activation of the ISR leads to cell cycle arrest as a mechanism to cope with cellular stress. In cells exposed to ER stress, GCN2 and PERK cooperate to phosphorylate eIF2α, which leads to cell cycle arrest through translational suppression of cyclin D[37]. ER stress also results in PERK-dependent induction of the p53 isoform p53/47, which promotes G_2 arrest through 14-3-3σ[38]. In T cells, arginine deprivation induces G_1 arrest through GCN2. T cells stimulated in the absence of arginine fail to induce cyclin D3 and CDK4, and these effects are rescued by knockout of GCN2[39]. In fission yeast, activation of Gcn2 through nitrogen starvation[40] and, interestingly, UV light[41] causes cell cycle arrest in G_1. However,

the molecular mechanisms acting downstream of Gcn2 to regulate the cell cycle in yeast have not been elucidated. The ability of amino acid deprivation and glucose deprivation to induce cell cycle inhibitors suggests that GCN2 may have additional unidentified roles in cell cycle regulation[42,43].

Physiological functions of GCN2

Given its function in amino acid sensing, GCN2 plays a crucial role in regulating metabolism. In wildtype mice deprived of the essential amino acid leucine, GCN2 suppresses protein synthesis in the liver[44] and mobilizes lipid sources as an alternative source of energy[45]. Although GCN2 knockout mice are overtly phenotypically normal when fed a complete diet, they cannot employ these metabolic adaptations under stress and rapidly become moribund upon the removal of one amino acid from their diet[44]. GCN2 also plays a role in regulating hepatic gluconeogenesis, as $GCN2^{-/-}$ mice or mice with a liver specific GCN2 knockout have deficiencies in maintaining glucose homeostasis while fasting[46]. Additionally, GCN2 influences feeding behaviors in animals by regulating an aversion response to food sources lacking an amino acid[47]. Interestingly, short-term removal of tryptophan from the diet induces resistance to ischemia-reperfusion tissue damage in mice, and this protection is dependent upon GCN2[48].

GCN2 functions in many other contexts in addition to metabolism. GCN2 is highly expressed in the brain and regulates synaptic plasticity and memory. In a Morris water maze, $GCN2^{-/-}$ mice exhibit enhanced long-term spatial memory after weak training and impaired long-term memory after strong training[49]. This is thought to be due to decreased expression of ATF4, which is an antagonist of the cyclic AMP response element binding protein (CREB) transcription factor. CREB is responsible for transcribing genes responsible for long-term memory. Thus, in $GCN2^{-/-}$ mice, CREB activity is increased in the hippocampus, resulting in increased memory and learning. However, too much stimulation appears to block synaptic plasticity[49].

Although PKR is the ISR kinase typically associated with defence against viral infections, GCN2 also plays a role in this process. $GCN2^{-/-}$ mice are more susceptible to both Sindbis virus (SV), an RNA virus[50], and mouse cytomegalovirus (MCMV), a DNA virus[51]. It has been

demonstrated that the SV genome activates GCN2 by binding to the HisRS-like domain[50]. The mechanism behind MCMV-dependent activation has not yet been elucidated, but in both cases GCN2 is thought to protect against viral infection by phosphorylating eIF2α to inhibit translation of viral proteins[50,51]. It has also been demonstrated that human immunodeficiency virus (HIV) RNA activates GCN2 in cultured cells, which is also likely due to the HIV RNA genome binding the HisRS-like domain of GCN2. Interestingly, HIV-1 and HIV-2 proteases cleave GCN2, apparently to counteract GCN2's inhibitory effect on viral protein translation[52].

GCN2 also plays an important role in the immune system, particularly in the context of cancer. It has been demonstrated that GCN2 relays signals from the immunosuppressive enzyme indoleamine 2,3-dioxygenase (IDO) to T lymphocytes. Both tumor cells themselves[53] and a subset of $CD19^+$ plasmacytoid dendritic cells (pDCs) present in tumor draining lymph nodes[54] express IDO. IDO participates in the first and rate-limiting step of tryptophan catabolism, creating local tryptophan depletion that activates GCN2 in both cytotoxic and regulatory T cells. In an antigen-specific manner, IDO^+ pDCs induce anergy in wildtype $CD8^+$ T cells and block their proliferation both *in vitro* and *in vivo*, while $GCN2^{-/-}$ $CD8^+$ T cells maintain normal levels of proliferation and responsiveness to antigen[55]. IDO^+ pDCs can also suppress $CD8^+$ T cell proliferation indirectly by activating T_{regs}. However, $GCN2^{-/-}$ T_{regs} exposed to IDO^+ pDCs are unable to suppress the proliferation of $CD8^+$ T cells in response to antigen[56]. Furthermore, overexpression of IDO in tumor cells prevents the accumulation of tumor-specific $CD8^+$ T cells *in vivo*[53]. These data indicate that IDO signaling through GCN2 may promote tumor growth by inhibiting $CD8^+$ T cells from recognizing and responding to tumor cells, thus preventing their elimination.

GCN2 activation in tumors

The tumor microenvironment is frequently characterized by nutrient deficiencies. Nutrient deprivation is typically thought to occur in the microenvironment due to poor perfusion. The rapid proliferation of tumor cells can outstrip the tumor's ability to form new vasculature. This is

compounded by the fact that tumor vasculature is often inadequately constructed, resulting in tortuous networks of leaky vessels, and therefore, inefficient delivery of nutrients to the tumor through the blood[1]. Tumor cells have increased metabolic demands as compared to normal cells, which can also result in nutrient deprivation as tumor cells rapidly consume the nutrients present in the microenvironment[57]. Amino acid deprivation in the tumor microenvironment can activate GCN2. Glucose deprivation can also activate GCN2, presumably due to tumors depleting amino acids as an alternative energy source when glucose is not available[58].

The PERK arm of the ISR is also relevant in tumorigenesis, as both glucose and oxygen deprivation perturb protein folding and induce ER stress[59,60]. PERK and GCN2 cooperate to signal through phospho-eIF2α and ATF4 to promote tumor cell survival. PERK also has functions outside the ISR, including direct phosphorylation and activation of the antioxidant transcription factor nuclear factor erythroid 2-like 2 (NRF2)[61] and phosphorylation of diacylglycerol, which mediates the activity of mechanistic target of rapamycin (mTOR) and RAC-alpha serine/threonine-protein kinase (AKT) under stress[62]. When $PERK^{-/-}$ Ras and Simian virus 40 (SV40) large T antigen transformed MEFs are injected subcutaneously into nude mice, they grow more slowly than their wildtype counterparts and display areas of apoptosis which overlap with areas of hypoxia[63]. A pro-tumorigenic role for PERK has been demonstrated in genetically engineered mouse models of mammary carcinoma and insulinoma[64,65].

Previous work from our lab demonstrated that GCN2 supports tumor cell survival both *in vitro* and *in vivo*[58]*.* Cells lacking GCN2 undergo apoptosis when cultured in media lacking an amino acid. Cells lacking GCN2 also have decreased survival under glucose deprivation and fail to induce ATF4 transcriptional targets when grown without glucose. In mouse xenograft models, knockdown of GCN2 in the human fibrosarcoma cell line HT1080 completely blocked tumor growth. $GCN2^{-/-}$ Ras and SV40 large T antigen transformed MEFs also formed drastically smaller tumors in nude mice as compared to $GCN2^{+/+}$ cells. These findings are clinically relevant as well. Increased GCN2 protein levels were found in human liver, breast, and lung tumors as compared

to normal tissue controls. Activation of GCN2, as evidenced by staining for its autophosphorylated form, was detected by immunohistochemistry (IHC) in human lung, breast, and colon cancer.

Similar observations were made with proteins downstream of GCN2 in the ISR signaling pathway. Cells containing a knock-in mutation of eIF2α in which serine 51 is converted to alanine to block its phosphorylation also undergo apoptosis when grown in media lacking an amino acid[58]. Ras and SV40 large T antigen transformed eIF2α S51A MEFs exhibited decreased tumor growth when injected into mice[63]. We found high eIF2α phosphorylation concomitant with GCN2 overexpression in human liver, breast, and lung tumors[58]. Cells lacking ATF4 also have decreased survival when grown without an amino acid or glucose[58]. *In vivo*, HT1080 cells with stable knockdown of ATF4 exhibit decreased tumor growth[58]. ATF4 was found to be overexpressed in samples from human glioblastoma, breast adenocarcinoma, cervical carcinoma, and melanoma[63,66]. Increased copy number of ATF4 has been documented in breast tumors as well[67].

Several processes downstream of GCN2 are thought to promote tumor cell survival. The GCN2-eIF2α-ATF4 pathway regulates a number of genes involved in amino acid biosynthesis, which can aid in meeting the metabolic demands of tumor cells. The sensitivity of HT1080 cells with stable ATF4 knockdown to glutamine deprivation can be rescued by addition of asparagine to the media or by overexpression of the ATF4 target ASNS[58]. Indeed, overexpression of ASNS in these cells partially rescues tumor growth in xenografts[58]. Cells containing the eIF2α S51A mutation or lacking GCN2 are compromised in their ability to undergo autophagy under amino acid deprivation[58]. Autophagy can be a pro-survival process in cancer not only by recycling amino acids and other nutrients but also by protecting cells from hypoxia and anoikis, maintaining cancer stem cell populations, and inducing therapeutic resistance[68]. GCN2 also promotes tumor angiogenesis under amino acid deprivation by inducing vascular endothelial growth factor (VEGF). Knockdown of GCN2 reduces VEGF induction in the human head and neck squamous cell carcinoma cell line UM-SCC-22B, and xenografts of these tumors contain fewer blood vessels than their wildtype counterparts[69].

Project aims

The goals of this project were two-fold. First, we wanted to characterize additional pathways downstream of GCN2 that promote cell survival under nutrient stress. For this, we focused on how GCN2 regulates cell proliferation during amino acid deprivation. This work demonstrates that GCN2-dependent phosphorylation of eIF2α translationally upregulates the cell cycle inhibitor $p21^{Cip1}$ through the presence of uORFs in its 5' UTR. Induction of p21 under nutrient stress results in cell cycle arrest in G_1 and enhances clonogenic survival after long-term exposure to amino acid deprivation. Secondly, we wanted to better define the role of GCN2 in tumorigenesis by using a genetically engineered mouse model of cancer in which tumors arise in their native microenvironment and are exposed to physiological levels of nutrient deprivation. The LSL-$Kras^{G12D}$;$p53^{fl/fl}$ model of soft tissue sarcoma was employed for this purpose. In this model, we found that loss of GCN2 did not impact tumor growth or animal survival. However, other proteins involved in the ISR were overexpressed or activated in the tumors, suggesting that ISR signaling is critical for sarcomas, and tumors can adapt to maintain activation of this pathway. We also identified that many of the ISR components are overexpressed in human soft tissue sarcoma, indicating that the results from the mouse model are clinically significant. Overall, this work further supports a pro-survival function for GCN2 in nutrient stressed cells and identifies a novel mechanism by which GCN2 protects cells from death during amino acid starvation.

CHAPTER II: TRANSLATIONAL UPREGULATION OF AN INDIVIDUAL P21^{CIP1} TRANSCRIPT VARIANT BY GCN2 REGULATES CELL PROLIFERATION AND SURVIVAL UNDER NUTRIENT STRESS

This chapter contributes to a manuscript of the same title submitted to *PLOS Genetics* (in press)

Introduction

$p21^{Cip1}$, a member of the CIP/KIP family of cell cycle inhibitors, is known to play a key role in regulating the transition from G_1 to S phase of the cell cycle. Under normal conditions, complexes of cyclin E and CDK2 are active in late G_1 phase and phosphorylate the retinoblastoma protein (pRb). Phosphorylated pRB dissociates from E2F transcription factors, resulting in the transactivation of genes required for progression into S phase. Many different stress conditions upregulate p21 expression to inhibit cell proliferation and allow time for recovery before cell division. When p21 is induced, it binds to and inhibits cyclin E:CDK2 complexes. This prevents full phosphorylation of pRB, resulting in G_1/S arrest[70].

p21 expression must be tightly controlled in order for cells to properly progress through the cell cycle. As a result, p21 is regulated at many levels, both transcriptionally and post-transcriptionally[71]. At the transcriptional level, p21 was first described as a p53 target and a major effector of cell cycle arrest in response to DNA damage[72,73]. However, many stressors, such as oncogenic Ras[74] and histone deacetylase inhibition[75], upregulate p21 transcription independently of p53. A variety of mechanisms regulate p21 levels post-transcriptionally. mRNA binding proteins, such as HuD[76] and HuR[77], bind to the 3' UTR of the p21 transcript to enhance its stability. Both ubiquitin-dependent and independent pathways regulate the stability of p21 protein[78]. Phosphorylation events also regulate p21 protein stability, as well as its binding partners and subcellular localization[79].

Interestingly, p21 is encoded by multiple transcript variants in both mice and humans[80,81]. Although much is known about the regulation of p21 expression as a whole, the regulation of the individual transcript variants is not understood. These transcript variants differ in the 5' UTRs but are identical in their coding sequence and thus produce the same protein. The 5' UTR of a transcript plays a crucial role in regulating its translation, suggesting that these variants might be differentially controlled at the translational level.

Here, we demonstrate that upstream open reading frames in the 5' UTR of an individual p21 transcript variant upregulate its translation during amino acid deprivation. This stress activates the serine/threonine kinase GCN2, which phosphorylates the eukaryotic translation initiation factor eIF2α[14]. Mutation of the uORFs in the p21 transcript variant or mutation of eIF2α preventing its phosphorylation blocks translational induction. Similarly, the translation of a second p21 transcript variant that lacks uORFs is not enhanced by eIF2α phosphorylation. Unlike many other known mechanisms of p21 upregulation under stress, GCN2-dependent regulation does not require p53 or the other p53 family members, p63 and p73. p21 induction is required for optimal G_1/S arrest and promotes cell survival under conditions of amino acid deprivation. Together, these findings uncover a novel mechanism of differential regulation of distinct p21 transcript variants at the translational level and establish GCN2 as a critical regulator of the cell cycle and cell survival.

Results

Multiple p21 transcript variants have been identified in mammals, but their significance remains unknown. In mice, there are two p21 transcripts generated by alternative promoter usage (Figure II-1A). The classical p21 transcript is designated as variant 1. Variant 2 is produced from a promoter located 2.8 kilobases upstream from the variant 1 promoter[80]. Both transcripts are ubiquitously expressed throughout mouse tissues[80]. These variants differ only in their 5' UTRs, suggesting that they undergo differential post-transcriptional regulation. Elements in the 5' UTR, such uORFs and internal ribosome entry sites (IRESes), play a major role in regulating translation. Analysis of the known mouse p21 transcript variants revealed that transcript variant 2 contains 5' uORFs, while transcript variant 1 does not. A diagram of the 5' uORFs is depicted in Figure II-1B. The first uORF of the transcript overlaps out of frame with the coding region for p21. uORFs 2 and 3 are located within the first uORF and are fully contained within the 5' UTR. Human p21 is also encoded by multiple transcripts, some of which contain uORFs in their 5' UTRs[81].

One of the best studied transcripts translationally regulated by uORFs is *ATF4*. While eIF2α phosphorylation leads to a general downregulation of protein synthesis, the presence of 5' uORFs in *ATF4* leads to its translational upregulation under these conditions[22,23]. Mouse *Atf4* contains two 5' uORFs. Under normal conditions, translation begins at the first uORF and then quickly reinitiates at the second uORF. Since the second uORF overlaps out of frame with the ATF4 coding region, no protein is produced. Upon eIF2α phosphorylation, the exchange of GDP to GTP on eIF2 is hampered. This delays translation reinitiation, allowing ribosomes to scan through uORF2 and begin translation at the ATF4 ORF[22].

To determine if p21 is regulated by eIF2α phosphorylation, SV40 large T antigen transformed MEFs were cultured in media lacking leucine to activate GCN2. Previous work has demonstrated that amino acid deprivation upregulates p21[43,58]. Leucine deprivation resulted in phosphorylation of eIF2α and induction of p21. This response was strictly dependent on GCN2, as GCN2$^{-/-}$ MEFs did not phosphorylate eIF2α or induce p21 under stress (Figure II-1C). MEFs containing a knock-in mutation of eIF2α in which serine 51 is converted to alanine to prevent phosphorylation were also unable to upregulate p21 under stress, indicating that GCN2-dependent phosphorylation of eIF2α is necessary for p21 induction upon amino acid starvation (Figure II-1C). The experiment was repeated with glutamine deprivation to ensure that these results were not specific to leucine deprivation. Similar results were observed in all three cell lines (Figure II-1D).

Next, we wanted to determine if dependence on GCN2 and phospho-eIF2α for p21 upregulation is a general stress response phenomenon or is restricted to nutrient deprivation. To do so, cells were exposed to ionizing radiation, a stress that induces p21 but does not activate the ISR. As shown in Figure II-1E, wildtype, GCN2$^{-/-}$, and eIF2α S51A cells all rapidly increased p21 expression in response to DNA damage. These data indicate that GCN2 loss specifically renders cells incapable of inducing p21 in response to amino acid deprivation.

After resolution of stress, p21 levels return to baseline. GCN2$^{+/+}$ MEFs were cultured without leucine for two days, and then returned to complete media for 16 hours. p21 induction

was robust after 48 hours of amino deprivation, but levels were barely detectable after a period of recovery (Figure II-1F). This indicates that p21 induction is reversible and cells can adjust p21 levels in response to their environment.

To confirm that these findings were not specific to MEFs, SQ20B cells, a human head and neck squamous cell carcinoma cell line, were transfected with non-targeting siRNA or siRNA against GCN2 and cultured without leucine. Upon leucine deprivation, the siNT-transfected SQ20Bs phosphorylated eIF2α and induced p21. Knockdown of GCN2 prevented eIF2α phosphorylation and reduced p21 induction by almost 70% (Figure II-1G). Thus, GCN2 regulates p21 in both human and murine cells.

It has been reported that amino acid deprivation also induces $p27^{Kip1}$, a cell cycle inhibitor closely related to p21[43]. To establish if GCN2 and eIF2α phosphorylation are responsible for its upregulation under amino acid deprivation, $GCN2^{+/+}$, $GCN2^{-/-}$, and eIF2α S51A MEFs cells were leucine deprived and immunoblotted for p27. All three cell lines induced p27 (Figure II-1H). The p27 5' UTR does not contain any uORFs, further supporting that eIF2α is not responsible for its upregulation under stress. Thus, p21 and p27 are regulated by different mechanisms under nutrient stress.

Next page: Figure II-1. p21 induction under amino acid deprivation requires GCN2 and eIF2α phosphorylation. (A) Schematic representation of the mouse p21 genomic locus. The gray boxes indicate the p21 ORF and the white boxes represent the UTRs. **(B)** The 5' regions of the two known mouse transcript variants of p21 are shown. The start codon for p21 is indicated in green capital letters. Variant 2 contains three 5' uORFs; the start and stop codons for each are indicated in red, blue, and purple, respectively. **(C)** Western blot analysis of p21 induction in leucine-deprived $GCN2^{+/+}$, $GCN2^{-/-}$, and eIF2α S51A MEFs. β-actin was used as a loading control. All samples were collected at the same time and the blots were run in parallel. **(D)** Western blot analysis of p21 induction in glutamine-deprived $GCN2^{+/+}$, $GCN2^{-/-}$, and eIF2α S51A MEFs. β-tubulin was used as a loading control. **(E)** Western blot analysis of p21 induction in irradiated $GCN2^{+/+}$, $GCN2^{-/-}$, and eIF2α S51A MEFs. Total eIF2α was used as a loading control. **(F)** Western blot analysis of the reversibility of p21 induction in $GCN2^{+/+}$ MEFs. β-tubulin was used as a loading control. **(G)** Western blot analysis of p21 induction in leucine-deprived SQ20B cells. Cells were transfected with either non-targeting siRNA (siNT) or siRNA against GCN2 (siGCN2). β-tubulin was used as a loading control. **(H)** Western blot analysis of p27 induction in leucine-deprived $GCN2^{+/+}$, $GCN2^{-/-}$, and eIF2α S51A MEFs. β-tubulin was used as a loading control.

Data information: Values below blot represent the fold change in total pixel intensity over control of p21, GCN2, or p27 normalized to the loading control for each lane.

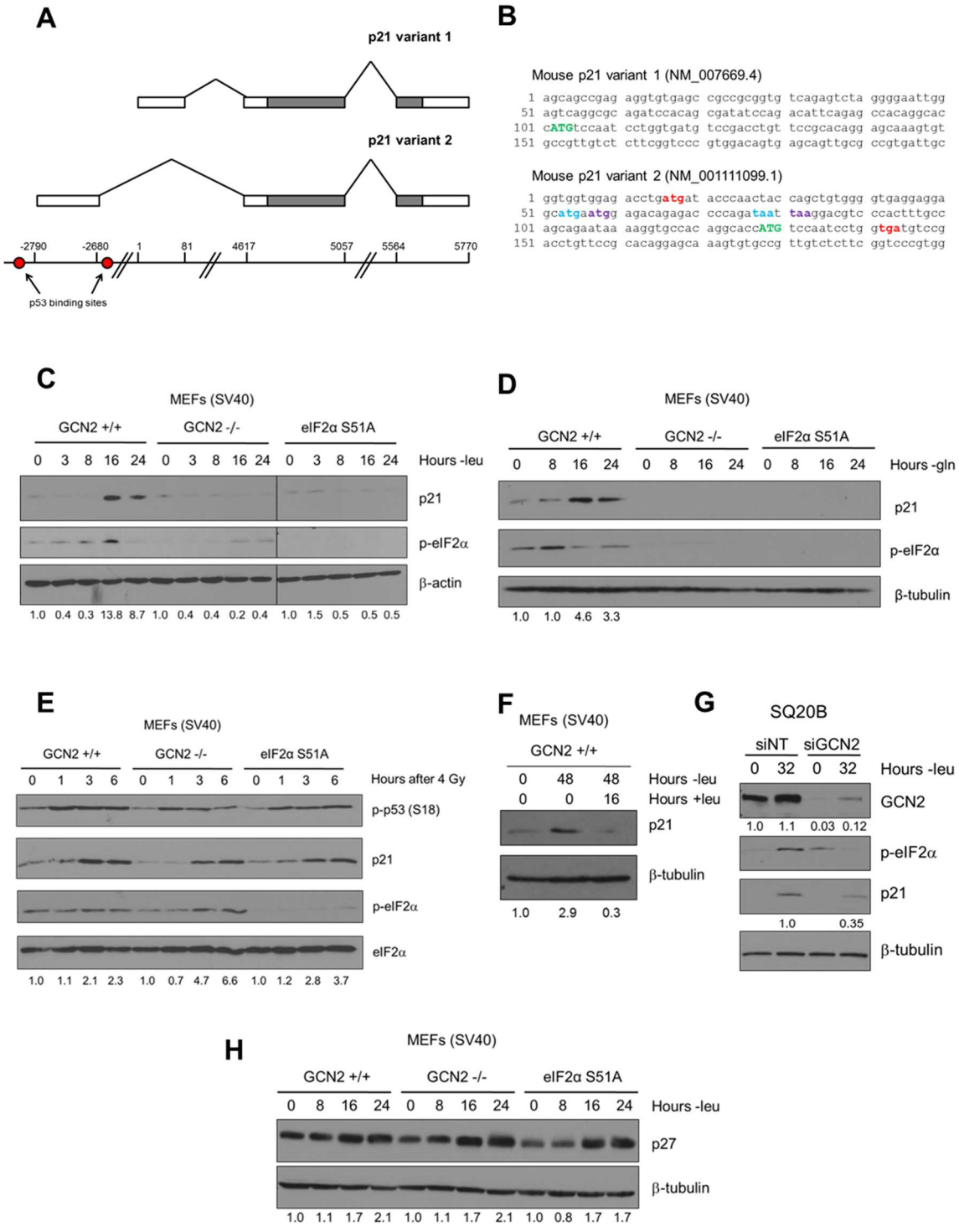
A
p21 variant 1
p21 variant 2
-2790
-2680
1
81
4617
5057
5564
5770
p53 binding sites
B
Mouse p21 variant 1 (NM_007669.4)
1 agcagccgag aggtgtgagc cgccgcggtg tcagagtcta ggggaattgg
51 agtcaggcgc agatccacag cgatatccag acattcagag ccacaggcac
101 cATGtccaat cctggtgatg tccgacctgt tccgcacagg agcaaagtgt
151 gccgttgtct cttcggtccc gtggacagtg agcagttgcg ccgtgattgc
Mouse p21 variant 2 (NM_001111099.1)
1 ggtggtggag acctgatgat acccaactac cagctgtggg gtgaggagga
51 gcatgaatgg agacagagac cccagataat taaggacgtc ccactttgcc
101 agcagaataa aaggtgccac aggcaccATG tccaatcctg gtgatgtccg
151 acctgttccg cacaggagca aagtgtgccg ttgtctcttc ggtcccgtgg
C
MEFs (SV40)
GCN2 +/+
GCN2 -/-
eIF2α S51A
0 3 8 16 24 0 3 8 16 24 0 3 8 16 24
Hours -leu
p21
p-eIF2α
β-actin
1.0 0.4 0.3 13.8 8.7 1.0 0.4 0.4 0.2 0.4 1.0 1.5 0.5 0.5 0.5
D
MEFs (SV40)
GCN2 +/+
GCN2 -/-
eIF2α S51A
0 8 16 24 0 8 16 24 0 8 16 24
Hours -gln
p21
p-eIF2α
β-tubulin
1.0 1.0 4.6 3.3
E
MEFs (SV40)
GCN2 +/+
GCN2 -/-
eIF2α S51A
0 1 3 6 0 1 3 6 0 1 3 6
Hours after 4 Gy
p-p53 (S18)
p21
p-eIF2α
eIF2α
1.0 1.1 2.1 2.3 1.0 0.7 4.7 6.6 1.0 1.2 2.8 3.7
F
MEFs (SV40)
GCN2 +/+
0 48 48
0 0 16
Hours -leu
Hours +leu
p21
β-tubulin
1.0 2.9 0.3
G
SQ20B
siNT
siGCN2
0 32 0 32
Hours -leu
GCN2
1.0 1.1 0.03 0.12
p-eIF2α
p21
1.0 0.35
β-tubulin
H
MEFs (SV40)
GCN2 +/+
GCN2 -/-
eIF2α S51A
0 8 16 24 0 8 16 24 0 8 16 24
Hours -leu
p27
β-tubulin
1.0 1.1 1.7 2.1 1.0 1.1 1.7 2.1 1.0 0.8 1.7 1.7

One of the best-known mechanisms of p21 regulation is at the transcriptional level through p53, and it has been previously established that p53 regulates both murine p21 transcript variants[80]. To evaluate if any p53 family members contribute to p21 upregulation under amino acid deprivation, p21 transcript levels were measured by qPCR in leucine-starved E1A transformed wildtype, $p53^{-/-}$, $p63^{-/-}$, and $p73^{-/-}$ MEFs. p21 transcript levels were upregulated in all cell lines in a time-dependent manner, although loss of any one of the p53 family members compromised basal levels of p21 mRNA (Figure II-2A). To confirm these results in a human cell line, glutamine-starved $p53^{+/+}$ and $p53^{-/-}$ HCT116s, a human colorectal adenocarcinoma cell line, were analyzed by western blot for p21 induction. Similar to the MEFs, a decrease in basal levels of p21 was observed in $p53^{-/-}$ cells, but loss of p53 did not prevent p21 upregulation under stress (Figure II-2B). Furthermore, the SQ20B cells shown in Figure II-1E express a nonfunctional mutant version of p53[82]. Overall, these results demonstrate that p53 and other p53 family members maintain p21 transcript levels in unstressed cells but are not necessary for p21 induction upon amino acid deprivation.

When p21 mRNA levels were measured in leucine-starved $GCN2^{+/+}$, $GCN2^{-/-}$, and eIF2α S51A MEFs, we observed a time-dependent increase in total p21 transcript in all three cell lines (Figure II-2C). Levels of the p21 transcript variants were also measured separately under leucine deprivation. Transcript variant 1 was the predominant variant present in the MEFs, with a relative abundance of six to eight times more than variant 2 in complete media (Figure II-2D). Under amino acid deprivation, increases in variant 1 are primarily responsible for the increase in total p21 mRNA (Figure II-2E). Interestingly, variant 2 levels increased modestly in $GCN2^{+/+}$ and eIF2α S51A MEFs under stress, while decreasing by half in $GCN2^{-/-}$ MEFs (Figure II-2F). This indicates that GCN2 plays a role independently of eIF2α in maintaining variant 2 mRNA levels under conditions of leucine deprivation.

The increase in p21 mRNA without a corresponding increase in p21 protein in the $GCN2^{-/-}$ and eIF2α S51A MEFs further supported that p21 is regulated at the translational level by eIF2α phosphorylation through GCN2. To directly measure p21 translation, we grew $GCN2^{+/+}$ and

GCN2$^{-/-}$ MEFs with or without leucine for 16 hours, labeled newly synthesized proteins with ^{35}S-methionine and ^{35}S-cystiene, and immunoprecipitated p21. GCN2$^{+/+}$ MEFs increased translation of p21 by approximately four-fold under leucine deprivation, while GCN2$^{-/-}$ MEFs showed no increase in p21 labeling under stress (Figure II-2G). Thus, GCN2 translationally upregulates p21 under nutrient stress.

To address the possibility that enhanced protein stability might also contribute to increased p21 levels under amino acid deprivation, we leucine starved GCN2$^{+/+}$ MEFs to initially induce p21 protein, and then switched the cells to complete or leucine-free media containing cycloheximide to block any new p21 protein synthesis. A time course analysis revealed that p21 protein half-life was approximately 80 minutes in complete media and 20 minutes in leucine-free media (Figure II-2H). Therefore, enhanced protein stability does not contribute to p21 induction under nutrient stress. Moreover, this experiment further supports the notion that translational control plays a major role in maintaining p21 protein levels under stress.

To assess the effects of amino acid deprivation on the translational efficiency of each p21 variant, luciferase reporter constructs were created by inserting either the 5' UTR of p21 variant 1 or 2 between the HindIII and NcoI restriction sites in a pGL3 reporter vector in which the SV40 promoter drives expression of luciferase. This produced a construct in which the luciferase coding sequence is located directly after the p21 ORF start codon (Figure II-3A). GCN2$^{+/+}$ MEFs were transfected with the p21 variant 1 5' UTR-luciferase and p21 variant 2 5' UTR-luciferase plasmids, and luciferase activity was measured during a time course of leucine deprivation. No change in luciferase activity was observed from the variant 1 construct, while luciferase activity from the p21 variant 2 construct increased in a time-dependent manner (Figure II-3B). These results indicate that translational upregulation is specific to p21 variant 2. Furthermore, the translational regulation was dependent on eIF2α phosphorylation, as there was no statistically significant increase in luciferase activity from the variant 2 construct in eIF2α S51A MEFs (Figure II-3B).

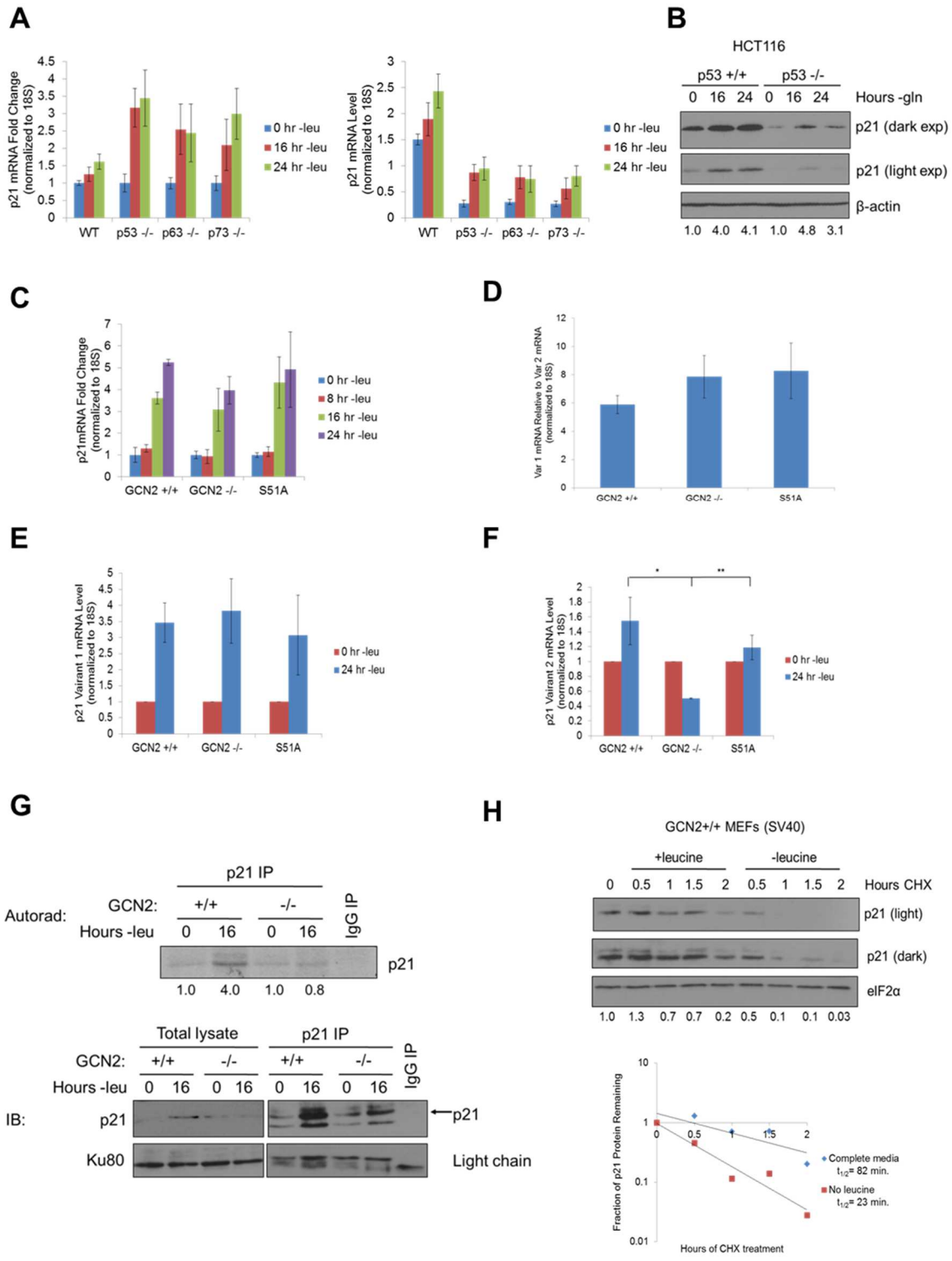
A
p21 mRNA Fold Change (normalized to 18S)
WT
p53 -/-
p63 -/-
p73 -/-
0 hr -leu
16 hr -leu
24 hr -leu
p21 mRNA Level (normalized to 18S)
B
HCT116
p53 +/+
p53 -/-
0 16 24 0 16 24
Hours -gln
p21 (dark exp)
p21 (light exp)
β-actin
1.0 4.0 4.1 1.0 4.8 3.1
C
p21mRNA Fold Change (normalized to 18S)
GCN2 +/+
GCN2 -/-
S51A
0 hr -leu
8 hr -leu
16 hr -leu
24 hr -leu
D
Var 1 mRNA Relative to Var 2 mRNA (normalized to 18S)
E
p21 Vairant 1 mRNA Level (normalized to 18S)
F
p21 Vairant 2 mRNA Level (normalized to 18S)
G
p21 IP
Autorad:
GCN2:
+/+
-/-
IgG IP
Hours -leu
0 16 0 16
p21
1.0 4.0 1.0 0.8
Total lysate
p21 IP
IB:
Ku80
Light chain
H
GCN2+/+ MEFs (SV40)
+leucine
-leucine
0 0.5 1 1.5 2 0.5 1 1.5 2
Hours CHX
p21 (light)
p21 (dark)
eIF2α
1.0 1.3 0.7 0.7 0.2 0.5 0.1 0.1 0.03
Fraction of p21 Protein Remaining
Hours of CHX treatment
Complete media
t1/2= 82 min.
No leucine
t1/2= 23 min.

Previous page: Figure II-2. GCN2 enhances p21 translation independently of p53. (A) qPCR for p21 was performed on RNA isolated from wildtype, $p53^{-/-}$, $p63^{-/-}$, and $p73^{-/-}$ MEFs deprived of leucine for the indicated times. p21 transcript levels were normalized to 18S rRNA. Left: Results are depicted as fold change over control for each cell line. Right: Results are depicted as absolute levels of normalized transcript. Data represent the average of three independent experiments ± S.E.M. **(B**) Western blot analysis of p21 induction in $p53^{+/+}$ and $p53^{-/-}$ HCT116s. β-actin was used as a loading control. Values below blot represent fold change in total pixel intensity over control of p21 normalized to the loading control for each lane. **(C)** qPCR for p21 was performed on RNA isolated from $GCN2^{+/+}$, $GCN2^{-/-}$, and eIF2α S51A MEFs deprived of leucine for the indicated times. p21 transcript levels were normalized to 18S rRNA and are depicted as fold change over control. Data are the average of three independent experiments ± S.E.M. **(D)** qPCR for p21 variants 1 and 2 was performed on RNA isolated from $GCN2^{+/+}$, $GCN2^{-/-}$, and eIF2α S51A MEFs grown in complete media. Levels of transcript variant 1 relative to transcript variant 2 were calculated using the $\Delta\Delta C_t$ method using 18S rRNA as the reference gene. Data represent the average of three independent experiments ± S.E.M. Results were not statistically significant. **(E)** qPCR for p21 variant 1 was performed on RNA isolated from $GCN2^{+/+}$, $GCN2^{-/-}$, and eIF2α S51A MEFs deprived of leucine for the indicated times. p21 variant 1 transcript levels were normalized to 18S rRNA. Results are depicted as fold change over control for each cell line. Data represent the average of four independent experiments ± S.E.M. There was no statistically significant difference in variant 1 induction among the three cell types. **(F)** qPCR for p21 variant 2 was performed on RNA isolated from $GCN2^{+/+}$, $GCN2^{-/-}$, and eIF2α S51A MEFs deprived of leucine for the indicated times. p21 variant 2 transcript levels were normalized to 18S rRNA. Results are depicted as fold change over control for each cell line. Data represent the average of four independent experiments ± S.E.M.; *$p<0.05$, **$p<0.01$. **(G)** Metabolic labeling of p21 under leucine deprivation. Top: Autoradiograph of ^{35}S-labeled p21 immunoprecipitated from $GCN2^{+/+}$ and $GCN2^{-/-}$ MEFs grown with or without leucine for 16 hours. Bottom: Western blot with cold amino acids to determine immunoprecipitation efficiency and verify induction of p21 in total cell lysates. **(H)** Measurement p21 protein half-life under replete and leucine starved conditions. $GCN2^{+/+}$ MEFs were initially grown in leucine-free media to induce p21 protein levels at time 0. Cells were then switched to complete or leucine-free media containing 50 μg/mL cycloheximide. Top: Western blot analysis of p21 protein levels during a time course of cycloheximide treatment. Total eIF2α was used as a loading control. Values below blot represent fold change in total pixel intensity over control of p21 normalized to the loading control for each lane. Bottom: Normalized p21 protein values were fit to exponential decay curves to calculate protein half-life.

In order to determine if the 5' uORFs in the p21 variant 2 transcript were responsible for translational upregulation under stress, point mutations to disrupt the uORF start codons were introduced into the constructs. Constructs were created with deletion of uORF1 (ΔuORF1), deletion of both uORFs 2 and 3 (ΔuORF2,3), and deletion of all three uORFs (ΔuORF1,2,3) (Figure II-3A). Again, $GCN2^{+/+}$ MEFs were transfected with these constructs, and luciferase activity was measured over a time course of leucine deprivation. Deletion of uORF1 or deletion of both uORFs 2 and 3 compromised induction of luciferase activity, demonstrating that all three uORFs promote translation under stress. The uORFs appear to be the only 5' elements regulation p21 translation since deletion of all three uORFs essentially blocked the increase in luciferase activity (Figure II-3C). Under basal conditions, deletion of either uORF1 or uORFs 2 and 3 modestly raised luciferase activity, indicating that all three uORFs are inhibitory to

translation under normal, unstressed conditions. The deletion of all three uORFs completely rescued basal luciferase activity to levels similar to that of p21 variant 1, which contains no uORFs (Figure II-3C). This suggests that under unstressed conditions, ribosomes tend to initiate translation at the uORFs instead of the p21 ORF.

As a positive control, luciferase assays were performed with ATF4 5' UTR constructs (Figure II-3D). In agreement with previous data[22], treatment with thapsigargin induced luciferase activity from the wildtype construct, and deletion of uORF2 increased basal translation levels while preventing induction in response to stress. This response is very similar to that seen with the deletion of p21 variant 2 uORFs. To confirm that the changes observed in luciferase activity were not due to changes in the transcript levels of the reporters, qPCR for luciferase was performed on GCN2$^{+/+}$ MEFs transfected with the 5' UTR constructs. No appreciable changes in luciferase mRNA were observed (Figure II-3E).

Next page: Figure II-3. GCN2-dependent translational upregulation of p21 is specific to variant 2 and mediated by the presence of 5' uORFs. (A) Partial sequence of p21 5' UTR luciferase reporter constructs. The p21 sequence is in lowercase letters, and the luciferase sequence is in capital letters. Restriction sites used to insert the p21 5' UTRs are underlined. The start codon for p21 is indicated in green capital letters. The start and stop codons for p21 variant 2 uORFs 1, 2, and 3 are in red, blue, and purple letters, respectively. The mutations created to disrupt the uORFs are indicated by arrows. **(B)** Luciferase assay using p21 5' UTR reporter constructs under leucine deprivation. Top: A schematic representation of the p21 variant 1 and 2 luciferase reporter constructs (not drawn to scale). Bottom: Luciferase activity from reporter constructs was measured in leucine-deprived GCN2$^{+/+}$ and eIF2α S51A MEFs and normalized to *Renilla* luciferase. Data are the average of three independent experiments ± S.E.M.; *p<0.05. **(C)** Luciferase assay using mutant p21 variant 2 5' UTR reporter constructs. Left: A schematic representation of the p21 variant 2 luciferase reporter constructs (not drawn to scale). Top right: Luciferase activity from reporter constructs was measured in leucine-deprived GCN2$^{+/+}$ MEFs. Bottom right: Relative basal translation levels of mutant p21 variant 2 reporter constructs in untreated cells. All results were normalized to *Renilla* luciferase. Data are the average of three (p21 variant 1 and p21 variant 2 ΔuORF1,2,3) or four (remaining constructs) independent experiments ± S.E.M.; *p<0.5, **p<0.01. **(D)** Dual luciferase assay using mutant ATF4 5' UTR reporter constructs. Top: Luciferase activity from reporter constructs was measured in GCN2$^{+/+}$ MEFs treated with 1 μM thapsigargin for 6 hours and normalized to *Renilla* luciferase activity. Bottom: Relative basal translation levels of ATF4 reporter constructs in untreated cells as measured by luciferase assay. Results are normalized to *Renilla* and depicted as fold change over the wildtype construct. Data represent the average of three independent experiments ± S.E.M. **(E)** qPCR for luciferase was performed on RNA isolated MEFs transfected with the p21 5' UTR reporter constructs. Luciferase transcript levels were normalized to 18S rRNA and are depicted as fold change over control. Data represent the average of three independent experiments ± S.E.M. No changes in luciferase transcript levels were statistically significant.

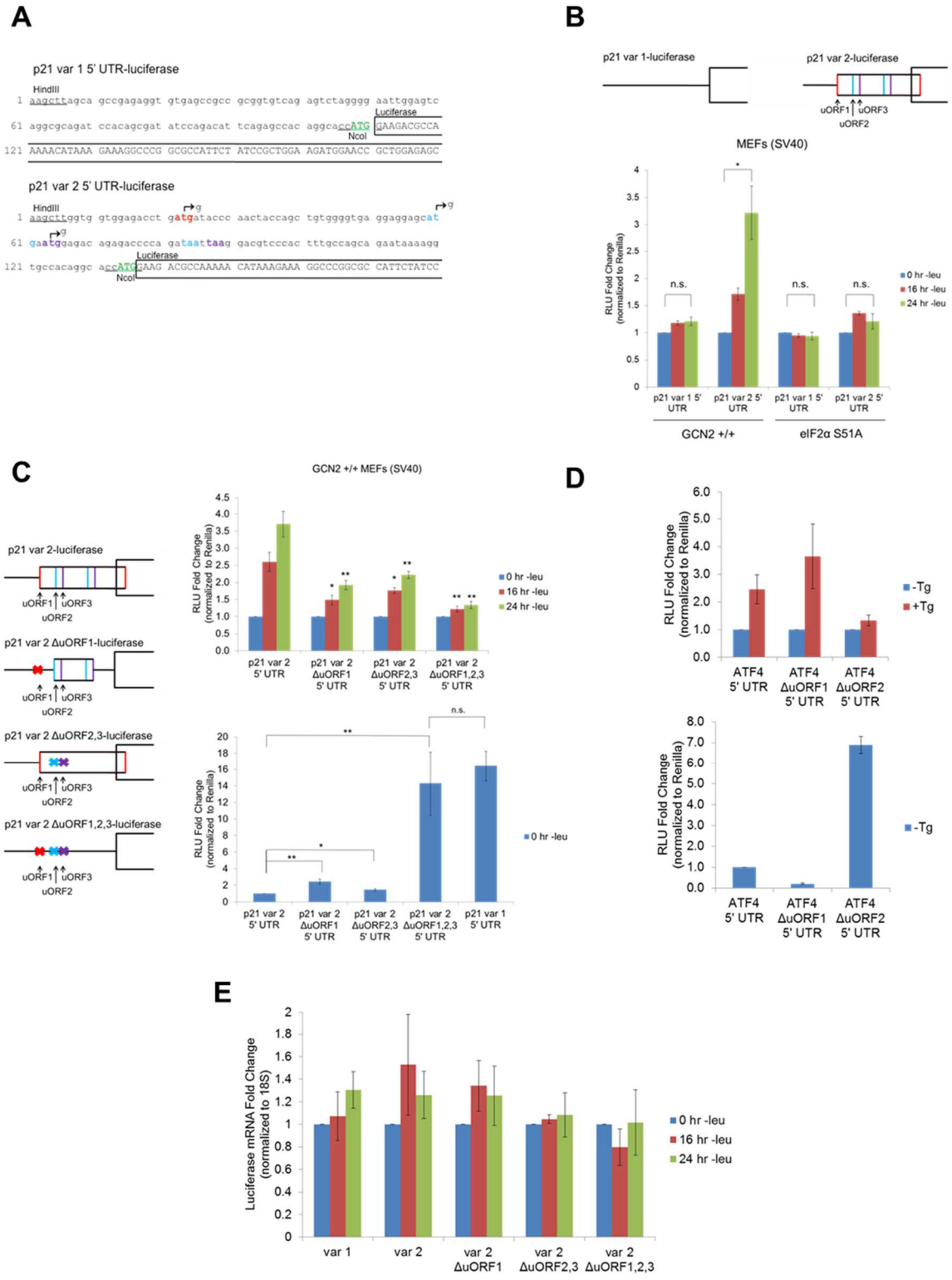
A
p21 var 1 5' UTR-luciferase
HindIII
Luciferase
NcoI
p21 var 2 5' UTR-luciferase
HindIII
Luciferase
NcoI
B
p21 var 1-luciferase
p21 var 2-luciferase
uORF1
uORF3
uORF2
MEFs (SV40)
RLU Fold Change (normalized to Renilla)
n.s.
0 hr -leu
16 hr -leu
24 hr -leu
p21 var 1 5' UTR
p21 var 2 5' UTR
GCN2 +/+
eIF2α S51A
C
p21 var 2-luciferase
p21 var 2 ΔuORF1-luciferase
p21 var 2 ΔuORF2,3-luciferase
p21 var 2 ΔuORF1,2,3-luciferase
GCN2 +/+ MEFs (SV40)
RLU Fold Change (normalized to Renilla)
p21 var 2 5' UTR
p21 var 2 ΔuORF1 5' UTR
p21 var 2 ΔuORF2,3 5' UTR
p21 var 2 ΔuORF1,2,3 5' UTR
p21 var 1 5' UTR
D
RLU Fold Change (normalized to Renilla)
-Tg
+Tg
ATF4 5' UTR
ATF4 ΔuORF1 5' UTR
ATF4 ΔuORF2 5' UTR
E
Luciferase mRNA Fold Change (normalized to 18S)
var 1
var 2
var 2 ΔuORF1
var 2 ΔuORF2,3
var 2 ΔuORF1,2,3

To ascertain if the two endogenous variants of p21 mRNA were translated with different efficiencies under stress, we leucine-starved GCN2$^{+/+}$ MEFs for 8, 12, 16, 20, and 24 hours and analyzed the distribution of the two p21 transcript variants in different polysome fractions. The polysome profiles for these time points are shown in Figure II-4A. p21 variant 1 exhibited a strong shift from the high to the low molecular weight polysomes at 16 hours, after which it began to recover towards its baseline distribution (Figure II-4B). This pattern of translational suppression and recovery is similar to that of the housekeeping gene β-actin, as opposed to ATF4, which is translationally upregulated under stress (Figure II-4C). The association of p21 variant 2 with polysomes changed very little with time. It exhibited slight decrease in association at 16 hours, followed by full recovery back to baseline at 24 hours. Thus, by 24 hours, p21 variant 2 is translated at its normal efficiency while variant 1 is still suppressed (Figure II-4B).

To determine the effect of leucine deprivation on global translation, we used the polysome profiles shown in Figure II-4A to calculate translational efficiency at each time point as previously described[83] and normalized to the translational efficiency in complete media. This value reflects the fraction of all mRNAs that are associated with polysomes under leucine deprivation as compared to complete media. Global translational efficiency reached its nadir of approximately 0.75 at 12 hours of leucine deprivation and then recovered to a nearly constant level of 0.9 (Figure II-4D). The kinetics of translational efficiency closely correlated with eIF2α phosphorylation, which reached its peak at 12 hours of leucine deprivation and then decreased to near baseline levels by 24 hours (Figure II-4D). Additionally, leucine deprivation resulted in decreased levels of eIF4G and hypophosphorylation of 4E-BP1, which may also contribute to translational suppression (Figure II-4D). Leucine deprivation also increased phosphorylation of the elongation factor eEF2 (Figure II-4D). However, inhibition of elongation by eEF2 phosphorylation would not alter mRNA association with polysomes[84].

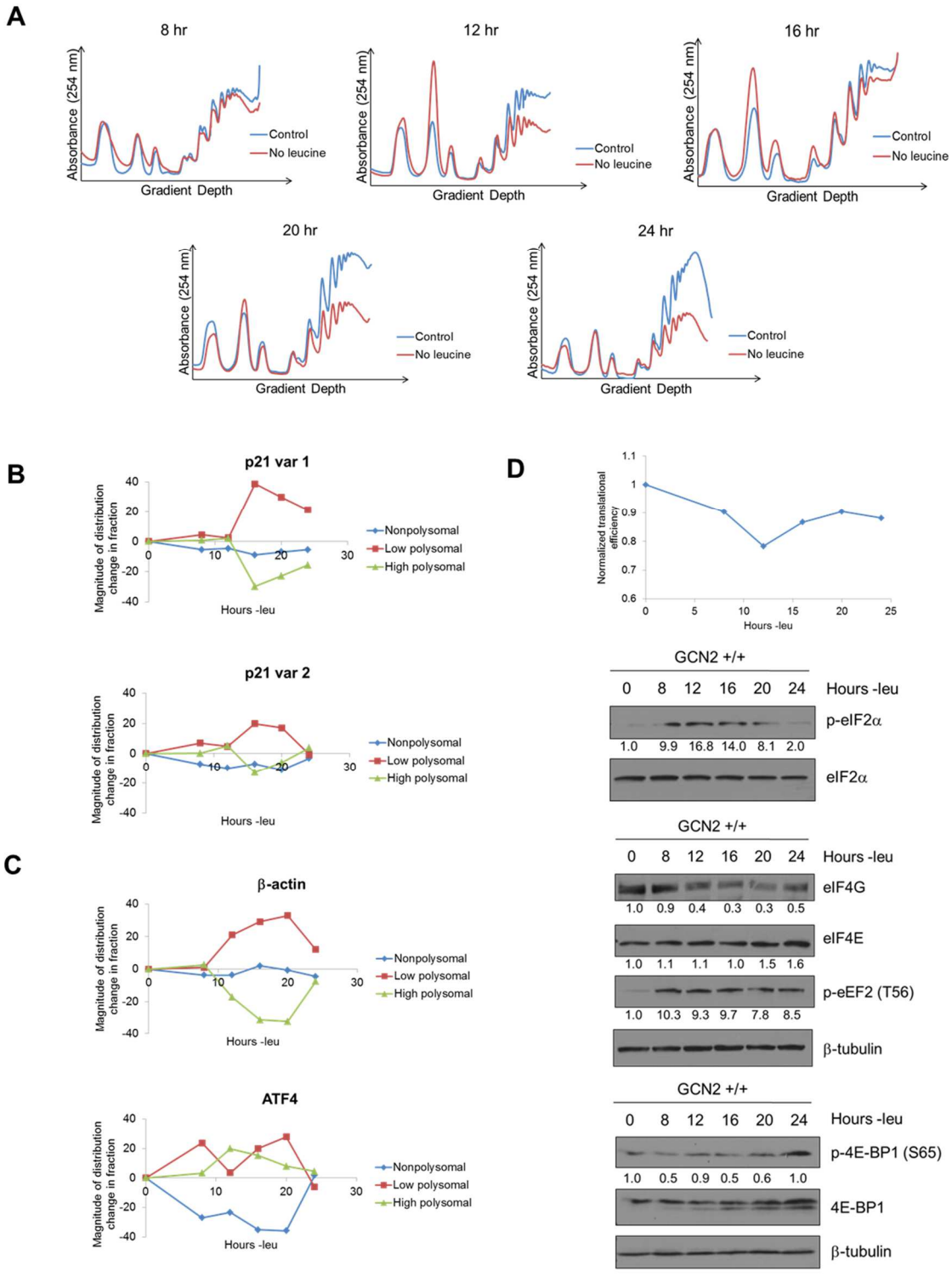
A
8 hr
12 hr
16 hr
20 hr
24 hr
Absorbance (254 nm)
Gradient Depth
Control
No leucine
B
p21 var 1
p21 var 2
Magnitude of distribution change in fraction
Hours -leu
Nonpolysomal
Low polysomal
High polysomal
C
β-actin
ATF4
D
Normalized translational efficiency
GCN2 +/+
0 8 12 16 20 24 Hours -leu
p-eIF2α
1.0 9.9 16.8 14.0 8.1 2.0
eIF2α
eIF4G
1.0 0.9 0.4 0.3 0.3 0.5
eIF4E
1.0 1.1 1.1 1.0 1.5 1.6
p-eEF2 (T56)
1.0 10.3 9.3 9.7 7.8 8.5
β-tubulin
p-4E-BP1 (S65)
1.0 0.5 0.9 0.5 0.6 1.0
4E-BP1
β-tubulin

Previous page: Figure II-4. Polysome profiling reveals differences between the translational efficiencies of p21 variants 1 and 2 under nutrient stress. (A) Polysome profiles of leucine-starved $GCN2^{+/+}$ MEFs over time. Lysates from $GCN2^{+/+}$ MEFs grown with or without leucine for 8, 12, 16, 20, and 24 hours were separated on 10 to 50% sucrose gradients. Polysome profiles of the gradients were generated by measuring absorbance at 254 nm. **(B)** Time course of p21 translational efficiency as measured by mRNA association with polysomes. qPCR was performed on fractions pooled from sucrose gradients. p21 transcript levels in each group were normalized to total transcript. **(C)** Time course of β-actin and ATF4 translational efficiency as measured by mRNA association with polysomes. qPCR was performed on fractions pooled from sucrose gradients. Transcript levels in each group were normalized to total transcript. **(D)** Time course of global translational efficiency in leucine-deprived $GCN2^{+/+}$ MEFs. Top: Time course of translational efficiency in leucine-deprived cells. Bottom: Western blot analysis of various components of the translational machinery in leucine-deprived $GCN2^{+/+}$ MEFs. Values below each blot represent the fold change in total pixel intensity over control normalized to β-tubulin (for eIF4G, eIF4E, p-eEF2), eIF2α (for p- eIF2α), or 4E-BP1 (for p-4E-BP1).

Additional mechanisms of p21 regulation under amino acid deprivation were also explored. It has been previously published that amino acid deprivation increases p21 mRNA stability[43]. To determine if this effect was GCN2 dependent, $GCN2^{+/+}$ and $GCN2^{-/-}$ MEFs were glutamine starved overnight, and then switched to complete media containing the transcriptional inhibitor 5,6-dichlorobenzimidazole 1-β-D-ribofuranoside (DRB) or glutamine-free media containing DRB. Cells were harvested over a time course, and p21 mRNA levels were measured by qPCR. In wildtype cells, the half-life of p21 mRNA was 2.84 hours in complete media, which increased to 3.47 hours in glutamine-free media. Similarly in $GCN2^{-/-}$ cells, the half-life of p21 mRNA was 2.73 hours in complete media and 3.49 hours in glutamine-free media (Figure II-5A). Thus, it does not appear that GCN2 plays a role in regulating p21 mRNA stability.

Interestingly, under glutamine or methionine deprivation, $GCN2^{-/-}$ MEFs are unable to upregulate p21 transcript levels, unlike $GCN2^{+/+}$ or eIF2α S51A MEFs (Figure II-5B,C). This may suggest that GCN2 is generally required for p21 transcriptional regulation under amino acid deprivation, but leucine deprivation specifically regulates another factor that compensates for GCN2 loss. Figure II-2A demonstrates that p53 family members are not required for p21 transcriptional upregulation under leucine deprivation. We further confirmed that they are not required for p21 transcriptional induction under glutamine deprivation (Figure II-5D). Therefore, p53 is not responsible for the differential ability of $GCN2^{-/-}$ MEFs to induce p21 transcript levels under glutamine or leucine deprivation. The role of the transcription factor Myc was also

analyzed. Myc is a suppressor of p21 transcription[71]. One possible scenario is that leucine deprivation results in derepression of p21 transcription through downregulation of Myc, while Myc levels remain high in glutamine-starved GCN2$^{-/-}$ MEFs. Surprisingly, Myc protein levels declined much more rapidly in GCN2$^{-/-}$ MEFs than in GCN2$^{+/+}$ MEFs under both glutamine and leucine deprivation (Figure II-5E), so such a scenario is not likely.

GCN2 has been reported to interact with members of the transforming growth factor β/bone morphogenic protein (TGFβ/BMP) signaling pathway[85]. It is also known that TGFβ signaling induces p21 transcription[86]. Therefore, we tested the possibility that TGFβ/BMP signaling induces p21 under amino acid deprivation. To do so, mothers against decapentaplegic homolog 4 (SMAD4), the common member of the TGFβ and BMP pathways, was knocked down in GCN2$^{+/+}$ MEFs, which were subsequently glutamine starved. SMAD4 knockdown greatly delayed the induction of both p21 transcript and protein levels (Figure II-5F,G), suggesting that SMAD4 plays a significant role in regulating p21 under glutamine deprivation. However, the mechanism is likely not straightforward since SMAD4 protein levels actually decrease under glutamine deprivation (Figure II-5G). Further work is necessary to determine if SMAD4 and GCN2 cooperate to regulate p21 under amino acid deprivation.

Next page: Figure II-5. Additional mechanisms of p21 regulation under stress. (A) Measurement of p21 mRNA half-life under replete and glutamine starved conditions. GCN2$^{+/+}$ and GCN2$^{-/-}$ MEFs were initially grown in glutamine-free media to induce p21 mRNA levels at time 0. Cells were then switched to complete or glutamine-free media containing 100 μg/mL DRB. p21 transcript levels were normalized to 18S rRNA and are depicted as fold change over control. mRNA levels were fit to exponential decay curves to calculate half-life. **(B)** qPCR for p21 was performed on RNA isolated from GCN2$^{+/+}$, GCN2$^{-/-}$, and eIF2α S51A MEFs deprived of glutamine for the indicated times. p21 transcript levels were normalized to 18S rRNA and are depicted as fold change over control. Data are the average of three independent experiments ± S.E.M. **(C)** qPCR for p21 was performed on RNA isolated from GCN2$^{+/+}$, GCN2$^{-/-}$, and eIF2α S51A MEFs deprived of methionine for the indicated times. p21 transcript levels were normalized to 18S rRNA and are depicted as fold change over control. Data are the average of three technical replicates ± standard deviation. **(D)** qPCR for p21 was performed on RNA isolated from wildtype, p53$^{-/-}$, p63$^{-/-}$, and p73$^{-/-}$ MEFs deprived of glutamine for the indicated times. p21 transcript levels were normalized to 18S rRNA. Results are depicted as fold change over control for each cell line. Data represent the average of three independent experiments ± S.E.M. **(E)** Western blot analysis of myc levels in leucine or glutamine deprived GCN2$^{+/+}$ and GCN2$^{-/-}$ MEFs. PARP and Ku80 were used as loading controls. **(F)** qPCR for p21 was performed on RNA isolated from glutamine-deprived GCN2$^{+/+}$ MEFs transfected with non-targeting siRNA (siNT) or siRNA against SMAD4 (siSMAD4). p21 transcript levels were normalized to 18S rRNA. Results are depicted as fold change over control for each cell line. Data represent the average of three technical replicates ± standard deviation. **(G)** Western blot analysis of p21 levels in glutamine-deprived GCN2$^{+/+}$ MEFs transfected with siNT or siSMAD4. Total eIF2α was used as a loading control.

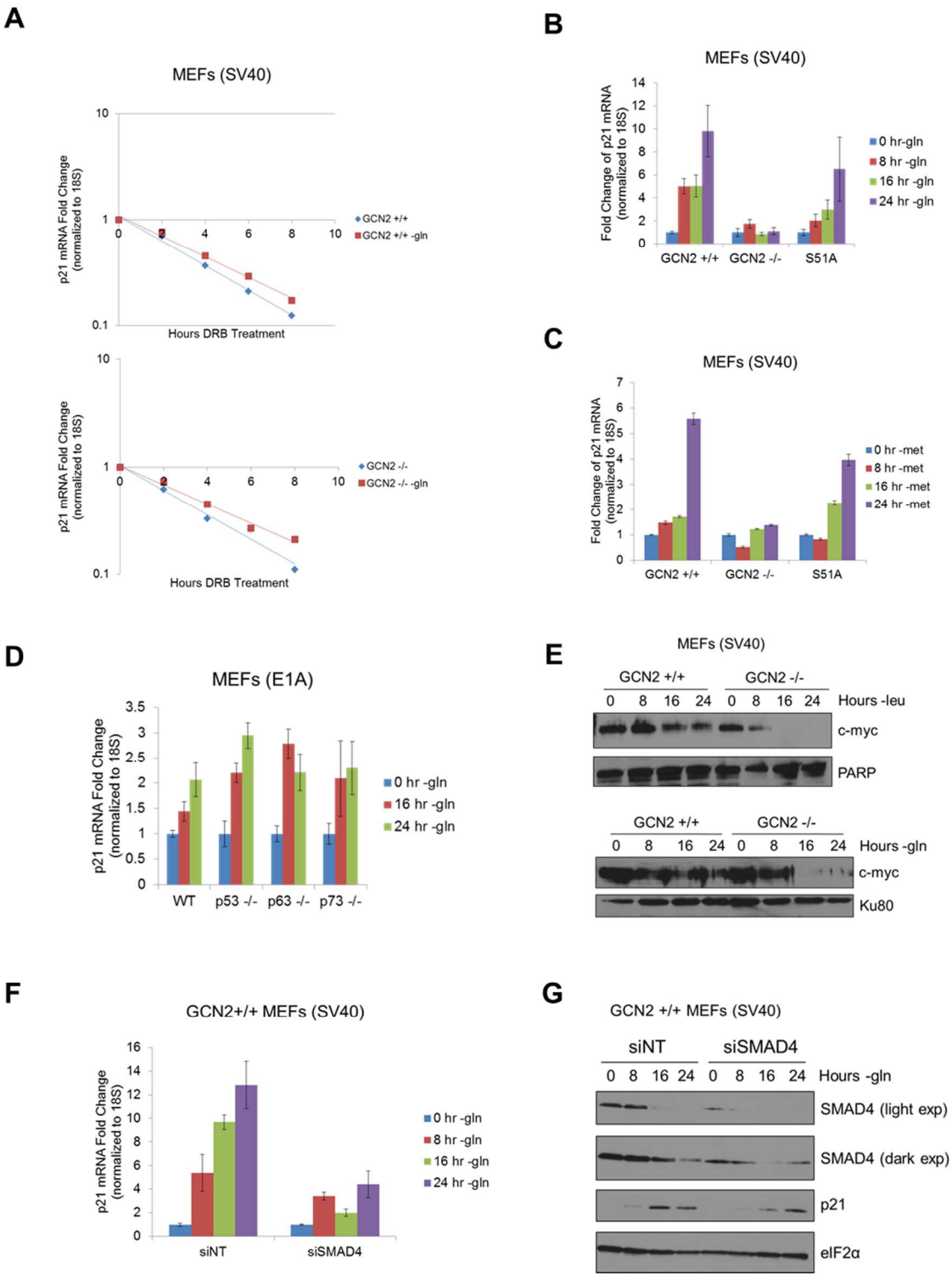
A
MEFs (SV40)
p21 mRNA Fold Change (normalized to 18S)
Hours DRB Treatment
GCN2 +/+
GCN2 +/+ -gln
GCN2 -/-
GCN2 -/- -gln
B
MEFs (SV40)
Fold Change of p21 mRNA (normalized to 18S)
0 hr-gln
8 hr -gln
16 hr -gln
24 hr -gln
GCN2 +/+
GCN2 -/-
S51A
C
MEFs (SV40)
Fold Change of p21 mRNA (normalized to 18S)
0 hr -met
8 hr -met
16 hr -met
24 hr -met
GCN2 +/+
GCN2 -/-
S51A
D
MEFs (E1A)
p21 mRNA Fold Change (normalized to 18S)
0 hr -gln
16 hr -gln
24 hr -gln
WT
p53 -/-
p63 -/-
p73 -/-
E
MEFs (SV40)
GCN2 +/+
GCN2 -/-
Hours -leu
c-myc
PARP
Hours -gln
c-myc
Ku80
F
GCN2+/+ MEFs (SV40)
p21 mRNA Fold Change (normalized to 18S)
0 hr -gln
8 hr -gln
16 hr -gln
24 hr -gln
siNT
siSMAD4
G
GCN2 +/+ MEFs (SV40)
siNT
siSMAD4
Hours -gln
SMAD4 (light exp)
SMAD4 (dark exp)
p21
eIF2α

Next, we sought to determine the functional consequences of p21 upregulation under amino acid starvation. We hypothesized that wildtype cells would undergo G_1/S arrest in response to amino acid deprivation, while cells lacking p21 would continue to proliferate. To this end, $GCN2^{+/+}$ MEFs were stably transfected with either non-targeting shRNA (shNT) or shRNA directed against p21 (shp21). The knockdown efficiency of two independent shp21 clones is shown in Figure II-6A. Leucine starvation resulted in a time-dependent increase in the G_1/S ratio of $GCN2^{+/+}$ shNT MEFs (Figure II-6B), as measured by flow cytometry. Knockdown of p21 resulted in a statistically significant decrease in the G_1/S ratio in both clones, indicating that p21 promotes cell cycle arrest under amino acid deprivation.

To confirm these results in a human cell line, SQ20B cells were transfected with either non-targeting siRNA (siNT) or siRNA against p21 (sip21). The knockdown efficiency of p21 is shown in Figure II-6C. An increase in the G_1/S ratio was observed in siNT transfected cells at 32 hours of leucine deprivation, while no appreciable change in the G_1/S ratio was detected in sip21 transfected cells (Figure II-6D). Thus, p21 regulates G_1/S arrest under amino acid deprivation in both murine and human cells.

To directly assess the role of GCN2 in cell cycle arrest, the degree of G_1/S cell cycle arrest was measured by flow cytometry in leucine-starved $GCN2^{-/-}$ MEFs. The phenotype was even stronger in these cells, as they did not undergo any measurable degree of G_1/S arrest by 32 hours of leucine starvation (Figures II-6E). This indicates that GCN2 is critically required for the induction of G_1/S arrest in response to leucine deprivation and likely regulates other factors that promote cell cycle arrest under stress. These results were also confirmed in SQ20B cells transfected with siNT or siGCN2 (Figure II-6F).

Previous findings showed that ER stress-induced phosphorylation of eIF2α by PERK and GCN2 in NIH 3T3 cells resulted in translational suppression of cyclin D1 and subsequent G_1 arrest[37,87]. To determine if a similar scenario occurred in this system, cyclin D1 protein levels were measured in leucine-starved $GCN2^{+/+}$ and $GCN2^{-/-}$ MEFs. Figure II-6G shows that cyclin D1 levels decreased over time in both cell lines. Therefore, under these study conditions, GCN2 does not

contribute to cell cycle regulation by modulating levels of cyclin D1. The GCN2-independent decrease in cyclin D1 and increase in p27 may explain why knockdown of p21 does not completely abolish the ability of MEFs to undergo G_1/S arrest in response to amino acid deprivation.

Next, we wanted to determine if p21 contributes to cell survival under amino acid deprivation. To do so, the shNT and shp21 MEF clones were cultured in complete media or media lacking leucine. After 72 hours, the viable cells were re-plated at low density in complete media. Virtually all shNT cells were able to recover from nutrient stress and form colonies. However, clonogenic survival was significantly reduced by approximately 40-50% in the two shp21 MEF clones after leucine deprivation (Figures II-6H). These results demonstrate that p21 is dispensable for cell growth under nutrient replete conditions but is critical for cell survival during the recovery from amino acid starvation. Furthermore, these results are consistent with another study which showed that p21 promotes cell survival under the combined stresses of complete amino acid and serum starvation independently of p53[88].

Next page: Figure II-6. p21 regulates G_1/S arrest and cell survival under conditions of amino acid deprivation. (A) Western blot analysis of the MEFs used in (B) to determine p21 knockdown efficiency. Values below blot represent the fold change in total pixel intensity over control of p21 normalized to the loading control for each lane. β-tubulin was used as a loading control. **(B)** G_1/S ratio of leucine-starved $GCN2^{+/+}$ MEFs stably transfected with non-targeting shRNA (shNT) or shRNA against p21 (shp21). DNA content was measured by propidium iodide staining and flow cytometry analysis. Data are the average of three independent experiments ± S.E.M.; * $p<0.05$, ** $p<0.01$. **(C)** Western blot analysis of the SQ20Bs used in (D) to determine p21 knockdown efficiency. Values below blot represent the fold change in total pixel intensity over control of p21 normalized to the loading control for each lane. β-tubulin was used as a loading control. **(D)** G_1/S ratio of leucine-starved SQ20Bs transfected with non-targeting siRNA (siNT) or siRNA against p21 (sip21). DNA content was measured by propidium iodide staining and flow cytometry analysis. Data are the average of four (siNT) or five (sip21) independent experiments ± S.E.M.; * $p<0.05$, ** $p<0.01$. **(E)** G_1/S ratio of $GCN2^{-/-}$ MEFs starved of leucine for the indicated times. DNA content was measured by propidium iodide staining and flow cytometry analysis. Changes in G_1/S ratio were not statistically significant. Data represent the average of three independent experiments ± S.E.M. **(F)** G_1/S ratio of leucine-starved SQ20Bs transfected with non-targeting siRNA (siNT) or siRNA against GCN2 (siGCN2). DNA content was measured by propidium iodide staining and flow cytometry analysis. The knockdown efficiency of siGCN2 is demonstrated in Figure II-1G. Data represent the average of three independent experiments ± S.E.M.; ** $p<0.01$. **(G)** Western blot analysis of cyclin D1 in leucine-starved $GCN2^{+/+}$ and $GCN2^{-/-}$ MEFs. Ku80 was used as a loading control. **(H)** Top: Clonogenic survival of control and p21 knockdown $GCN2^{+/+}$ MEFs exposed to long-term leucine starvation. Data are the average of three independent experiments ± S.E.M; *$p<0.05$, **$p<0.01$. Bottom: Representative picture of control and p21 knockdown MEFs from the clonogenic survival assay after one week of colony formation.

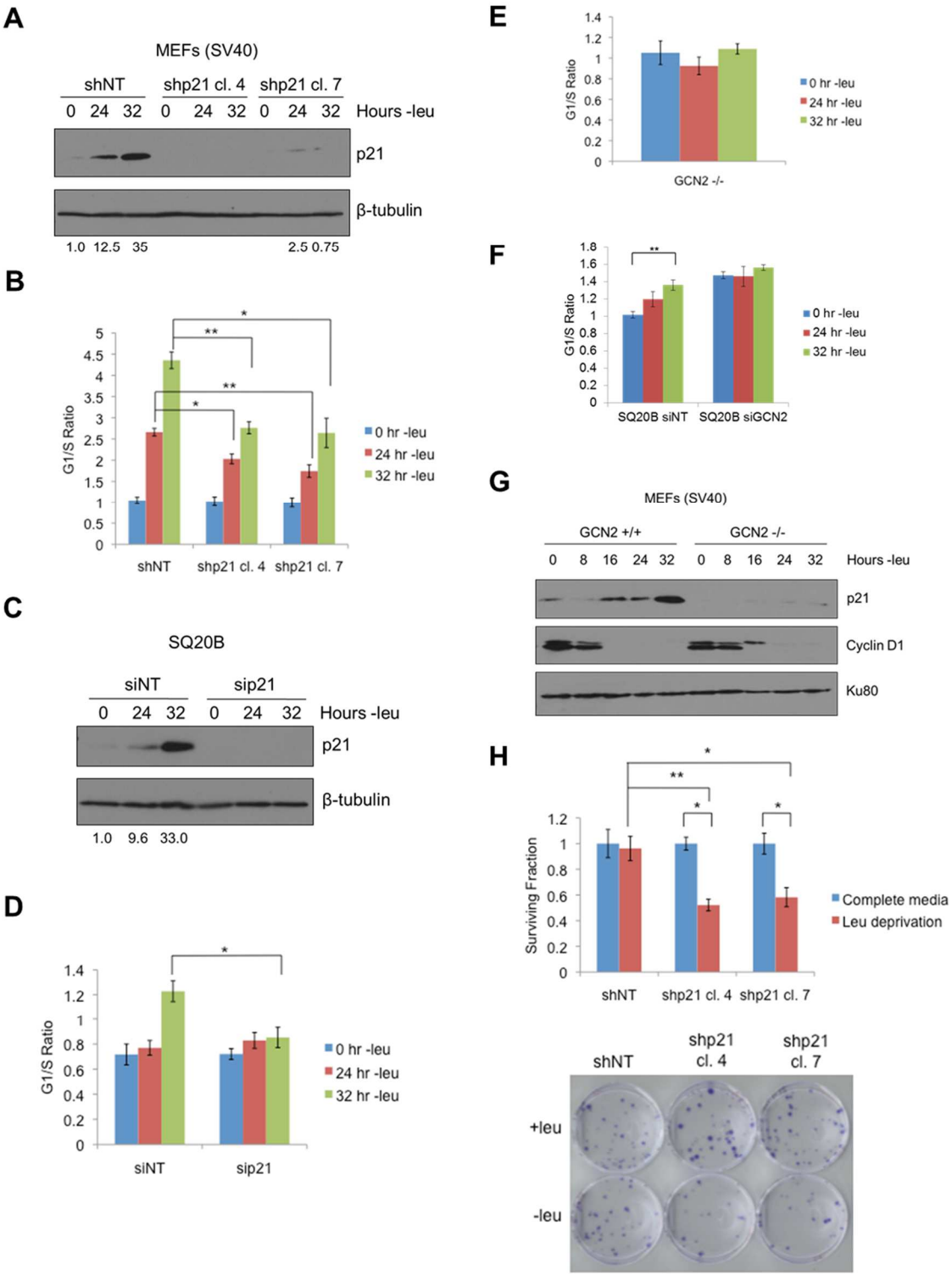
A
MEFs (SV40)
shNT
shp21 cl. 4
shp21 cl. 7
0 24 32 0 24 32 0 24 32
Hours -leu
p21
β-tubulin
1.0 12.5 35
2.5 0.75
B
G1/S Ratio
0 hr -leu
24 hr -leu
32 hr -leu
shNT
shp21 cl. 4
shp21 cl. 7
C
SQ20B
siNT
sip21
0 24 32 0 24 32
Hours -leu
p21
β-tubulin
1.0 9.6 33.0
D
G1/S Ratio
0 hr -leu
24 hr -leu
32 hr -leu
siNT
sip21
E
G1/S Ratio
0 hr -leu
24 hr -leu
32 hr -leu
GCN2 -/-
F
G1/S Ratio
0 hr -leu
24 hr -leu
32 hr -leu
SQ20B siNT
SQ20B siGCN2
G
MEFs (SV40)
GCN2 +/+
GCN2 -/-
0 8 16 24 32 0 8 16 24 32
Hours -leu
p21
Cyclin D1
Ku80
H
Surviving Fraction
Complete media
Leu deprivation
shNT
shp21 cl. 4
shp21 cl. 7
+leu
-leu

Discussion

Cells have evolved multiple mechanisms to regulate p21 at the post-transcriptional level. However, translational regulation of p21 has been largely unexplored. Here, we demonstrate a novel mechanism of translational control of a specific p21 transcript variant that regulates cell proliferation and survival under nutrient stress. GCN2 activation and subsequent phosphorylation of eIF2α translationally upregulates a p21 mRNA variant with 5' uORFs. Many genes are upregulated by eIF2α phosphorylation indirectly through activation of the ATF4 transcriptional program[26,89]. However, the number of genes known to be directly translationally upregulated by eIF2α phosphorylation is much smaller. In addition to ATF4, several other genes, such as ATF5[25], GADD34[24], CCAAT/enhancer-binding protein homologous protein (CHOP)[90], inhibitor of Bruton's tyrosine kinase α (IBTKα)[91], and protein kinase C η (PKCη)[92], are also translationally upregulated by eIF2α phosphorylation due the presence of uORFs in the 5' UTR. These studies into p21 regulation expand on the known targets of translational upregulation by phosphorylation of eIF2α and provide greater understanding of the functional outcomes of ISR activation.

These results suggest a model in which under normal, unstressed conditions, translation typically initiates at the uORFs in the p21 variant 2 transcript, resulting in very little production of p21. Initiation at uORF1 would fail to produce a protein because it overlaps out of frame with the p21 coding sequence. Initiation at uORFs 2 and 3 likely do not produce a protein because they are located very close to the p21 coding sequence, which does not provide ribosomes sufficient time to reinitiate translation at the p21 ORF. When GCN2 phosphorylates eIF2α, translation initiation is delayed. This promotes leaky scanning through the uORFs and increases the likelihood that ribosomes will begin translation at the p21 ORF (Figure II-7).

This mechanism of translation regulation also offers an explanation for the existence of multiple p21 transcript variants that encode for the same protein. While this work focused on the two mouse p21 mRNA variants, humans also have multiple p21 mRNA variants that are likely regulated in a similar manner[81]. Some of these variants contain an overlapping 5' uORF, while the others contain none. We speculate that p21 transcript variants with 5' uORFs provide an

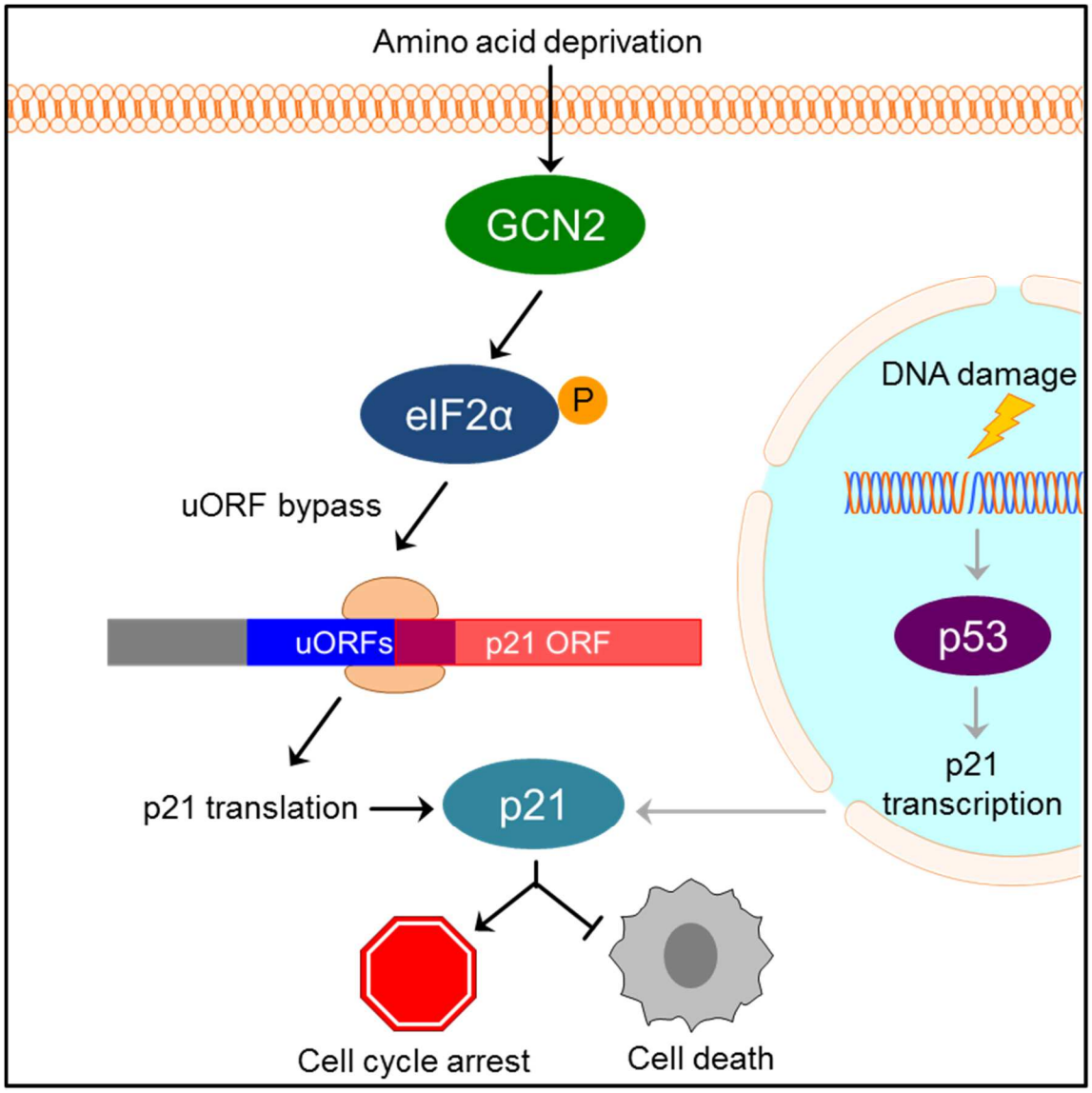

Figure II-7. Model of p21 translational regulation. Upon amino acid deprivation, GCN2 phosphorylates eIF2α, which delays translation initiation. This results in ribosomes bypassing 5' uORFs in the p21 variant 2 transcript and beginning translation at the p21 ORF, resulting in p21 upregulation under stress. This pathway is distinct from p53-dependent transcriptional upregulation of p21. Induction of p21 upon nutrient deprivation leads to G_1/S arrest and promotes cell survival.

advantage to cells by allowing them to upregulate p21 under stress conditions that would normally repress translation. Translation is one of the highest energy consuming processes in the cell, which is why it is often suppressed to conserve resources under stress. Under these conditions, proliferation is not favored and upregulation of p21 provides an advantage to cells by promoting cell cycle arrest. However, the variants without 5' uORFs ensure that cells are not

restricted to express p21 only when eIF2α is phosphorylated. Other stresses, such as DNA damage, do not suppress translation but still require cell cycle arrest to allow time for recovery. In these cases, cells could still translate p21 efficiently to respond to stress even though eIF2α remains unphosphorylated.

From a functional standpoint, this study provides a link between the nutrient-sensing capabilities of GCN2 and the mammalian cell cycle. Many proteins that respond to nutrient levels impinge upon the cell cycle. Amino acids are also sensed by mTOR, one of the master metabolic switches of the cell. mTOR activity is inhibited upon amino acid deprivation, resulting in G_1 arrest through decreased production and increased turnover of cyclin D1[93,94] and upregulation of the cell cycle inhibitor p27[95]. Amino acid starvation also increases the half-life of both p21 and p27 mRNA[43]. Glucose deprivation activates AMPK, a major cellular energy regulator, which phosphorylates and stabilizes p53, resulting in p21 induction[42]. Glucose deprivation also perturbs protein folding and activates the ISR initiator and endoplasmic reticulum resident kinase PERK, which induces G_1 arrest by suppressing cyclin D1 translation[87]. Here, we provide additional links between the cell's nutrient sensing and cell cycle machinery by demonstrating that GCN2 directly links amino acid availability with cell cycle progression by translationally upregulating a transcript variant of p21.

The induction of p21 promotes cell cycle arrest when nutrients are scarce and conditions are not favorable for division. As a likely consequence of continued proliferation in a nutrient-poor environment, cells lacking p21 exhibit decreased survival after exposure to amino acid deprivation. These findings may have important implications for cancer. Tumor cells often exist in a nutrient-poor microenvironment due to inadequate tumor perfusion and increased metabolic demands of tumor cells[1]. Our lab has previously shown that GCN2 is overexpressed in human tumors, and loss of GCN2 slows or inhibits tumor growth in mouse xenograft models of cancer[58]. Downstream of GCN2, p21 may serve to promote tumor cell survival in areas where nutrients are limiting. This fits with observations that p21 has both pro- and anti-tumorigenic properties[96]. In general, limiting cell division would slow tumor growth. However, in areas lacking adequate

nutrient supply, p21-dependent cell cycle arrest would allow tumor cells to remain dormant and survive adverse conditions that would otherwise lead to cell death. Understanding the mechanism of p21 regulation and its function will greatly enhance the development of targeted therapeutics against the GCN2-eIF2α-p21 pathway.

CHAPTER III: SIGNALING THROUGH ALTERNATIVE INTEGRATED STRESS RESPONSE PATHWAYS COMPENSATES FOR GCN2 LOSS IN A MOUSE MODEL OF SOFT TISSUE SARCOMA

This chapter contributes to a manuscript of the same title submitted to *Scientific Reports* (in revision).

Introduction

Many of the stressors that activate the ISR are encountered in the tumor microenvironment. Tumor vasculature is often poorly constructed, resulting in leaky, tortuous vessels that cannot deliver nutrients efficiently to tumor cells. The high metabolic rate of tumor cells also leads to rapid consumption of nutrients that are available to the cells. This results oxygen, glucose, and amino acid deprivation in areas of the tumor[1]. Hypoxia and glucose deprivation both interfere with proper protein folding, resulting in endoplasmic reticulum (ER) stress and PERK activation[59,60], while amino acid deprivation activates GCN2[2,3]. The cell autonomous stress of oncogene activation through c-Myc places high demands on protein synthesis and can also activate PERK[97].

Previous research from many groups, including our own, has shown that ISR activation promotes tumor cell survival. *In vitro*, cells lacking PERK exhibit decreased clonogenic survival after exposure to hypoxia[63]. PERK$^{-/-}$ cells with activated c-Myc also have greatly reduced clonogenic survival[97]. *In vivo*, PERK$^{-/-}$ cells injected into the flanks of nude mice form much smaller tumors than their wildtype counterparts[63,98]. Additionally, hypoxic and apoptotic areas of PERK null tumors overlap, indicating that PERK supports tumor cell survival under hypoxia *in vivo*[63]. Similarly, cells lacking GCN2 undergo apoptosis when grown in media lacking an amino acid. Loss of GCN2 in xenograft models of cancer greatly inhibits or even prevents tumor growth[58].

While these results are promising, it is necessary to test the role of ISR kinases in genetically engineered mouse models (GEMMs) of cancer. The majority of conditions known to activate the ISR in tumor cells, such as hypoxia and low nutrient levels, are non-cell autonomous and dictated by the tumor microenvironment. Cells grown subcutaneously in mice as xenografts are not exposed to physiological levels of microenvironmental stress. Many important components of the tumor microenvironment, such as stromal cells, immune cells, and blood vessels, are altered or absent in xenograft models[99]. GEMMs provide the benefit of modeling the

growth of tumors in their native microenvironment, which allows for a more accurate assessment of the contribution of these kinases to tumor growth.

The ISR kinase PERK has been studied in GEMMs. $PERK^{fl/fl}$;MMTV-cre mice crossed to MMTV-neu mice resulted in the specific deletion of PERK in the mammary glands of tumor-prone MMTV-neu mice. Results from this study showed that loss of PERK in mammary carcinomas slowed tumor growth and reduced the number of metastases to the lungs[64]. In a second model, mice expressing SV40 large T antigen specifically in the beta cells of the pancreas were crossed to $PERK^{-/-}$ mice. Loss of PERK resulted in the formation of fewer and smaller insulinomas in mice[65]. In general, the results of PERK loss in GEMMs recapitulate the observations made in xenograft models.

Although the role of PERK in tumorigenesis has been characterized in both xenograft and genetically engineered mouse models of cancer, GCN2 has yet to be studied in a GEMM. Our lab's previous studies in the HT1080 human sarcoma cell line revealed that knockdown of GCN2 completely blocked tumor growth in a xenograft model[58]. Here, these studies are expanded to GCN2 null mice crossed to genetic model of soft tissue sarcoma developed by Kirsch and colleagues[100]. Surprisingly, in autochthonous tumors, loss of GCN2 did not affect tumor initiation or progression and did not increase the lifespan of tumor-bearing mice. Analysis of the tumors at the molecular level revealed several mechanisms of compensation for GCN2 loss. Mice on a C57BL6 background exhibited increased signaling through PERK to maintain levels of phosphorylated eIF2α in tumors, while mixed background mice upregulated ATF4 independently of eIF2α phosphorylation levels to maintain ISR signaling. Overall, this study reveals the importance of ISR signaling in tumorigenesis and defines mechanisms by which sarcomas can become resistant to ISR inhibition. As small molecule inhibitors of the ISR kinases are currently under development, this study has clinical relevance to their testing in animal models and insight into ways tumor cells may circumvent their effects.

Results

To study the role of GCN2 in tumorigenesis, $GCN2^{-/-}$ mice were crossed to LSL-$Kras^{G12D/wt}$;$p53^{fl/fl}$ mice to obtain GCN2 wildtype, heterozygous, and null mice on an LSL-$Kras^{G12D/wt}$;$p53^{fl/fl}$ background (Figure III-1A). Sarcoma formation was induced in these mice by injection of adenovirus expressing cre recombinase (Ad-cre) into the right leg muscle. This resulted in the formation of soft tissue sarcomas in nearly 100% of mice. Grossly, the sarcomas grew rapidly and essentially took over the normal muscle tissue in the leg (Figures III-1B,C). At the microscopic level, the tumors were highly dedifferentiated with complete loss of normal tissue architecture (Figure III-1D). To determine if the tumors were undergoing oxygen and nutrient deprivation, hypoxia levels were assessed by performing immunohistochemistry for the hypoxia marker carbonic anhydrase 9 (CA9). Tumors demonstrated extensive areas of hypoxia (Figure III-1E).

To determine if the GCN2 arm of the ISR was activated in the sarcomas in response to stress, tumors and normal muscle from $GCN2^{+/+}$, $GCN2^{+/-}$, and $GCN2^{-/-}$ mice were homogenized and immunoblotted for total and phosphorylated GCN2. As previously observed in human patient samples[58], GCN2 was overexpressed in tumor tissue as compared to normal tissue in wildtype and heterozygous mice. Phosphorylation of GCN2 was detected in the wildtype and heterozygous mice, indicating that GCN2 was activated in the tumors (Figure III-1F). Since GCN2 in normal muscle tissue could not be detected by western blot, its overexpression at the mRNA level was confirmed by qPCR (Figure III-1G).

Next page: Figure III-1. Development of a genetically engineered mouse model to study the role of GCN2 in sarcomagenesis. (A) Breeding scheme to generate $GCN2^{+/+}$, $GCN2^{+/-}$, and $GCN2^{-/-}$ mice on an LSL-$Kras^{G12D/wt}$;$p53^{fl/fl}$ background. **(B)** Gross morphology of sarcomas compared to normal leg. The right leg was injected with Ad-cre, while the left leg served as a normal tissue control. **(C)** Gross morphology of sarcomas compared to normal leg. The size of a typical sarcoma (left) is compared to size of the normal leg (right) from the same mouse. **(D)** Typical histology of normal muscle (top) and soft tissue sarcoma (bottom) stained with hematoxylin and eosin. Magnification is 40X. Normal muscle and tumor shown are from the same animal. **(E)** Immunohistochemistry for CA9 in two sarcomas, along with the no primary antibody control. Tissue sections were counterstained with hematoxylin. Magnification is 100X. **(F)** Western blot analysis of phosphorylated and total GCN2 in homogenized normal muscle tissue (N) and soft tissue sarcomas (T). β-tubulin was used as a loading control. **(G)** qPCR analysis of *GCN2* levels in sarcoma and muscle tissue. *GCN2* levels were normalized to the geometric mean of the reference genes β-actin and 18S rRNA. Data are represented as the average value for each genotype ± S.E.M.;*$p<0.05$, **$p<0.01$

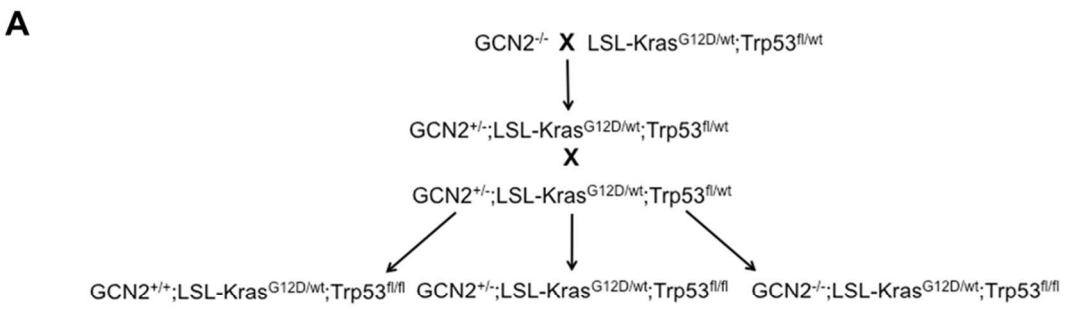
A
GCN2-/- X LSL-KrasG12D/wt;Trp53fl/wt
GCN2+/-;LSL-KrasG12D/wt;Trp53fl/wt
X
GCN2+/-;LSL-KrasG12D/wt;Trp53fl/wt
GCN2+/+;LSL-KrasG12D/wt;Trp53fl/fl
GCN2+/-;LSL-KrasG12D/wt;Trp53fl/fl
GCN2-/-;LSL-KrasG12D/wt;Trp53fl/fl


B

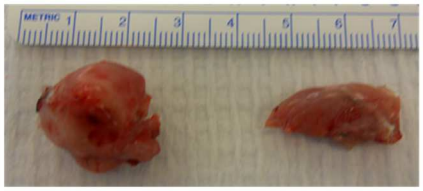
C

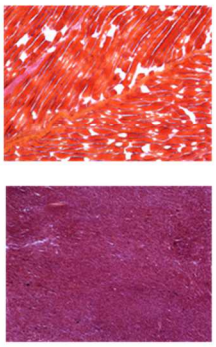
D

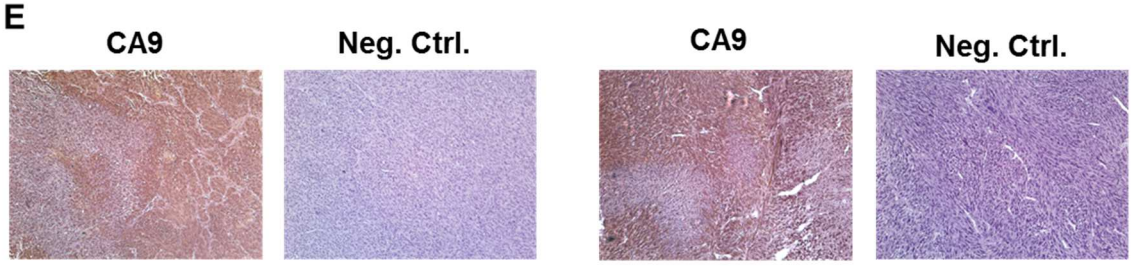
E
CA9
Neg. Ctrl.
CA9
Neg. Ctrl.

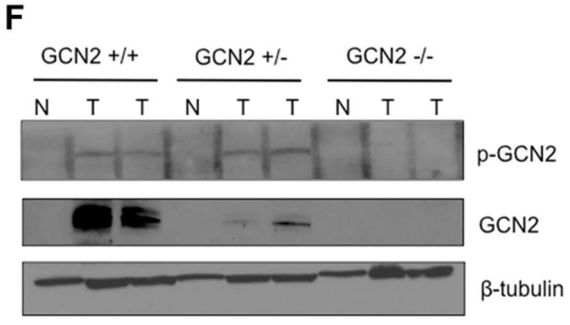
F
GCN2 +/+
GCN2 +/-
GCN2 -/-
N T T N T T N T T
p-GCN2
GCN2
β-tubulin

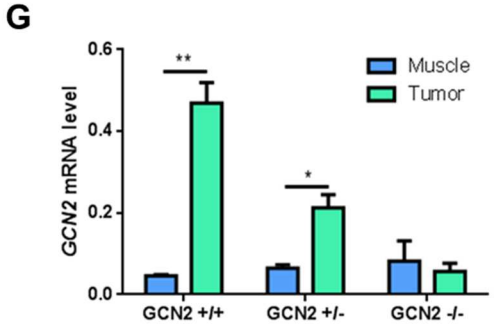
G
GCN2 mRNA level
0.6
0.4
0.2
0.0
**
*
Muscle
Tumor
GCN2 +/+
GCN2 +/-
GCN2 -/-

Tumor volume was measured in the mice over time. As shown in Figure III-2A, palpable tumors formed in most mice between 50 to 80 days post-injection. Tumor measurements were fit to exponential growth curves, and doubling times were calculated from the growth curves to determine the tumor growth rates. Loss of GCN2 did not affect tumor growth. Regardless of the GCN2 status of the mice, all tumors had a doubling time of three to four days, and the differences among the three genotypes were not statistically significant (Figure III-2B).

Kaplan-Meier curves were generated for both time to tumor formation after Ad-cre injection and time to death after tumor detection. There were no statistically significant differences in survival among the three genotypes, indicating that GCN2 did not affect tumor initiation or tumor progression in this model (Figures III-2C,D). To ensure that using both male and female mice did not obscure the effects of GCN2, survival curves based on the sex of the mice were generated. These data show that tumor initiation and progression were identical in males and females (Figure III-2E,F).

The $GCN2^{-/-}$ mice used in this study were on a C57BL6 background, while the LSL-$Kras^{G12D/wt}$;$p53^{fl/fl}$ mice were on a mixed background. To determine if genetic heterogeneity of the mixed background mice masked the effects of GCN2, we obtained C57BL6 LSL-$Kras^{G12D/wt}$;$p53^{fl/fl}$ mice to carry out the experiments on a uniform genetic background. While tumors initiated in the C57BL6 mice within a much narrower window (40 to 50 days for most mice), loss of GCN2 still had no effect on tumor growth rate, tumor free survival, or overall survival of the mice (Figure III-3A-D). There was no difference in survival between C57BL6 males and females (Figure III-3E,F).

Next page: Figure III-2. GCN2 does not affect tumor growth or survival of sarcoma-bearing mice on a mixed background. (A) Measurements of tumor volume over time in $GCN2^{+/+}$, $GCN2^{+/-}$, and $GCN2^{-/-}$ mixed background mice. The line through the set of measurements for each mouse represents the best fit exponential growth equation of the tumor. **(B)** Tumor doubling time was calculated from the best fit exponential growth equations shown in (A). The average doubling time ± standard deviation is depicted for each genotype. Results were not statistically significant. **(C)** Kaplan-Meier curves depicting the time from Ad-cre injection to tumor formation for each GCN2 genotype. Results were not statistically significant. **(D)** Kaplan-Meier curves depicting the time from tumor detection to euthanasia for each GCN2 genotype. The major euthanasia criterion was a tumor volume exceeding 1000 mm^3. Results were not statistically significant. **(E)** Kaplan-Meier curves depicting the time from Ad-cre injection to tumor formation for males and females. Results were not statistically significant. **(F)** Kaplan-Meier curves depicting the time from tumor detection to euthanasia for males and females. Results were not statistically significant.

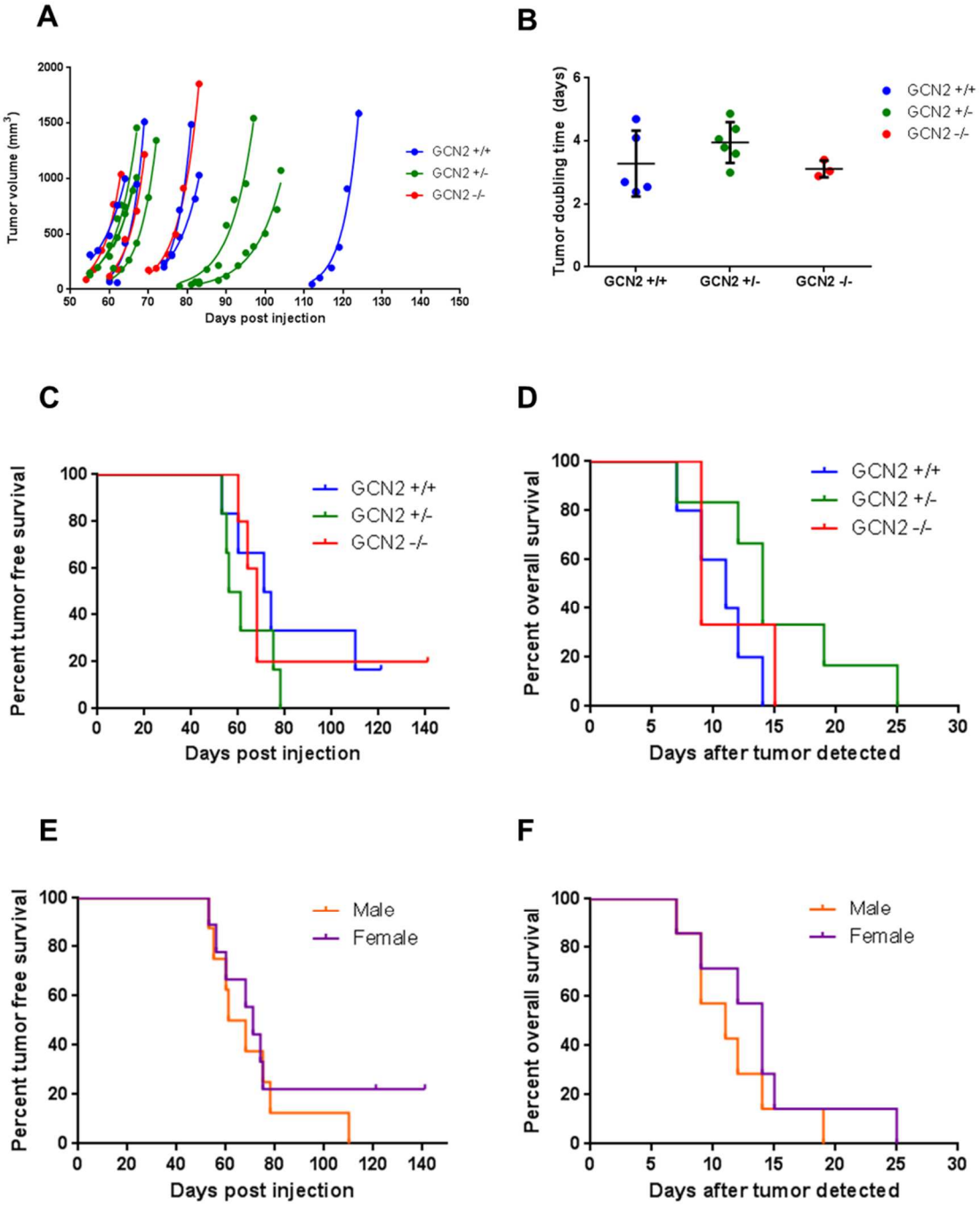
A
Tumor volume (mm3)
2000
1500
1000
500
0
50 60 70 80 90 100 110 120 130 140 150
Days post injection
GCN2 +/+
GCN2 +/-
GCN2 -/-
B
Tumor doubling time (days)
6
4
2
0
GCN2 +/+
GCN2 +/-
GCN2 -/-
C
Percent tumor free survival
100 80 60 40 20 0
0 20 40 60 80 100 120 140
Days post injection
GCN2 +/+
GCN2 +/-
GCN2 -/-
D
Percent overall survival
100 80 60 40 20 0
0 5 10 15 20 25 30
Days after tumor detected
GCN2 +/+
GCN2 +/-
GCN2 -/-
E
Percent tumor free survival
100 80 60 40 20 0
0 20 40 60 80 100 120 140
Days post injection
Male
Female
F
Percent overall survival
100 80 60 40 20 0
0 5 10 15 20 25 30
Days after tumor detected
Male
Female

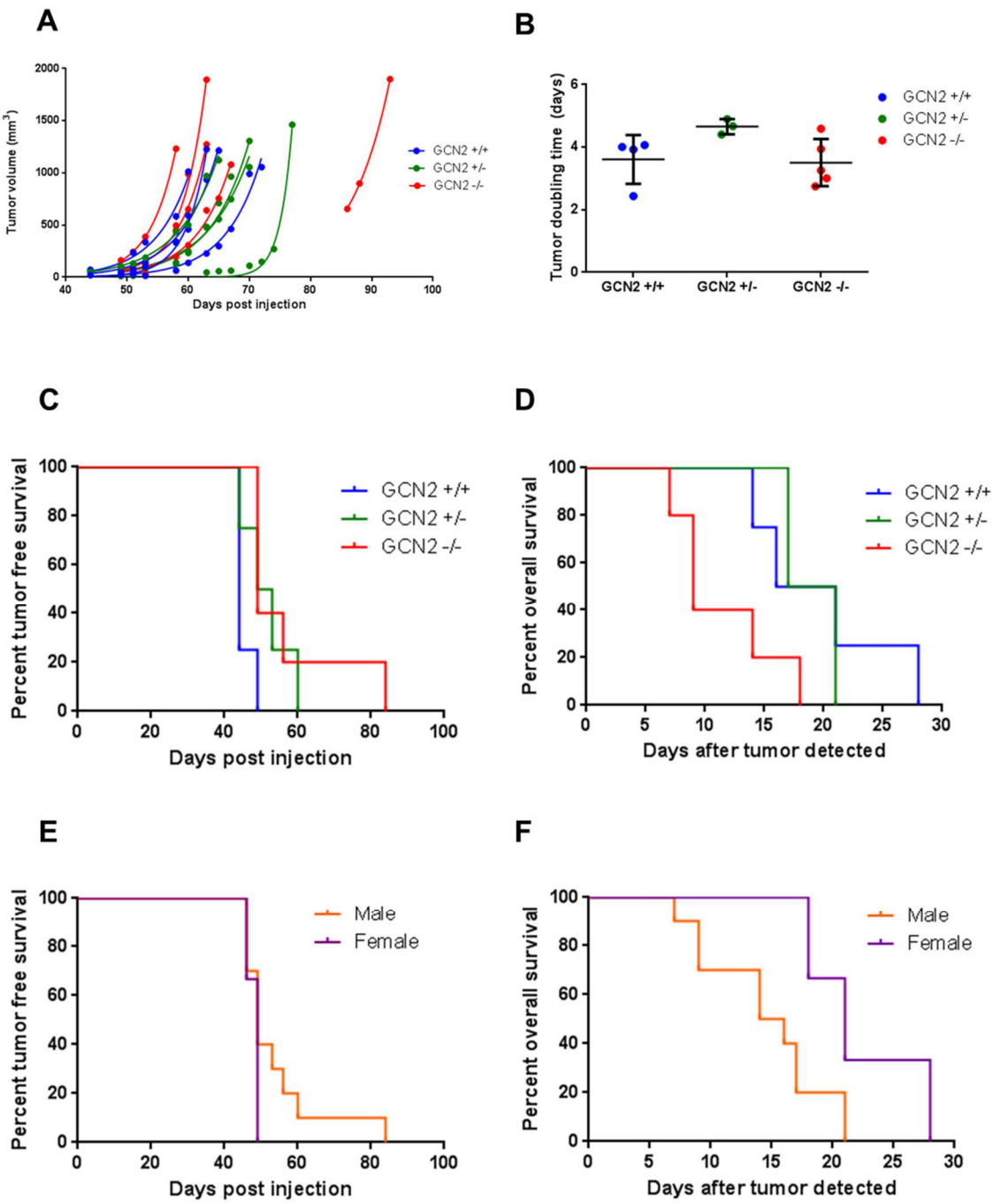
A
Tumor volume (mm3)
Days post injection
GCN2 +/+
GCN2 +/-
GCN2 -/-
B
Tumor doubling time (days)
GCN2 +/+
GCN2 +/-
GCN2 -/-
C
Percent tumor free survival
Days post injection
GCN2 +/+
GCN2 +/-
GCN2 -/-
D
Percent overall survival
Days after tumor detected
GCN2 +/+
GCN2 +/-
GCN2 -/-
E
Percent tumor free survival
Days post injection
Male
Female
F
Percent overall survival
Days after tumor detected
Male
Female

Previous page: Figure III-3. GCN2 does not affect tumor growth or survival of sarcoma-bearing mice on a C57BL6 background. (A) Measurements of tumor volume over time in $GCN2^{+/+}$, $GCN2^{+/-}$, and $GCN2^{-/-}$ C57BL6 mice. The line through the set of measurements for each mouse represents the best fit exponential growth equation of the tumor. **(B)** Tumor doubling time was calculated from the best fit exponential growth equations shown in (A). The average doubling time ± standard deviation is depicted for each genotype. Results were not statistically significant. **(C)** Kaplan-Meier curves depicting the time from Ad-cre injection to tumor formation for each GCN2 genotype. Results were not statistically significant. **(D**) Kaplan-Meier curves depicting the time from tumor detection to euthanasia for each GCN2 genotype. The major euthanasia criterion was a tumor volume exceeding 1000 mm^3. Results were not statistically significant. **(E)** Kaplan-Meier curves depicting the time from Ad-cre injection to tumor formation for males and females. Results were not statistically significant. **(F)** Kaplan-Meier curves depicting the time from tumor detection to euthanasia for males and females. Results were not statistically significant.

Next, we wanted to determine if loss of GCN2 affected downstream signaling through the ISR in tumor tissue. Western blot analysis of tumor lysates revealed that loss of GCN2 did reduce levels of eIF2α phosphorylation in mixed background mice. A repeat of the analysis on a small, independent sample of tumors produced similar results (Figure III-4A). Quantification of the p-eIF2α to total eIF2α ratio showed that $GCN2^{-/-}$ mixed background sarcomas had a statistically significant decrease in eIF2α phosphorylation (Figure III-4B). Signaling through other branches of the ISR was examined by measuring PERK and PKR phosphorylation in the tumors. PERK phosphorylation was detected in almost all tumors to varying degrees, while PKR was phosphorylated rather uniformly in all tumors (Figure III-4C). These data indicated that all relevant branches of the ISR are activated in this sarcoma model and that PERK and PKR are responsible for the residual eIF2α phosphorylation detected in $GCN2^{-/-}$ tumors. An analysis of normal muscle tissue indicated that, similar to GCN2, the sarcomas had overexpressed and activated PERK and PKR. Total eIF2α and phospho-eIF2α were also increased in tumors as compared to normal tissue controls (Figure III-5A). Staining of the membrane with Ponceau revealed that, overall, normal muscle tissue and sarcoma tissue have very different patterns of protein expression (Figure III-5B).

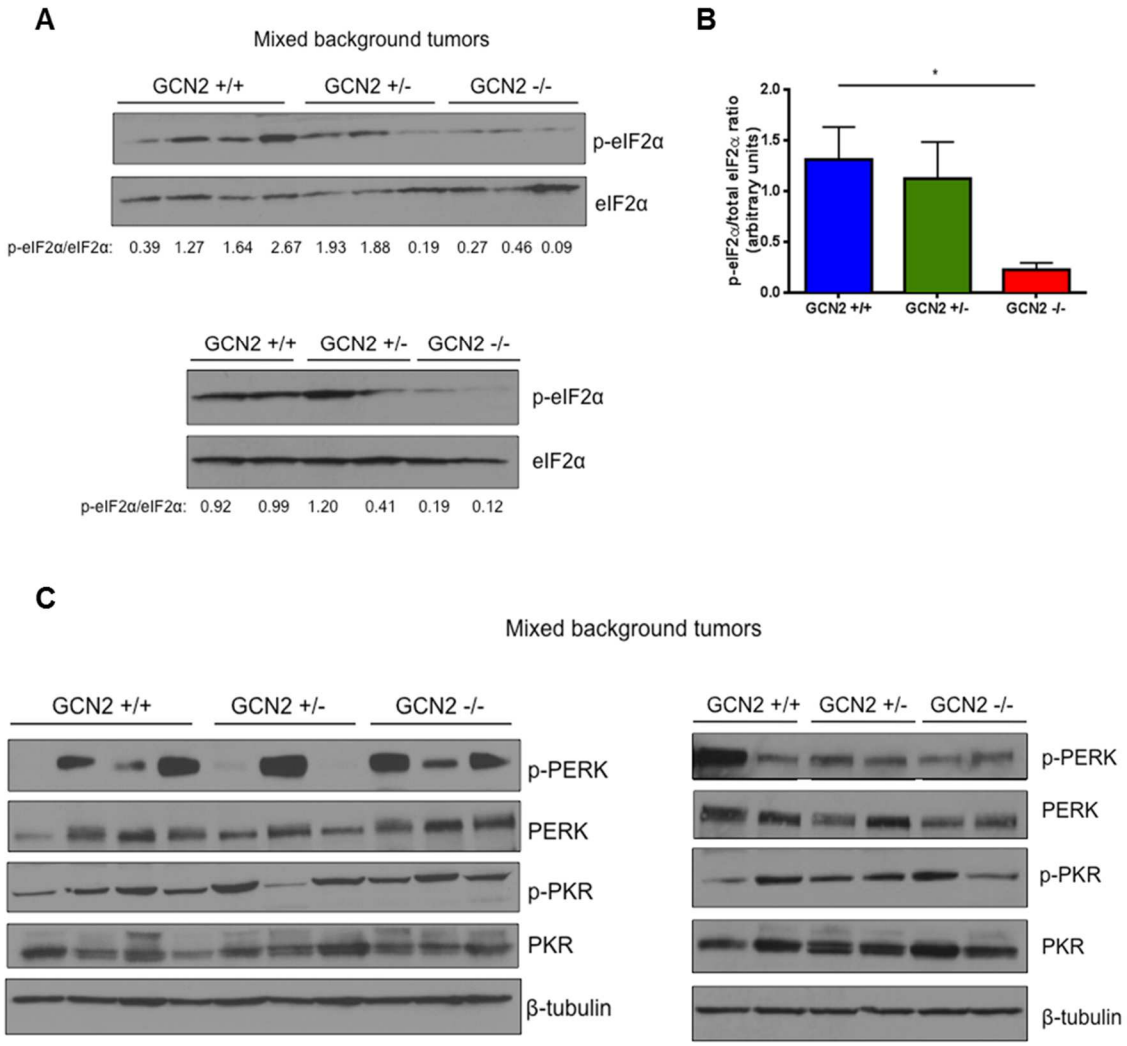

Figure III-4. Loss of GCN2 reduces eIF2α phosphorylation in mixed background sarcomas. (A) Western blot analysis on two independent samples of tumor homogenates for levels of phosphorylated and total eIF2α in mixed background tumors. The ratio of phosphorylated to total eIF2α is displayed below each blot. **(B)** Graphical representation of the phosphorylated to total eIF2α ratios calculated from the blots in (A). Data are represented as the average value for each genotype ± S.E.M.; *p<0.05. **(C)** Western blot analysis on two independent samples of tumor homogenates for levels of phosphorylated and total PERK and phosphorylated and total PKR in mixed background tumors. β-tubulin was used as a loading control.

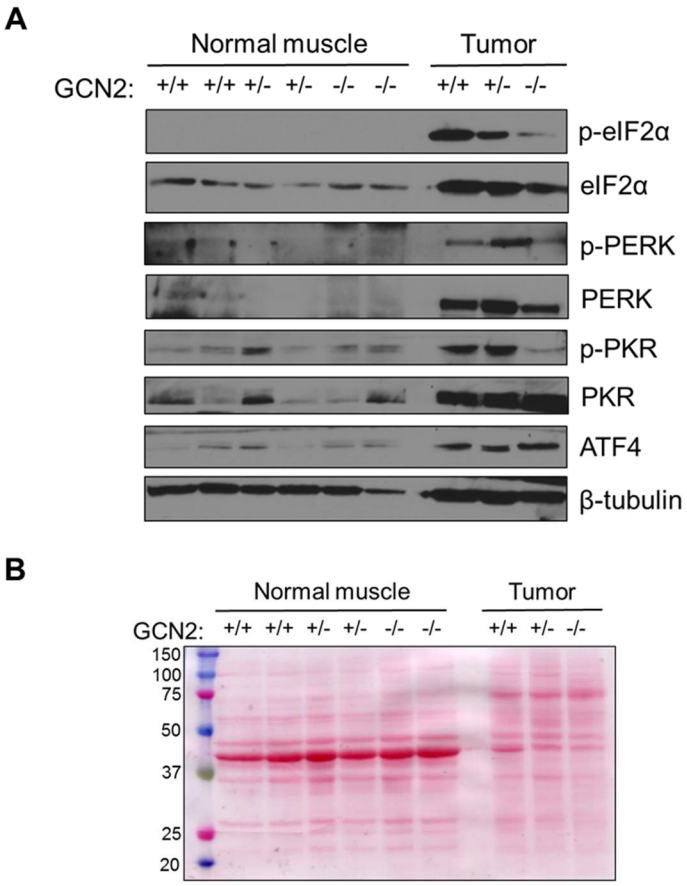

Figure III-5. ISR proteins are overexpressed and activated in sarcomas. Western blot analysis for various ISR proteins and their phosphorylated, active forms in both normal muscle tissue and tumor tissue. β-tubulin was used as a loading control. **(B)** Ponceau staining of total tissue lysates from normal muscle and tumor tissue.

The examination of ISR signaling was repeated in the C57BL6 tumors. Interestingly, the GCN2 status of these mice did not affect levels of eIF2α phosphorylation in the sarcomas (Figure III-6A). There was no statistically significant difference in the p-eIF2α to total eIF2α ratio in GCN2$^{-/-}$ mice as compared to the other genotypes (Figure III-6B). As observed in the mixed background tumors, PKR was phosphorylated in all C57BL6 tumors. However, substantially increased PERK phosphorylation was detected almost exclusively in GCN2$^{-/-}$ tumors (Figure III-6C). This suggests that in the C57BL6 tumors, PERK compensates for loss of GCN2, resulting in maintenance of eIF2α phosphorylation levels. To determine if other arms of the Unfolded Protein Response

(UPR) were activated in addition to PERK, we performed PCR on RNA isolated from normal muscle and tumor for X-box binding protein 1 (XBP1) splicing. Similar basal levels of spliced XBP1 were observed in normal muscle tissue, regardless of GCN2 status. However, enhanced XBP1 splicing in tumors was only observed in GCN2$^{-/-}$ mice, suggested that loss of GCN2 sensitizes cells to ER stress in the disease state only (Figure III-6D). Intriguingly, in a mouse model of Alzheimer's disease, another pathological condition that activates the ISR, knockout of GCN2 also results in compensatory activation of PERK in the brains of affected animals, leading to no improvements in memory decline[101].

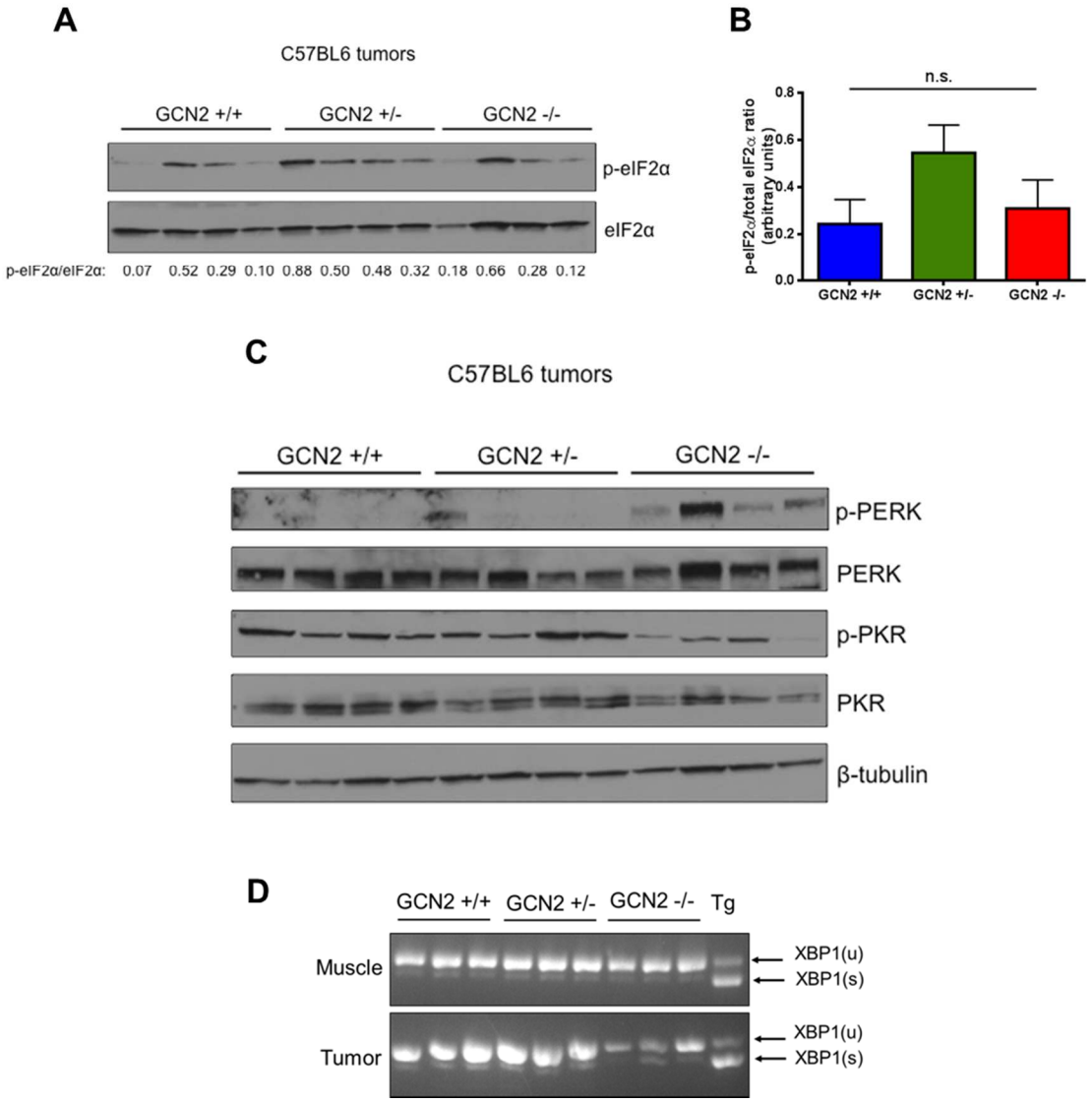

Previous page: Figure III-6. Loss of GCN2 does not reduce eIF2α phosphorylation in C57BL6 sarcomas, potentially due to compensation by PERK. (A) Western blot of tumor homogenates for levels of phosphorylated and total eIF2α in C57BL6 tumors. The ratio of phosphorylated to total eIF2α is displayed below each blot. **(B)** Graphical representation of the phosphorylated to total eIF2α ratios calculated from the blots in (A). Data are represented as the average value for each genotype ± standard error of the mean. Results are not statistically significant. **(C**) Western blot analysis of tumor homogenates for levels of phosphorylated and total PERK and phosphorylated and total PKR in C57BL6 tumors. β-tubulin was used as a loading control. **(D)** PCR analysis of XBP1 splicing in normal muscle and tumor tissue. The tumor sample below each muscle sample is from the same mouse. Mouse embryonic fibroblasts treated with 500 nM thapsigargin (Tg) for 8 hours were used as a positive control for XBP1 splicing.

Next, ISR signaling downstream of eIF2α phosphorylation was analyzed by immunoblotting for ATF4 in tumors. As expected from the similar levels of eIF2α phosphorylation, GCN2 status did not affect ATF4 protein levels in C57BL6 tumors (Figure III-7A,B). However, in the mixed background GCN2$^{-/-}$ tumors, in which there was a significant decrease in eIF2α phosphorylation, ATF4 protein levels were minimally affected (Figure III-7C). While there was a small decrease in ATF4 in both GCN2$^{+/-}$ and GCN2$^{-/-}$ tumors, it was not statistically significant (Figure III-7D). To further confirm that ATF4 was expressed similarly regardless of GCN2 status, mRNA levels of the ATF4 target genes ASNS, ATF3, and ULK1 were measured by qPCR. All three genes were expressed at the same level in GCN2$^{+/+}$ and GCN2$^{-/-}$ tumors (Figures III-7E-G). This suggested that the mixed background tumors compensated for GCN2 loss by upregulating ATF4 independently of eIF2α phosphorylation status.

Next page: GCN2$^{-/-}$ mixed background sarcomas do not express lower levels of ATF4, in spite of reduced eIF2α phosphorylation. (A) Western blot analysis on tumor homogenates for levels of ATF4 in C57BL6 tumors. β-tubulin was used as a loading control. The ratio of ATF4 to β-tubulin is displayed below each blot. ATF4 was probed on the same blot as total and phospho-PERK and total and phospho-PKR (Figure III-6C), so the β-tubulin loading control is the same in both figures. **(B)** Graphical representation of the ATF4 to β-tubulin ratios calculated from the blots in (A). Data are represented as the average value for each genotype ± standard error of the mean. Results are not statistically significant. **(C)** Western blot analysis on two independent samples of tumor homogenates for levels of ATF4 in mixed background tumors. β-tubulin was used as a loading control. The ratio of ATF4 to β-tubulin is displayed below each blot. **(D)** Graphical representation of the ATF4 to β-tubulin ratios calculated from the blots in (C). Data are represented as the average value for each genotype ± standard deviation. Results are not statistically significant. **(E)** qPCR analysis of *ASNS* levels in GCN2$^{+/+}$ and GCN2$^{-/-}$ sarcomas. *ASNS* levels were normalized to the geometric mean of the reference genes β-tubulin, β-actin, and 18S rRNA. Data are represented as the average value for each genotype ± standard deviation. Results are not statistically significant. **(F)** qPCR analysis of *ATF3* levels in GCN2$^{+/+}$ and GCN2$^{-/-}$ sarcomas. *ATF3* levels were normalized to the geometric mean of the reference genes β-tubulin, β-actin, and 18S rRNA. Data are represented as the average value for each genotype ± standard deviation. Results are not statistically significant. **(G)** qPCR analysis of *ULK1* levels in GCN2$^{+/+}$ and GCN2$^{-/-}$ sarcomas. *ULK1* levels were normalized to the geometric mean of the reference genes β-tubulin, β-actin, and 18S rRNA. Data are represented as the average value for each genotype ± standard deviation. Results are not statistically significant.

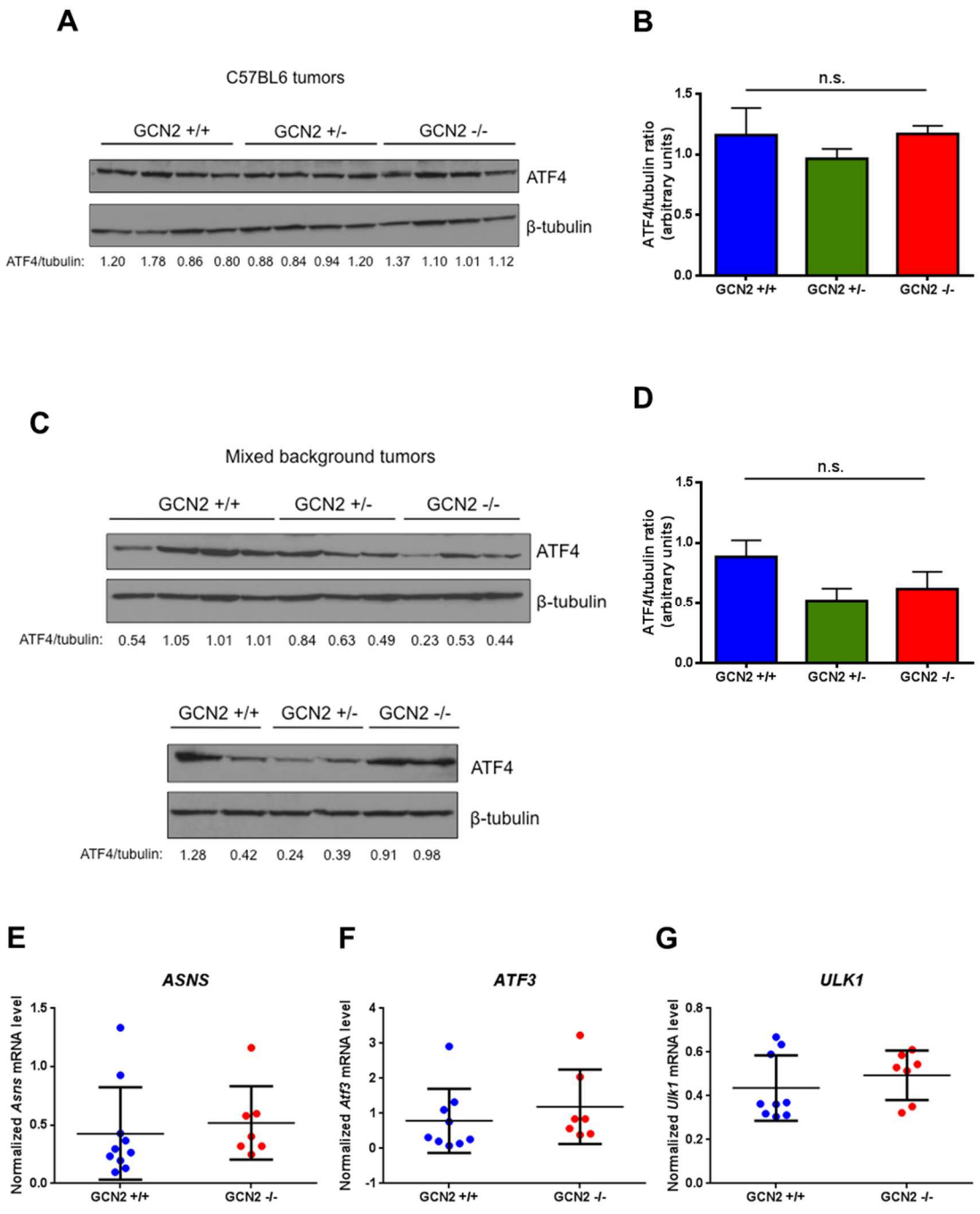
A
C57BL6 tumors
GCN2 +/+
GCN2 +/-
GCN2 -/-
ATF4
β-tubulin
ATF4/tubulin: 1.20 1.78 0.86 0.80 0.88 0.84 0.94 1.20 1.37 1.10 1.01 1.12
B
n.s.
ATF4/tubulin ratio (arbitrary units)
1.5
1.0
0.5
0.0
GCN2 +/+
GCN2 +/-
GCN2 -/-
C
Mixed background tumors
GCN2 +/+
GCN2 +/-
GCN2 -/-
ATF4
β-tubulin
ATF4/tubulin: 0.54 1.05 1.01 1.01 0.84 0.63 0.49 0.23 0.53 0.44
GCN2 +/+
GCN2 +/-
GCN2 -/-
ATF4
β-tubulin
ATF4/tubulin: 1.28 0.42 0.24 0.39 0.91 0.98
D
n.s.
ATF4/tubulin ratio (arbitrary units)
1.5
1.0
0.5
0.0
GCN2 +/+
GCN2 +/-
GCN2 -/-
E
ASNS
Normalized Asns mRNA level
1.5
1.0
0.5
0.0
GCN2 +/+
GCN2 -/-
F
ATF3
Normalized Atf3 mRNA level
4
3
2
1
0
-1
GCN2 +/+
GCN2 -/-
G
ULK1
Normalized Ulk1 mRNA level
0.8
0.6
0.4
0.2
0.0
GCN2 +/+
GCN2 -/-

One mechanism by which GCN2$^{-/-}$ tumors could maintain ATF4 protein levels under conditions of reduced eIF2α phosphorylation is by increasing levels of *ATF4* transcript. This could be accomplished directly through transcriptional upregulation or indirectly through an increase in ATF4 copy number. First, ATF4 copy number was measured in GCN2$^{+/+}$ and GCN2$^{-/-}$ sarcomas with a TaqMan copy number assay. Normal muscle tissue was used as a copy number control. ATF4 amplification was observed in two GCN2$^{+/+}$ tumors, but no GCN2$^{-/-}$ tumors (Figure III-8A). qPCR analysis of *ATF4* mRNA in GCN2$^{+/+}$ and GCN2$^{-/-}$ tumors demonstrated equal levels of transcript in both genotypes (Figure III-8B). Thus, GCN2$^{-/-}$ sarcomas do not directly or indirectly upregulate *ATF4* transcript levels.

A second mechanism by which GCN2$^{-/-}$ tumors could maintain ATF4 levels is through mutations in the protein that enhance its expression. For example, mutations of the 5' uORFs could uncouple ATF4 expression from eIF2α phosphorylation, and mutations in the beta transducin repeat containing ubiquitin protein ligase (β-TrCP) recognition motif or the oxygen dependent degradation (ODD) domain could enhance ATF4 protein stability. To assess this possibility, the three exons of ATF4 were sequenced in both GCN2$^{+/+}$ and GCN2$^{-/-}$ tumors. *De novo* mutations were not detected in either GCN2$^{+/+}$ or GCN2$^{-/-}$ tumors. However, there were differences in previously known ATF4 SNPs. Five SNPs clustered into two distinct groups, which we designated as SNP Profile A and B (Figure III-8C). The majority of mice were heterozygous at all five loci, although both GCN2$^{+/+}$ and GCN2$^{-/-}$ mice homozygous for either SNP Profile A or B were identified. Four of the five SNPs are located in the 5' UTR of ATF4, but they do not interfere with the 5' uORFs. The remaining SNP in the coding region results in a synonymous codon change. Thus, it does not appear that these SNPs would affect ATF4 expression levels. The lack of substantial differences in ATF4 copy number, transcript levels, and coding sequence between GCN2$^{+/+}$ and GCN2$^{-/-}$ mixed background sarcomas suggests that another factor is regulating ATF4 protein expression *in trans* to maintain levels ATF4 levels in GCN2$^{-/-}$ tumors.

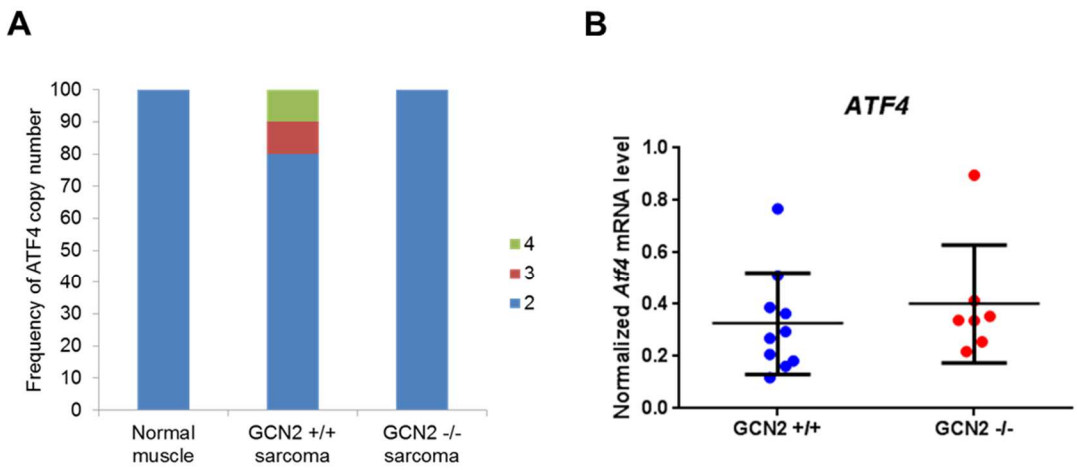

C

Reference SNP	mRNA Position	Location	SNP Profile A Nucleotide	SNP Profile B Nucleotide
rs32207233	290	5' UTR	A	G
rs31773570	342	5' UTR	A	G
rs13461824	350	5' UTR	T	C
rs13461823	572	5' UTR	C	G
rs13461826	1266	Residue 224 (Pro→Pro)	A	G

RefSeq ID: NM_009716.3 → NP_033846.2

Figure III-8. Maintenance of ATF4 protein expression in mixed background GCN2$^{-/-}$ sarcomas likely occurs *in trans*. (A) Copy number analysis of ATF4 in normal muscle tissue, GCN2$^{+/+}$ sarcomas, and GCN2$^{-/-}$ sarcomas in mixed background mice. Copy number increases were detected in two GCN2$^{+/+}$ sarcomas (normal muscle n=3, GCN2$^{+/+}$ sarcoma n=10, GCN2$^{-/-}$ sarcoma n=7). **(B)** qPCR analysis of *ATF4* levels in GCN2$^{+/+}$ and GCN2$^{-/-}$ sarcomas. *ATF4* levels were normalized to the geometric mean 3of the reference genes β-tubulin, β-actin, and 18S rRNA. Data are represented as the average value for each genotype ± standard deviation. Results are not statistically significant. **(C)** ATF4 SNPs detected in mixed background sarcomas. Two variations of ATF4 alleles were found in the mice, with five SNPs clustering in distinct patterns. These are designated as SNP Profile A and SNP Profile B. The nucleotide position of each SNP in the mRNA is indicated, along with the region of the mRNA in which the SNP is located.

The results in this mouse model demonstrate that ISR signaling is an important component of sarcoma biology. To determine if there is evidence of enhanced ISR signaling in human sarcomas, the online database Oncomine (www.oncomine.org, Compendia Bioscience, Ann Arbor, MI) was used to compare the expression of ISR-related genes in sarcoma samples and normal tissue controls using the Detwiller sarcoma dataset[102]. We chose to focus on undifferentiated pleomorphic sarcoma (UPS), also known as malignant fibrous histiocytoma (MFH), since the LSL-Kras$^{G12D/wt}$;p53$^{fl/fl}$ model most closely resembles this sarcoma subtype at

the genetic level[103]. Both PKR (EIF2AK2) and PERK (EIF2AK3) were overexpressed in UPS samples, along with eIF2α (EIF2S1). Unfortunately, GCN2 (EIF2AK4) expression was not measured in this study (Figure III-9A).

ATF4 mRNA levels were the same in normal tissue and tumor tissue. However, this is not surprising since ATF4 is primarily regulated at the translational level. As an indirect way to examine ATF4 expression, a number of ATF4 transcriptional targets were analyzed in the same dataset. To assemble an unbiased list of ATF4 targets, we utilized published microarray data to identify genes whose expression was reduced by at least two-fold in $ATF4^{-/-}$ cells treated with the ER stress inducing agent tunicamycin as compared to tunicamycin-treated $ATF4^{+/+}$ cells[26]. To ensure only direct ATF4 transcriptional targets were analyzed, we used a published ChIP-seq study to exclude genes whose promoters were not bound by ATF4 during tunicamycin treatment[89]. This resulted in a list of 26 ATF4 targets, which included genes such as amino acyl tRNA synthetases, amino acid transporters, and enzymes regulating redox balance. Of the 26 ATF4 target genes, 15 were significantly overexpressed in human UPS samples as compared to normal tissue. All but two of these genes were expressed in sarcomas at levels at least two-fold higher than normal tissue. Only one gene of the 26 was significantly underexpressed, and one gene from the list was not measured in this study. The remaining genes did not show evidence of differential expression (Figure III-9B). This analysis reveals that many ATF4 target genes are overexpressed in human patient samples, indicating that ISR activation in sarcomas is a clinically relevant phenomenon and not just restricted to mouse models.

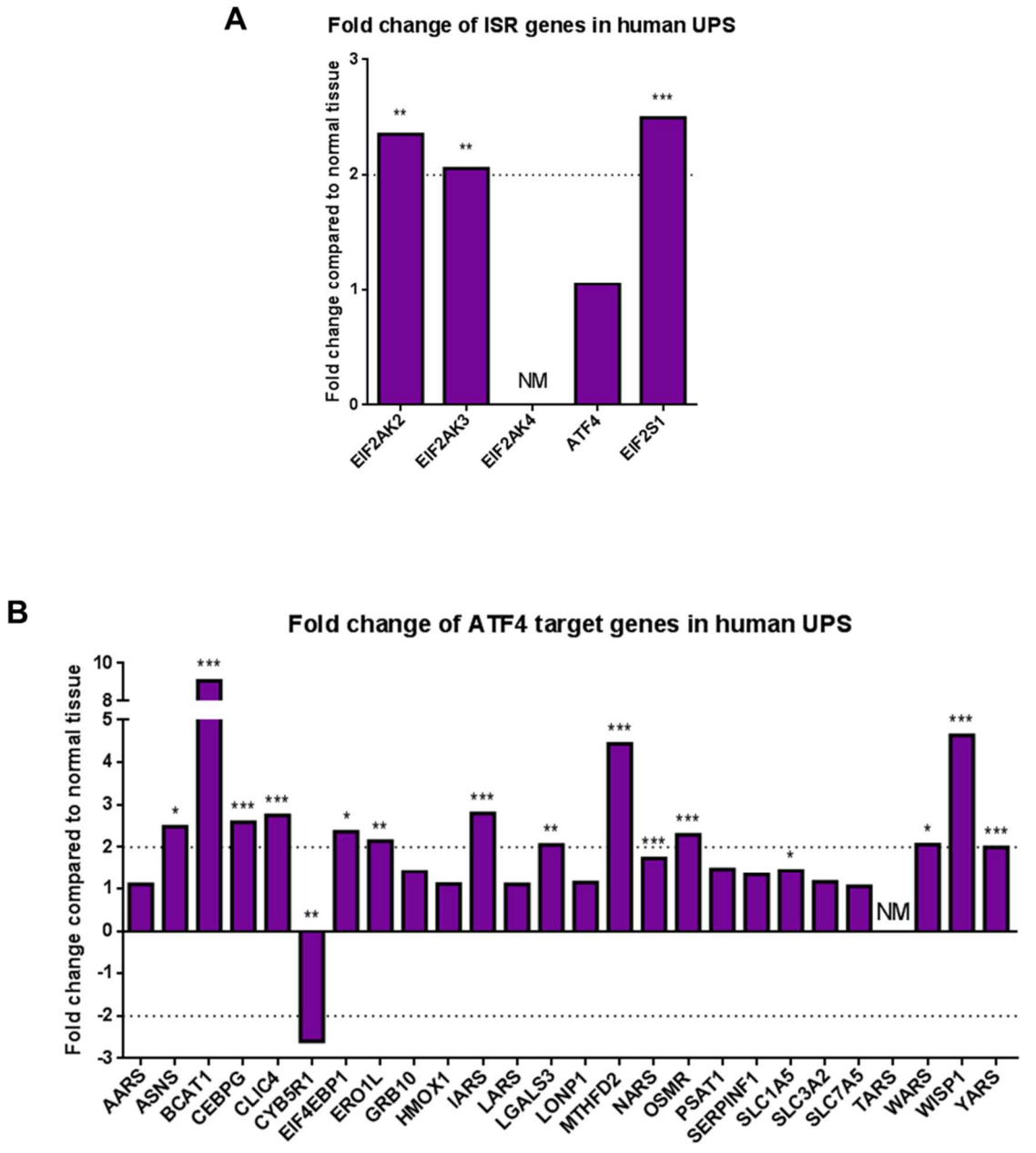

Figure III-9. Many genes involved in ISR signaling are overexpressed in human undifferentiated pleomorphic sarcoma. (A) Analysis of overexpression of ISR-related genes in human undifferentiated pleomorphic sarcoma using the Detwiller dataset in Oncomine. Data are represented as fold change over normal tissue control; **p<0.01, ***p<0.001, NM=not measured. **(B)** Analysis of over- and underexpression of ATF4 target genes in human undifferentiated pleomorphic sarcoma using the Detwiller dataset in Oncomine. Data are represented as fold change over normal tissue control; *p<0.05, **p<0.01, ***p<0.001, NM=not measured.

Discussion

This study demonstrates the role of GCN2 in a genetically engineered mouse model of soft tissue sarcoma. Although GCN2 was both overexpressed and activated in the sarcomas, loss of GCN2 had no significant overt effect on tumor growth or animal survival. It appears that the tumors acquired various mechanisms to compensate for GCN2 loss, resulting in maintenance of ISR signaling. Sarcomas derived from GCN2$^{-/-}$ C57BL6 mice utilized PERK to sustain eIF2α phosphorylation, while sarcomas derived from GCN2$^{-/-}$ mixed background mice upregulated ATF4 regardless of reduced eIF2α phosphorylation. Although loss of GCN2 did not slow tumor growth, the development of these alternative signaling mechanisms indicates that the ISR is crucial for tumor cell survival. Additionally, many ISR-related genes are overexpressed in human sarcoma samples, indicating our observations in the mouse model are clinically relevant.

These experiments highlight the importance of using genetically engineered mouse models of cancer to study the tumor microenvironment. Our lab previously utilized flank xenograft models to study the role of GCN2 in tumorigenesis and found that Ras transformed GCN2$^{-/-}$ MEFs formed extremely small tumors, while stable knockdown of GCN2 in the HT1080 human sarcoma cell line completely blocked tumor growth[58]. These results can most likely be attributed to the subcutaneous microenvironment of the xenograft model. When tumor cells are injected beneath the skin, they initially lack a blood supply to provide them with oxygen and nutrients. Loss of GCN2 renders cells extremely sensitive to amino acid deprivation[58], and thus they probably undergo apoptosis before they can establish vasculature to deliver nutrients to the tumor site. In autochthonous tumor models, tumors are exposed to physiologically relevant levels of nutrients as they develop, which helps to support their initial growth.

Genetically engineered mouse models are not without their limitations, however. One caveat of this particular model is that GCN2 is absent from the very beginning of tumor formation. A more clinically relevant approach would be to block GCN2 activity after initial tumor development. In this type of model, GCN2 inhibition may slow tumor growth since the tumors have time to become reliant upon GCN2 to survive nutrient stress. This could be modeled

genetically by utilizing dual recombinase technology[104,105] to excise GCN2 after activation of $Kras^{G12D}$ and deletion of p53 to initiate sarcomagenesis. Moreover, our results do not exclude a potential role of GCN2 in tumor growth in other settings or tissue of origin, such as epithelial tumors.

The ultimate goal of studying the roles of ISR kinases in mouse models is to determine the therapeutic efficacy of kinase inhibition on tumor growth. Several specific small molecule inhibitors of PERK have been identified[106-108], while the currently known GCN2 inhibitors are non-specific and require further development[109]. Of these drugs, the PERK inhibitor GSK2656157 has been tested in xenograft models, with promising results[110]. However, this work suggests that testing small molecule inhibitors of the ISR will yield more accurate results in GEMMs, rather than xenograft models. As the characterization of ISR inhibitors continues, GEMMs should become an important tool to evaluate their effects.

A second clinically relevant finding from this study is the mechanism by which tumors compensate for GCN2 loss, as tumors treated with small molecular inhibitors of ISR kinases may rely on similar pathways to become drug resistant. In this study, PERK activation was observed in the absence of GCN2. This suggests that combining inhibitors against multiple ISR kinases might effectively combat drug resistance. ATF4 upregulation independent of eIF2α phosphorylation status was also observed. ATF4 is more difficult to directly target because it is a transcription factor. However, the downstream processes that ATF4 regulates, such as autophagy, amino acid biosynthesis, and redox signaling, are more amenable drug targets. Combination treatment with an ISR inhibitor and inhibitors of ATF4-regulated processes may also be an effective method to block signaling through this pathway. Continued studies with genetically engineered mouse models will provide insights into useful therapies to target this pathway in cancer.

CHAPTER IV: CONCLUSIONS AND FUTURE DIRECTIONS

GCN2-dependent translational regulation of p21

Chapter II describes a novel mechanism of p21 regulation at the translational level, which is regulated by GCN2. Under normal conditions when abundant nutrients are present and eIF2α is not phosphorylated, translation initiates at the upstream open reading frames in p21 transcript variant 2, resulting in no p21 protein production. Under conditions of amino acid deprivation, GCN2 is activated and phosphorylates eIF2α. This delays translation initiation and results in ribosomes beginning translation at the open reading frame for p21. p21 induction results in cell cycle arrest and prevents cells from proliferating when sufficient nutrients to do so are not present in the environment. Therefore, p21 exerts pro-survival functions under conditions of nutrient stress. In cells that lack p21, clonogenic survival is reduced after exposure to long-term amino acid deprivation.

This work offers greater insight into how GCN2 exerts its pro-survival function in amino acid starved cells. GCN2 is typically thought to promote survival through translational suppression and initiation of the ATF4 transcriptional program. However, as this study shows, other proteins, such as p21, can be translationally upregulated by eIF2α phosphorylation and contribute to the protective functions of the ISR. Future studies are needed to fully determine the whole range of proteins that are translationally upregulated by eIF2α phosphorylation. Attempts to identify these proteins have centered on performing microarrays on mRNA obtained from polysome profiles[91,111]. One drawback of this approach is that it is limited by the probes used in the arrays. In the case of p21, current microarray probes only recognize the coding region of the transcripts and do not distinguish between the variants. Thus, the translational upregulation of p21 variant 2 likely could not be identified by this method because variant 1 is more abundant and its translational suppression masks the upregulation of variant 2. One way to obtain a more complete picture would to be to take the less biased approach of RNA-Seq on mRNAs obtained from polysome profiling. Another helpful tool would be a publicly available program designed to identify upstream open frames in transcripts. NCBI offers a program called ORF Finder (http://www.ncbi.nlm.nih.gov/gorf/gorf.html) which identifies ORFs in a given sequence. This tool

is limited by a minimum ORF size of 50 nucleotides. However, much smaller uORFs can affect translation, as seen with both p21 and ATF4. The ideal program for this purpose would focus on the 5' UTR and identify all uORFs with no size limits.

In this study, several methodologies were used to measure p21 translation, each with their own advantages. ^{35}S labeling of newly synthesized proteins is useful in that it provides a direct measurement of translation. However, in the case of p21 translation, it is limited by the fact that both variants encode the same protein, and, therefore, their individual contributions to translation cannot be studied. The 5' UTR-luciferase reporter assays are one method that can distinguish the translational regulation of each p21 variant. The constructs are also easily genetically manipulated, which helps to provide a mechanistic understanding of translational control. Here, the upstream uORFs in the luciferase reporters were mutated to demonstrate that these elements promote p21 variant 2 translation under conditions of eIF2α phosphorylation. Polysome profiling is the only technique that can measure the translation of endogenous transcript variants. Although we clearly saw enhanced translation of p21 under leucine deprivation by ^{35}S labeling and specific translational upregulation of variant 2 by the 5' UTR-luciferase reporter assays, we were unable to detect greater association of p21 variant 2 with polysomes under stress. One potential explanation for these differing results is that the number of total ribosomes associated with variant 2 may not change under stress, but the number of ribosomes associated with the p21 ORF increases. For example, the majority of variant 2 may be associated with four ribosomes, but under normal conditions three ribosomes are associated with the uORFs and one is associated with the ORF, while all four ribosomes are associated with the ORF under stress. This would not alter the transcript's position in the gradient, but it would enhance its translational efficiency. Ribosomal profiling[112,113] would be required to test this hypothesis in order to determine the exact sequences that ribosomes are associated with in complete media versus leucine deprivation.

This work also suggests that any stressor that activates the ISR will induce p21 because phosphorylation of eIF2α is the upstream event that promotes p21 translation. Future studies should focus on analyzing p21 induction in response to the full range of stressors that activate the ISR kinases in order to determine if this is indeed the case. We performed a preliminary study to investigate if ER stress upregulated p21 through eIF2α phosphorylation. In PERK$^{+/+}$ MEFs, thapsigargin (Tg) treatment induced p21, while this response was absent in PERK$^{-/-}$ MEFs and eIF2α S51A MEFs (Figure IV-1). Thus, it appears that p21 induction is a more universal part of the ISR and not specific to GCN2 activation. This increases the physiological relevance of this p21 regulatory mechanism since a variety factors, such as UV irradiation, glucose deprivation, viral infection, proteosome inhibition, heat shock, and oxidative stress, signal through the ISR[16].

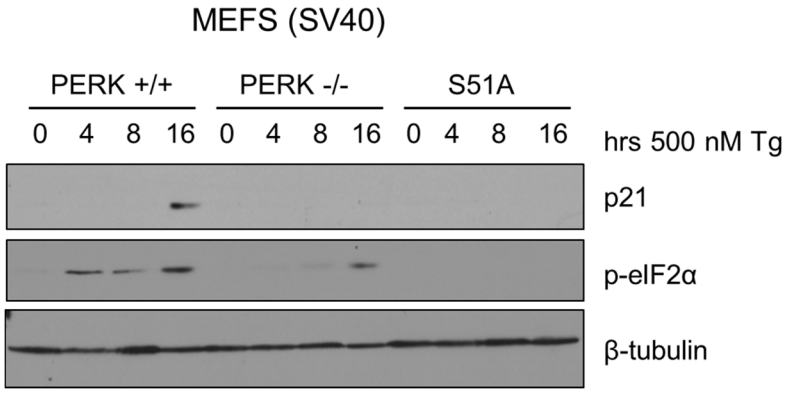

Figure IV-1. ER stress induces p21 through PERK-dependent phosphorylation of eIF2α. Western blot analysis of p21 induction in thapsigargin (Tg) treated PERK$^{+/+}$, PERK$^{-/-}$, and eIF2α S51A MEFs. β-tubulin was used as a loading control

In addition to the mechanism of p21 translational regulation, the functional consequences of p21 upregulation under amino acid deprivation are also important. Nutrient availability is critical for proliferation, as cells must synthesize proteins and membranes and replicate their DNA in order to divide. This work establishes GCN2 as an important regulator of the cell cycle under nutrient stress. One observation of note is that loss of p21 partially inhibits G_1/S arrest under leucine deprivation, while cells lacking GCN2 completely fail to undergo G_1/S arrest (Figures II-6B,E). This suggests that GCN2 controls other proteins involved in cell cycle regulation besides p21. We subsequently analyzed all known mouse transcripts of the Ink4 and Cip/Kip families of

cell cycle inhibitors for the presence of uORFs (Table IV-1). Like p21, mouse $p18^{Ink4c}$ is encoded by two transcript variants that are generated by alternate promoters and differ only in their 5' UTRs, but unlike p21, both transcript variants contain multiple uORFs. p18 variant 1 contains five uORFs, while p18 variant 2 contains three uORFs (Table IV-1). These two variants are conserved in humans. We also found that the only known mouse transcript for $p19^{Ink4d}$ contains one uORF (Table IV-1). However, in humans, p19 is encoded by two transcripts, neither of which contains uORFs. Based on this analysis, future experiments should address if GCN2 translationally upregulates p18 and if p18 upregulation contributes to cell cycle arrest under amino acid deprivation. In addition to translationally upregulating cell cycle inhibitors, GCN2 activation may also lead to transcriptional upregulation of cell cycle inhibitors or transcriptional or translational suppression of cell cycle activators to induce cell cycle arrest.

Table IV-1. Mouse cell cycle inhibitor transcripts analyzed for uORFs

NCBI Reference Sequence	Gene	uORF Position(s)	ORF Position
NM_007670.4	Cdkn2b ($p15^{Ink4b}$)	NA	236-628
NM_001040654.1	Cdkn2a ($p16^{Ink4a}$)	NA	82-588
NM_009877.2	Cdkn2a (ARF)	NA	97-606
NM_001301368.1	Cdkn2c ($p18^{Ink4c}$)	33-92, 92-148, 668-706, 773-904, 1081-1155	1159-1665
NM_007671.3	Cdkn2c ($p18^{Ink4c}$)	11-43, 138-194, 146-160	227-733
NM_009878.3	Cdkn2d ($p19^{Ink4d}$)	133-180	261-761
NM_009875.4	Cdkn1b ($p27^{Kip1}$)	NA	520-1113
NM_001161624.1	Cdkn1c ($p57^{Kip2}$)	NA	208-1254
NM_009876.4	Cdkn1c ($p57^{Kip2}$)	NA	209-1216

Interestingly, several studies have shown that Gcn2 regulates a G_1 checkpoint in the fission yeast *Schizosaccharomyces pombe* in response to stressors such as nitrogen starvation[40] and UV irradiation[41]. As there is no homologue of p21 in fission yeast, cell cycle arrest downstream of Gcn2 in *S. pombe* must occur through a different factor. Based on this work, it

would be interesting to determine if the *S. pombe* CDK inhibitor Rum1 contributes to this response because there are two transcript variants of *rum1*, one of which contains 5' uORFs and one which does not[114]. This would establish the translational upregulation of cell cycle inhibitors as an evolutionarily conserved stress response.

Furthermore, GCN2's ability to control cell proliferation may play a role in pulmonary hypertension in humans. One subtype of pulmonary hypertension known as pulmonary capillary hemangiomatosis (PCH) is characterized by the hyperproliferation of capillaries in the interstitial tissue, blood vessels, and airways of the lungs. This disease has an extremely high rate of mortality, and the only known cure is lung transplantation[115]. Recently, loss-of-function mutations in GCN2 have been identified in both familial autosomal recessive cases and sporadic cases of PCH[116]. The pathways downstream of GCN2 that regulate capillary function are not known. This study suggests the uncontrolled proliferation of capillaries in PCH may be due loss of GCN2-dependent regulation of the cell cycle inhibitor p21

In the case of GCN2 activation, p21 likely promotes cell survival through its ability to suppress cell proliferation under nutrient stress. Here, we showed that knockdown of p21 leads to decreased clonogenic survival after exposure to leucine deprivation. One attractive direction for future studies would be to elucidate the contribution of each p21 transcript variant to cell survival and cell cycle arrest under amino acid deprivation. Based on our model, loss of p21 variant 2 should decrease cell survival under leucine deprivation, while loss of p21 variant 1 should have little effect. Similarly, loss of p21 variant 2 should have a much greater effect than variant 1 on preventing cell cycle arrest in response to leucine deprivation. This experiment offers some intriguing technical challenges. p21 variants 1 and 2 could be individually targeted by siRNA or shRNA that bind to unique sequences in their 5' UTRs, but knockdown efficiency would be difficult to assess because both transcripts produce the same protein. Another possibility is to use genome editing to target either variant 1 or variant 2, but the unique region of variant 2 is located within the p21 promoter, specifically between the two p53 binding sites (Figure II-1A). Thus, regulation of p21 variant 1 may also be disrupted by this method. A combination approach using

genome editing to eliminate p21 variant 1 and siRNA or shRNA against variant 2 may be best. Based on our model, cells lacking variant 1 should be able to undergo G_1/S arrest and survive exposure to leucine deprivation. Knockdown of variant 2 in these cells should then inhibit these effects.

One of the most intriguing findings of this study that requires further investigation is the ability of GCN2 to regulate p21 transcription independently of eIF2α phosphorylation. GCN2$^{-/-}$ MEFs were incapable of inducing p21 transcription under glutamine and methionine deprivation (Figure II-5B,C). Moreover, GCN2$^{-/-}$ MEFs were unable to maintain levels of p21 variant 2 mRNA under leucine deprivation (Figure II-2F). In contrast, eIF2α S51A MEFs were able to induce p21 mRNA levels under all conditions tested. These results were unexpected because GCN2 is only known to phosphorylate itself and eIF2α. Therefore, kinase screens should be performed to identify additional targets of GCN2 phosphorylation in order to explain the phenotype of GCN2$^{-/-}$ MEFs. One particular family of potential targets is the TGFβ/BMP signaling pathway. GCN2 was found to interact with SMAD4, mothers against decapentaplegic homolog 1 (SMAD1), and transforming growth factor beta receptor 1 (TGFBR1) in a high throughput screen[85]. In this study, we found that knockdown of SMAD4 significantly blocked p21 transcriptional upregulation under glutamine deprivation. Future work should confirm these interactions, determine if these interaction partners are GCN2 phosphorylation targets, and elucidate the signaling pathway through which GCN2 and TGFβ/BMP signaling regulate p21 transcription under nutrient stress

In conclusion, Chapter II describes the mechanism by which GCN2 translationally upregulates the cell cycle inhibitor p21 under nutrient stress. Upregulation of p21 leads to decreased cell proliferation under stress and contributes to the pro-survival function of GCN2 signaling. This work opens avenues for many future studies, including identifying novel targets of translational upregulation by eIF2α phosphorylation, establishing p21 induction as a general consequence of ISR signaling, demonstrating translational upregulation of cell cycle inhibitors as an evolutionarily conserved stress response mechanism, and discovering additional targets of GCN2 phosphorylation. Overall, this model of GCN2-dependent translational regulation solidifies

our current understanding of translational regulation under stress, but also provides many new opportunities to explore the pathways that interconnect nutrient sensing with the cell cycle and GCN2's role in regulating this process, both transcriptionally and translationally, across species.

The role of GCN2 in tumorigenesis

Chapter III describes the use of the LSL-Kras$^{G12D/wt}$;p53$^{fl/fl}$ mouse model of soft tissue sarcoma to study the role of GCN2 in an autochthonous tumor model. Although prior studies in xenograft models indicated that GCN2 supported tumor growth, no difference in tumor growth or animal survival was observed between GCN2$^{+/+}$ and GCN2$^{-/-}$ mice on a mixed or C57BL6 background. However, the tumors developed compensatory mechanism to maintain ISR signaling in the absence of GCN2, indicating that this pathway is important for tumor cell survival. These findings are relevant to human soft tissue sarcoma, as overexpression of ISR-related genes was also observed in clinical patient samples.

The major conclusion from this work is that loss of GCN2 does not affect tumor growth in soft tissue sarcoma. A second significant finding is that tumors were able to compensate for GCN2 loss through other ISR pathway members. Sarcomas from mixed background mice upregulated ATF4 in spite of reduced eIF2α phosphorylation, and sarcomas from C57BL6 mice displayed activation of PERK. Since the sarcomas developed mechanisms to sustain ISR signaling, it suggests that this pathway is essential for tumor cell survival. However, at this point, these data are only correlative. The next important step for this work is to block signaling through these compensatory pathways to demonstrate the ISR truly is critical for tumor cell survival. Ideally, the best method to block ISR signaling is to prevent eIF2α phosphorylation, as this is the hub of the ISR. However, mice homozygous for the eIF2α S51A mutation die shortly after birth[117], and therefore cannot be crossed to a tumor model. One way to circumvent this issue is to generate cell lines from the soft tissue sarcomas, introduce the eIF2α S51A mutation via CRISPR and a template containing the mutation for homologous repair, and inject the eIF2α S51A sarcoma cells orthotopically into the leg muscles of syngeneic mice. Another option using genetic

models is to cross mixed background GCN2$^{-/-}$;LSL-Kras$^{G12D/wt}$;p53$^{fl/fl}$ mice to ATF4$^{fl/fl}$ mice to generate GCN2$^{-/-}$;ATF4$^{fl/fl}$;LSL-Kras$^{G12D/wt}$;p53$^{fl/fl}$ mice in order to test the combined deletion of GCN2 and ATF4 on tumor growth and animal survival upon sarcoma initiation. Similarly, C57BL6 GCN2$^{-/-}$;LSL-Kras$^{G12D/wt}$;p53$^{fl/fl}$ mice can be crossed to PERK$^{fl/fl}$ mice to generate GCN2$^{-/-}$;PERK$^{fl/fl}$;LSL-Kras$^{G12D/wt}$;p53$^{fl/fl}$ mice. PERK inhibitors are now commercially available, so tumor-bearing C57BL6 GCN2$^{-/-}$;LSL-Kras$^{G12D/wt}$;p53$^{fl/fl}$ mice could also be treated with one of these compounds to test the combined inactivation of GCN2 and PERK on tumor growth. Experiments such as these can definitively determine the role of the ISR in sarcoma growth.

The compensatory ISR signaling in GCN2$^{-/-}$ tumors poses interesting mechanistic questions. These are very important to address because small molecule inhibitors of ISR kinases are currently in development and may enter clinical trials in the future. In the C57BL6 mice, the activation of PERK in the absence of GCN2 is a relatively straightforward method to sustain ISR signaling. However, it is not clear what is activating PERK and why this is nearly exclusive to GCN2$^{-/-}$ tumors. One potential explanation is that GCN2 is the primary ISR kinase responsible for eIF2α phosphorylation in the tumors. When GCN2 is not present, tumor cells lose their ability to suppress translation under stress, causing them to deplete their ATP supplies. The drop in ATP levels would affect chaperone activity, resulting in the accumulation of unfolded proteins and PERK activation. Although such an experiment would be difficult to carry out *in vivo*, cell lines can be generated from C57BL6 GCN2$^{+/+}$ and GCN2$^{-/-}$ sarcomas and cultured without amino acids. Based on the observations in the animal model, one would expect that only GCN2$^{-/-}$ tumor cells would activate PERK in response to amino acid deprivation. Since this is thought to occur through the accumulation of unfolded proteins, treating the cells with a chemical chaperone, such as 4-phenylbutric acid (4-PBA) should block PERK activation. ATP levels can be measured throughout a time course of amino acid deprivation by high performance liquid chromatography (HPLC) to ascertain if ATP levels change over time, and, if so, how this correlates with the timing of PERK activation.

In the GCN2$^{-/-}$ mixed background mice, the maintenance of high ATF4 levels despite a substantial decrease in eIF2α phosphorylation also requires mechanistic explanation. Based on the observations that ATF4 copy number or mRNA levels were not increased in GCN2$^{-/-}$ tumors and that there were no mutations detected in ATF4, we concluded that another factor must be regulating ATF4 expression *in trans* in GCN2$^{-/-}$ mice. This could be achieved by GCN2$^{-/-}$ tumors downregulating proteins responsible for ATF4 degradation, such as β-TrCP[118] or egl-9 family hypoxia-inducible factor 3 (PHD3)[119], or upreguating proteins that stabilize ATF4, such as p300[120]. In the Detwiller data set utilized in this study to examine gene expression in human UPS, β-TrCP expression is decreased in UPS by 3.48 fold with a p-value of 7.33x10^{-5}, and PHD3 expression is decreased in UPS by 1.71 fold with a p-value of 0.03. p300 expression levels were not significantly different between UPS and normal tissue. These data suggest that β-TrCP would be a logical candidate for follow up. Decreased expression of β-TrCP needs to be confirmed in the mouse model of UPS, specifically in GCN2$^{-/-}$ tumors as compared to GCN2$^{+/+}$ tumors. Then, β-TrCP can be re-expressed to wildtype levels in GCN2$^{-/-}$ mixed background sarcoma cell lines to determine if this reduces ATF4 protein levels and tumor growth in an orthotopic model. Phosphorylation of ATF4 is also required for interaction with β-TrCP[118], so decreases in this post-translational modification could also stabilize ATF4 levels in GCN2$^{-/-}$ tumors. Comparing levels of phosphorylated ATF4 between GCN2$^{+/+}$ and GCN2$^{-/-}$ tumors by immunoblot would help to address if GCN2$^{-/-}$ tumor cells utilize the mechanism of reducing ATF4 phosphorylation to maintain its expression.

Since the LSL-Kras$^{G12D/wt}$;p53$^{fl/fl}$ soft tissue sarcoma model is intrinsically resistant to ISR inhibition through GCN2, it is a good model to study the efficacy of combination therapy. While GCN2 loss on its own does not affect tumor growth in this model, GCN2 inhibition may synergize with another therapeutic modality to slow or prevent tumor growth. The current mainstays of cancer therapy are surgery, chemotherapy, and radiation therapy. All three modalities are currently used clinically to treat and manage sarcoma[121,122]. Future work should focus on determining if GCN2 loss improves outcomes in LSL-Kras$^{G12D/wt}$;p53$^{fl/fl}$ mice treated with these

currently used methods. Another interesting study would be a combination of GCN2 loss and treatment with pazopanib, a small molecule inhibitor of several tyrosine kinases involved in angiogenesis, which recently received FDA approval in 2012 for the treatment of advanced soft tissue sarcoma[123]. Blocking tumor angiogenesis may result in more nutrient deprivation in the tumor microenvironment, and thus greater sensitivity to GCN2 loss, resulting in greater tumor control than with either therapy alone.

One observation in this study that is consistent with previous work is that GCN2 is overexpressed in tumors as compared to normal tissue. Our lab has previously observed increased GCN2 expression in human lung, liver, breast, and colon cancer and in mammary tumors from MMTV-neu mice by immunohistochemistry and western blot[58]. Here, we demonstrate that GCN2 is also overexpressed at the mRNA and protein level in the LSL-$Kras^{G12D/wt}$;$p53^{flfl}$ mouse model of soft tissue sarcoma. Very little is known about the regulation of GCN2 itself, so this model provides a system to study how GCN2 is upregulated in cancer. Since GCN2 upregulation at the mRNA level was observed in sarcoma, PROMO[124,125] was used in a preliminary analysis to identify transcription factor binding sites in the first 2000 bases of the mouse and human GCN2 promoters. Using the most stringent search conditions, yin yang 1 (YY1) was identified as a common GCN2 transcription factor in both species. YY1 is of interest because it has been shown to be upregulated in many different cancer types[126]. Studies into YY1 and other potential oncogenic transcription factors will lead to greater insight into the regulation of GCN2 itself in tumors and may lead to additional therapeutic opportunities to inhibit the ISR in cancer.

Although blocking ISR signaling through GCN2 did not affect tumor growth in the LSL-$Kras^{G12D/wt}$;$p53^{fl/fl}$ model of soft tissue sarcoma, inhibiting GCN2 may be an effective therapy in other cancer types. The role of GCN2 in cancers of epithelial origin should also be investigated because carcinomas comprise the vast the majority of cancers in the humans. The LSL-$Kras^{G12D/wt}$;$p53^{fl/fl}$ model could easily be repurposed to study the role of GCN2 in carcinomas by changing the tissues exposed to cre recombinase. For example, intranasal administration of Ad-

cre induces lung adenocarcinomas[127], and crossing LSL-Kras$^{G12D/wt}$p53$^{fl/fl}$ mice to mice expressing cre under the control of the pancreas-specific Pdx1 promoter results in pancreatic adenocarcinoma[128]. We have also observed GCN2 overexpression in human breast cancer and the MMTV-neu mouse mammary adenocarcinoma model[58], so it may also be worthwhile to cross MMTV-neu mice to GCN2$^{-/-}$ mice to study the effects of GCN2 loss in this particular type of cancer. Another cancer of interest is acute lymphoblastic leukemia (ALL). One common treatment for ALL is asparaginase, which hydrolyzes circulating asparagine. Leukemia cells are particularly sensitive to asparaginase treatment because they synthesize very little of their own asparagine, and are thus dependent on high levels of circulating asparagine to maintain their growth. It has been previously demonstrated that GCN2 promotes the survival of normal lymphocytes during asparaginase treatment[129], but it has yet to been determined if inhibition of GCN2 will enhance cancer cell death in a mouse model of ALL treated with asparginase.

In conclusion, Chapter III demonstrates that loss of GCN2 does not impact tumor growth or animal survival in the LSL-Kras$^{G12D/wt}$;p53$^{fl/fl}$ mouse model of soft tissue sarcoma. Compensation by other ISR signaling proteins is observed, indicating that the ISR is important for tumor cell survival and that tumor cells are able to adapt to maintain ISR signaling. This is supported clinically by the observation that many ISR proteins are upregulated in human sarcoma. This model offers many opportunities for further study, including demonstrating the requirement for the ISR in sarcomagenesis, analyzing the molecular mechanisms behind the development of resistance against ISR inhibition, testing synergy between GCN2 inhibition and other therapeutic modalities, and elucidating how GCN2 itself is regulated in cancer. Overall, this study expands upon the current xenograft and genetically engineered mouse models to study the role of the ISR in cancer. Although, to our knowledge, this is the first report that inhibition of one ISR signaling protein has no apparent effect on tumor growth, this model will be a valuable resource to begin to understand how tumors can adapt to ISR inhibition, which is highly clinically relevant, given the current development of small molecule inhibitors of the ISR kinases as cancer therapeutics.

The connection: a potential role for GCN2-dependent regulation of p21 in cancer

The role of GCN2 in p21 regulation and the role of GCN2 in tumorigenesis may potentially be linked. When tumor cells are exposed to nutrient stress in the tumor microenvironment, GCN2 is activated, as shown by our laboratory's previous work and in Chapter III[58]. Activated GCN2 phosphorylates eIF2α, leading to translational upregulation of p21, as demonstrated in Chapter II. Cancer is a disease of uncontrolled proliferation, and at first, upregulation of a cell cycle inhibitor appears to be counterintuitive in the context of a tumor cell. However, in order for cells to proliferate, sufficient nutrients must be available. In a local context, cell cycle inhibition is favorable if the microenvironment is nutrient deprived and the resources to proliferate are not available. Our lab's previous work showed by IHC that activated GCN2 is present in patches throughout the tumor, as opposed to global activation in the whole tumor[58]. This suggests that if GCN2 does induce p21 in tumor cells, its expression would be restricted to areas of stress only. Moreover, p21 variant 2 is translated inefficiently under nutrient replete conditions (Figure II-3C), which would further restrict p21 expression to areas of stress. This would specifically allow stressed tumor cells to remain dormant until conditions improve and then resume division once the microenvironment is more favorable for growth. Indeed, several lines of evidence from this study support this view. First, cells exposed to leucine deprivation upregulate p21 and then are able to downregulate it again when supplied with complete media (Figure II-1F). Furthermore, wildtype cells show complete recovery from long-term amino acid starvation, as measured by clonogenic survival, while cells lacking p21 are compromised in their ability to form colonies after exposure to long-term nutrient stress (Figure II-6H). This indicates that induction of p21 in response to amino acid deprivation does not induce permanent growth arrest. Rather, cells are able regulate their p21 levels in response to nutrient levels in their environment and proliferate again once the stress is removed.

GCN2-dependent regulation of p21 agrees with the currently accepted model that p21 can function as both an oncogene and a tumor suppressor[96]. In the context of p21 upregulation in a nutrient-deprived local microenvironment, inhibition of proliferation promotes tumor cell survival

by allowing cells to evade death from nutrient stress. However, in the context of a nutrient replete local microenivronment, induction of p21 would inhibit the proliferation of cells that are metabolically able to divide, and thus slow tumor growth. p21 was first identified as a transcriptional target of p53[72], and thus thought to act as a classical tumor suppressor. However, spontaneous tumors arise in $p53^{-/-}$ mice at an average age of 4.5 months[130], while spontaneous tumors do not arise in $p21^{-/-}$ mice until an average age of 16 months[131]. This large disparity in tumor onset suggests that p21 does not function purely as tumor suppressor downstream of p53. Furthermore, in human cancers, p21 loss-of-function mutations are rarely found, as opposed to the high frequency of p53 loss and mutation[132]. In support of a tumor suppressor role, in some human cancers, high p21 levels are correlated with a favorable prognosis, and p21 suppression is associated with increased metastasis and poor survival. However, in other cancers, p21 has an oncogenic role as evidenced by its overexpression associating with poor prognosis, poor survival, and increased recurrence and metastasis[96]. Previously, the opposing functions of p21 have been associated with its subcellular localization. In the nucleus, p21 can suppress proliferation by binding to and inhibiting cyclin:CDK complexes and proliferating cell nuclear antigen (PCNA). In the cytoplasm, p21 binds to and inhibits various proteins that regulate apoptosis, including procaspase 3, caspase 8, caspase 10, and apoptosis signal regulating kinase 1 (ASK1)[133]. The cytoplasmic activities would allow tumor cells to evade apoptosis and contribute to tumor progression. GCN2-dependent regulation of p21 offers another explanation for why p21 is oncogenic in some cases, especially in cancers, such as multiple myeloma, in which nuclear localization of p21 correlates with poor survival[134].

To begin to address a potential oncogenic role of p21 through the ISR, we immunoblotted for p21 in normal muscle and sarcoma tissue from the mixed background LSL-$Kras^{G12D/wt}$;$p53^{fl/fl}$ mice. Increased expression of p21 was observed in tumor tissue concomitant with activation of the ISR (Figure IV-2). p21 was still induced in $GCN2^{-/-}$ sarcomas, likely because these tumors still have some phosphorylated eIF2α due to PERK and PKR activation (data not shown). Importantly, p53 is deleted in these tumors, which agrees with our experiments in cell culture that

p53 is not required for p21 induction in response to amino acid deprivation. Since p53, but not p21, is typically mutated in cancers, this type of mechanism would allow most tumors to regulate their proliferation in response to nutrient levels in the microenvironment regardless of their p53 status. In human soft tissue sarcoma, previous work demonstrated that 53% of tumors were positive for p21 staining in the absence of p53 staining. Overall, 76% of soft tissue sarcomas stained positive for p21, indicating that this protein may play a significant role in sarcoma biology[135]. To further associate p21 induction in tumors with activation of the ISR, immunohistochemistry can be used to determine if p21 and phospho-eIF2α colocalize in sarcomas, both in humans and in the mouse model. It would also be interesting to determine if tumors specifically upregulate p21 transcript variants that can be translationally upregulated by eIF2α phosphorylation since the model put forth in this work predicts that these will provide a survival benefit under stress.

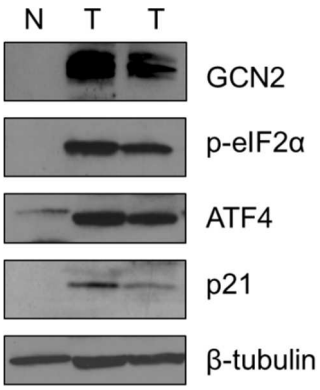

Figure IV-2. p21 is upregulated concomitantly with the ISR in LSL-Kras$^{G12D/wt}$;p53$^{fl/fl}$ sarcomas. Western blot analysis of ISR proteins and p21 in normal muscle (N) and tumor (T) from mixed background GCN2$^{+/+}$ mice. β-tubulin was used as a loading control. These panels were from the same blot shown in Figure III-1F, so the GCN2 and β-tubulin panels are identical between these two figures.

In summary, translational regulation of p21 through eIF2α phosphorylation may have physiological significance in the context of cancer, including the soft tissue sarcoma model studied in this work. Upregulation of p21 in areas of the tumor experiencing nutrient stress would allow cells to survive under conditions that cannot support the high rate of proliferation typically exhibited by cancer cells. This idea is supported by numerous studies demonstrating that p21 has

oncogenic functions in particular contexts. Moreover, we have demonstrated that p21 is induced in LSL-Kras$^{G12D/wt}$;p53$^{fl/fl}$ sarcomas in the absence of p53, which indicates that this mechanism can operate nearly universally in tumors, even the majority that have mutated or inactive p53. Future studies will be necessary to determine if ISR signaling is required for the p21 upregulation observed in sarcomas to firmly place this novel mechanism of p21 regulation in a physiological context. Doing so would expand our understanding of the outcomes of ISR signaling both *in vitro* and *in vivo*, allowing us to develop better targeted therapies against the ISR for cancer patients.

CHAPTER V: MATERIALS AND METHODS

Cell culture, transfection, and plasmids. All MEF cell lines and SQ20B cells were maintained in Dulbecco's Modified Eagle Medium (DMEM) supplemented with 10% fetal bovine serum (FBS), penicillin, and streptomycin. $GCN2^{-/-}$ and eIF2α S51A MEFs were additionally grown with nonessential amino acids and 55 μM β-mercaptoethanol. HCT116 cell lines were maintained in McCoy's 5A media supplemented with 10% FBS, penicillin, and streptomycin. $GCN2^{+/+}$ MEFs were stably transfected with pSM2-shNT (Open Biosystems) or pLKO-shp21 (Sigma) plasmids using Lipofectamine 2000 (Invitrogen) according to the manufacturer's protocol. SQ20B cells were transfected with ON-TARGETplus SMARTpool siNT, siGCN2, sip21, or siSMAD4 (Thermo Scientific) using Lipofectamine RNAiMAX (Invitrogen) according to the manufacturer's protocol.

Western blotting on cell lysates. Cells were lysed in Nonidet P-40 (NP-40) buffer (1% NP-40, 1 mM phenylmethylsulfonyl fluoride, 1X Complete Mini protease inhibitor cocktail [Roche], 1X phosphatase inhibitor cocktail 2 [Sigma] in PBS). Protein concentrations of lysates were determined using 660 nm Protein Assay Reagent (Thermo Scientific), according to the manufacturer's protocol. Equal amounts of protein were resolved on sodium dodecyl sulfate polyacrylamide gels and transferred to polyvinylidene fluoride membranes. Membranes were blocked with 5% non-fat dried milk in TBS-T (20 mM Tris, 137 mM NaCl, 0.1% Tween-20; pH 7.6) and then incubated in primary antibody. Following primary antibody incubation, membranes were washed three times with 1% non-fat dried milk in TBS-T, incubated in secondary antibody, and then washed three more times with 1% non-fat dried milk in TBS-T. Proteins were visualized by incubating membranes in ECL chemicals and exposing to film. Bands were quantified using ImageJ software. The following primary antibodies were used for western blotting: 4E-BP1, β-tubulin, cyclin D1, eIF2α, eIF4E, eIF4G, GCN2, Ku80, p27, p-4E-BP1, PARP, p-eEF2, p-eIF2α, p-p53, SMAD4 (all from Cell Signaling); β-actin (Sigma), c-myc (Santa Cruz), and p21 (BD Pharmigen). The secondary antibodies used were anti-rabbit HRP and anti-mouse HRP from Thermo Scientific.

Metabolic labeling. GCN2$^{+/+}$ and GCN2$^{-/-}$ MEFs were grown in complete or leucine-free media for 16 hours. To label newly synthesized proteins, cells were methionine and cysteine starved for 30 minutes and then labeled with 75 µCi/mL of Easy Tag Express Protein Labeling Mix (Perkin Elmer) for 30 minutes. Cells were washed with PBS and lysed in NET-2 lysis buffer (50 mM Tris, 75 mM NaCl, 1% NP-40, 1 mM phenylmethylsulfonyl fluoride, 1X Complete Mini protease inhibitor cocktail [Roche], 1X phosphatase inhibitor cocktail 2 [Sigma]; pH 7.4). Lysates were precleared with protein A/G agarose beads. 300 µg of lysate was incubated with 1 µg of p21 antibody or 1 µg of mouse IgG conjugated to protein A/G agarose beads overnight at 4 °C with end-over-end tumbling. Beads were washed four times with NET-2 wash buffer (50 mM Tris, 75 mM NaCl, 0.05% NP-40; pH 7.4) and one time with PBS. Immunoprecipitates were resolved on sodium dodecyl sulfate polyacrylamide gels. Gels were incubated in fixing solution (10% glacial acetic acid, 20% methanol, 3% glycerol), washed in deionized water, and incubated in Enlightening Autoradiography Enhancer (Perkin Elmer). Gels were air-dried overnight and exposed to film at -80 °C.

Plasmid construction and luciferase assay. p21 5' UTR luciferase reporter constructs were generated by inserting the 5' UTR sequences of the two known mouse p21 mRNA variants between the HindIII and NcoI restriction sites in the pGL3-Promoter vector (Promega). The 5' UTRs were purchased as oligonucleotides from Integrated DNA Technologies. Dual luciferase assays (Promega) were performed according to the manufacturer's instructions. Cells were co-transfected with *Renilla* luciferase (pRL-TK vector, Promega) for normalization.

Polysome extraction. Polysome extractions were performed as previously described[136]. Briefly, cells were treated with 0.1 mg/mL cycloheximide for three minutes at 37 °C to halt translation. Cells were washed twice with ice-cold PBS containing 0.1 mg/mL cycloheximide and then harvested in polysome extraction buffer (0.3 M NaCl, 15 mM $MgCl_2$, 15 mM Tris-HCl, pH 7.6; 1% Triton X-100, 0.1 mg/mL cycloheximide, 1 mg/mL heparin). Lysates were cleared by

centrifugation and loaded onto 10-50% sucrose gradients. Gradients were spun at 35,000 rpm for 190 minutes in a SW41Ti rotor. 1 mL fractions were collected from the gradients using the Brandel density gradient fractionation system. Fractions were brought to two mL with water. 3 mL of 8 M guanidine HCl was added to fractions, followed by extensive vortexing. One volume of 100% ethanol was added to fractions. The fractions were vortexed and incubated overnight at -20 °C. Fractions were spun at 10,000 x *g* for 45 minutes at 4 °C. RNA pellets were washed with ice-cold 75% ethanol and spun again at 10,000 x *g* for 30 minutes at 4 °C. RNA pellets were air-dried, resuspended in 400 µL TE buffer, pH 7.5 (10 mM Tris, 1mM EDTA). RNA was precipitated overnight in 0.3 M sodium acetate, pH 5.5 and 2.5 volumes 100% ethanol. Fractions were spun at 10,000 x *g* for 20 minutes at room temperature. The RNA pellet was washed with 400 µL ice-cold 75% ethanol and spun again at 10,000 x *g* for 20 minutes at room temperature. RNA pellets were air-dried and resuspended in 50 µL water. 25 µL from each fraction was pooled according to the following scheme: nonpolysomal- fractions 4, 5, 6, and 7; low molecular weight polysomal- fractions 8, 9, and 10; high molecular weight polysomal- fractions 11 and 12. LiCl was added to the pooled fractions at a final concentration of 2.5M. RNA was precipitated at -20 °C for 30 minutes. Pooled fractions were spun at 10,000 x *g* for 30 minutes at 4 °C. The RNA pellet was washed with 75% ethanol and spun again at 10,000 x *g* for 15 minutes at room temperature. The RNA was resuspended in 100 µL water, and the LiCl precipitation and ethanol wash was repeated. The resulting RNA was purified over RNeasy columns (QIAgen), according the manufacturer's protocol. RNA eluted from the column was used for qPCR analysis.

Cell cycle analysis. Cells were harvested, washed with 1% FBS in PBS, resuspended in PBS, and fixed in ice-cold ethanol. The fixed cells were washed with 1% FBS in PBS, resuspended in PBS, and treated with phosphate citric acid buffer (192 mM Na_2HPO_4; 4 mM citric acid, pH 7.8). Cells were resuspended in PI/Rnase buffer (50 µg/mL propidium iodide, 267 µg/mL Rnase A, 1% FBS in PBS) to stain DNA. DNA content was measured using a FACSCalibur flow cytometer on

populations of 20,000 cells per sample. The percentage of cells in each phase of the cell cycle was calculated using Flo Jo software.

Clonogenic survival assay. Cells were grown in media with or without leucine. After 72 hours, viable cells were replated at low density in complete media and incubated for one week. Colonies were fixed with a solution of 10% methanol and 10% acetic acid and then stained with 0.4% crystal violet in 20% ethanol.

Mice and soft tissue sarcoma generation. $GCN2^{-/-}$ mice (Jackson Laboratories), LSL-$Kras^{G12D/wt}$ mice, and $p53^{fl/fl}$ mice were previously described[30,137,138]. LSL-$Kras^{G12D/wt}$;$p53^{fl/fl}$ mice were injected with 2.5 x 10^7 PFU of Ad5CMVcre (University of Iowa Gene Transfer Vector Core) in the upper leg muscle to induce sarcomas. Adenovirus was prepared by diluting in MEM media, adding $CaCl_2$ to a final concentration of 9.6 mM, and incubating for 15 minutes to allow calcium phosphate precipitates to form. Animals were monitored three times weekly for tumor formation by palpitation. Once detected, tumors were measured three times weekly by calipers. The tumor volume was calculated for each individual mouse as [(tumor leg length x tumor leg width^2 x 0.52) – (normal leg length x normal leg width^2 x 0.52)]. Mice were euthanized once the tumor volume met or exceeded 1000 mm^3. Tumor tissue and normal muscle tissue were harvested from mice and either snap-frozen in liquid nitrogen for western blot and qPCR analysis or fixed overnight in 10% neutral buffered formalin for histopathological analysis. All animal experiments were performed in accordance with the “Guide for the Care and Use of Laboratory Animals” of the National Research Council of the National Academies and approved by the University of Pennsylvania Institutional Animal Care and Use Committee. Use of recombinant virus in animals was approved by the University of Pennsylvania Institutional Biosafety Committee.

Histopathology. Tumors were rinsed in PBS and fixed in 10% neutral buffered formalin overnight. Fixed tumors were washed with a series of PBS, 50% ethanol, 70% ethanol, 95%

ethanol, and 100% ethanol for one hour each. Tissues were then embedded in paraffin, sectioned, and stained with hematoxylin and eosin or used for immunohistochemistry.

Immunohistochemistry. Paraffin embedded tissues were dewaxed with a series of xylene, 100% ethanol, 95% ethanol, 80% ethanol, 70% ethanol, and distilled water washes. Antigen retrieval was carried by incubating slides for 10 minutes at 95 °C in universal antigen retrieval solution (R&D Systems). Endogenous peroxidases were quenched with a 15 minute incubation in 2.25% hydrogen peroxide. Endogenous avidin and biotin were blocked using an avidin/biotin blocking kit (Vector Laboratories). Tissue sections were blocked using normal goat serum, and then incubated in CA9 antibody (Millipore) diluted 1:50 overnight at 4 °C. Sections were washed twice with PBS for five minutes each. Tissue sections were then incubated in biotinylated rabbit IgG (Vector Laboratories) for 30 minutes at 37 °C. Sections were washed twice in PBS for five minutes each. Slides were incubated in Vectastain Elite ABC solution (Vector Laboratories) for 30 minutes at 37 °C, and then washed twice in PBS for five minutes each. Signal was developed using 3,3'-diaminobenzidine (DAB) peroxidase substrate (Vector Laboratories). Slides were washed in water and counterstained with hematoxylin. Tissues were dehydrated with a series of water, 70% ethanol, 95% ethanol, 100% ethanol, and xylene washes and then mounted.

Western blotting on tissue lysates. 50 mg pieces were cut from snap-frozen tumors or normal muscle and placed on ice in tissue lysis buffer (50 mM HEPES, pH 7.4; 150 mM NaCl, 1.5 mM $MgCl_2$, 1 mM EGTA, 1% Triton X-100, 1 mM phenylmethylsulfonyl fluoride, 1X Complete Mini protease inhibitor cocktail [Roche], and 1X phosphatase inhibitor cocktail 2 [Sigma]). Tissues were homogenized on ice by electric homogenizer and then incubated on ice for 10 minutes. Lysates were cleared by centrifugation at maximum speed for 10 minutes. Protein concentrations of lysates were determined using 660 nm Protein Assay Reagent (Thermo Scientific), according to the manufacturer's protocol. Equal amounts of protein were resolved on 4-15% gradient Tris-HCl polyacrylamide gels and transferred to polyvinylidene fluoride membranes. Membranes were

blocked with 5% non-fat dried milk in TBS-T (20 mM Tris, 137 mM NaCl, 0.1% Tween-20; pH 7.6) and then incubated in primary antibody. Following primary antibody incubation, membranes were washed three times with 1% non-fat dried milk in TBS-T, incubated in secondary antibody, and then washed three more times with 1% non-fat dried milk in TBS-T. Proteins were visualized by incubating membranes in ECL chemicals and exposing to film. Bands were quantified using ImageJ software. The following primary antibodies were used: β-tubulin, eIF2α, GCN2, p-eIF2α, PERK, p-PERK (all from Cell Signaling), ATF4, PKR (both from Santa Cruz), p-GCN2 (Bioss), and p-PKR (Millipore). The secondary antibodies used were anti-rabbit HRP and anti-mouse HRP from Thermo Scientific.

qPCR. RNA isolated from polysome fractions, total RNA harvested from cells using TRIzol (Ambion), and RNA isolated from homogenized snap frozen tissue using an Rneasy Mini Kit (QIAgen) were subjected to qPCR analysis. RNAs were reversed transcribed using AMV reverse transcriptase (Promega) and random hexamer primers (Invitrogen). The resulting cDNAs served as templates for qPCR using Power SYBR Green PCR Master Mix (Applied Biosystems). Data were analysed using the Applied Biosystems 7300 System Software. PCR reaction conditions were 50 °C for two minutes, 95 °C for 10 min, followed by 40 cycles of 95 °C for 15 seconds and 60 °C for one minute. A list of primers used is in Table V-1.

Table V-1. Primer sequences used for qPCR analysis

Primer Name	Sequence (5' to 3')
18S forward	CAATTACAGGGCCTCGAAAG
18S reverse	AAACGGCTACCACATCCAAG
ASNS forward	CAATTACAGGGCCTCGAAAG
ASNS reverse	TCTTATCGGCTGCATTCCAAAC
ATF3 forward	GAGGATTTTGCTAACCTGACACC
ATF3 reverse	TTGACGGTAACTGACTCCAGC
ATF4 forward	CCTGAACAGCGAAGTGTTGG
ATF4 reverse	TGGAGAACCCATGAGGTTTCAA
β-actin forward	GGCTGTATTCCCCTCCATCG
β-actin reverse	CCAGTTGGTAACAATGCCATGT
β-tubulin forward	GATCGGTGCTAAGTTCTGGGA
β-tubulin reverse	AGGGACATACTTGCCACCTGT
Luciferase forward	CTCACTGAGACTACATCAGC
Luciferase reverse	TCCAGATCCACAACCTTCGC
p21 total forward	CGAGAACGGTGGAACTTTGAC
p21 total reverse	CCAGGGCTCAGGTAGACCTT
p21 var 1 forward	TCCAGACATTCAGAGCCACAG
p21 var 1 reverse	ACGGGACCGAAGAGACAAC
p21 var 2 forward	AGGAGGAGCATGAATGGAGAC
p21 var 2 reverse	GGACATCACCAGGATTGGAC
ULK1 forward	ACATCCGAGTCAAGATTGCTG
ULK1 reverse	GCTGGGACATAATGACCTCAGG

Copy number analysis. Genomic DNA was isolated from snap frozen tumor or normal muscle tissue using a DNeasy Blood and Tissue Kit (QIAgen). DNA was digested with RNase A to remove any contaminating RNA. Copy number analysis on genomic DNA was performed using a TaqMan copy number assay with primers recognizing exon three of mouse ATF4 (Applied Biosystems, assay ID Mm00618542_cn), according to the manufacturer's protocol. The ATF4 copy number assay was duplexed with a TaqMan copy number reference assay against TRFC (Applied Biosystems) for normalization. Data were analyzed using Copy Caller software.

XBP1 splicing assay. RNA was isolated from normal muscle and tumor tissue and reversed transcribed into cDNA as described in the above qPCR section. To detect XBP1 splicing, PCR was performed with primers that flank the splice site in the XBP1 transcript, resulting in the

amplification of both spliced (368 bp) and unspliced (394 bp) transcript variants. PCR reaction conditions were 95 °C for one minute; 40 cycles of 95 °C for 20 seconds, 50 °C for 20 seconds, and 68 °C for one minute; and 68 °C for four minutes. Primer sequences are available in Table V-2. Spliced and unspliced XBP1 were resolved on a 3% agarose gel and visualized with ethidium bromide under UV light.

Table V-2. Primer sequences used for XBP1 splicing assay

Primer Name	Sequence (5' to 3')
XBP1 forward	AAGTGGTGGATTTGGAAGAAGA
XBP1 reverse	GGAGTTCCTCCAGACTAGCAGA

ATF4 sequencing. Genomic DNA was isolated from tumors as described under "copy number analysis." Exons 1, 2, and 3 of ATF4 were individually amplified by PCR using Herculase II high fidelity DNA polymerase (Agilent Technologies). PCR reaction conditions were 95 °C for two minutes; 30 cycles of 95 °C for 20 seconds, 55 °C for 20 seconds, and 72 °C for 30 seconds; and 72 °C for three minutes. A list primers used is Table V-3. PCR products were purified using a QIAquick PCR Purification kit (QIAgen). Purified PCR products were sequenced at the University of Pennsylvania Genomics Analysis Core.

Table V-3. Primers for ATF4 sequencing

Primer Name	Sequence (5' to 3')
ATF4 exon 1 forward	GTGATAACCTGGCAGCTTCG
ATF4 exon 1 reverse	CAGGCAACGCAAACAAGG
ATF4 exon 2 forward	TCCAGGCTCTTCACGAAATC
ATF4 exon 2 reverse	CCATATGAAAAGGGCACACC
ATF4 exon 3 forward	TTCTGCCTCCCGAATATGAC
ATF4 exon 3 reverse	CAAGCACAAAGCACCTGACT

Statistical analysis. All statistical analyses for p21-related experiments were performed using a two-tailed Student's t test assuming homoscedasticity. Survival data were analyzed using the log-rank (Mantel-Cox) test. In Oncomine, differential expression analysis is performed using an independent, two-sample, one-tailed Welch's t-test. All other sarcoma experiments were analyzed using a two-tailed Welch's t-test. A p-value less than 0.05 was considered statistically significant for all analyses.

REFERENCES

1. Vaupel, P., Kallinowski, F. & Okunieff, P. Blood flow, oxygen and nutrient supply, and metabolic microenvironment of human tumors: a review. *Cancer Res* **49**, 6449-65 (1989).

2. Wek, S.A., Zhu, S. & Wek, R.C. The histidyl-tRNA synthetase-related sequence in the eIF-2 alpha protein kinase GCN2 interacts with tRNA and is required for activation in response to starvation for different amino acids. *Mol Cell Biol* **15**, 4497-506 (1995).

3. Wek, R.C., Jackson, B.M. & Hinnebusch, A.G. Juxtaposition of domains homologous to protein kinases and histidyl-tRNA synthetases in GCN2 protein suggests a mechanism for coupling GCN4 expression to amino acid availability. *Proc Natl Acad Sci U S A* **86**, 4579-83 (1989).

4. Dong, J., Qiu, H., Garcia-Barrio, M., Anderson, J. & Hinnebusch, A.G. Uncharged tRNA activates GCN2 by displacing the protein kinase moiety from a bipartite tRNA-binding domain. *Mol Cell* **6**, 269-79 (2000).

5. Zaborske, J.M. et al. Genome-wide analysis of tRNA charging and activation of the eIF2 kinase Gcn2p. *J Biol Chem* **284**, 25254-67 (2009).

6. Qiu, H., Garcia-Barrio, M.T. & Hinnebusch, A.G. Dimerization by translation initiation factor 2 kinase GCN2 is mediated by interactions in the C-terminal ribosome-binding region and the protein kinase domain. *Mol Cell Biol* **18**, 2697-711 (1998).

7. Qiu, H., Dong, J., Hu, C., Francklyn, C.S. & Hinnebusch, A.G. The tRNA-binding moiety in GCN2 contains a dimerization domain that interacts with the kinase domain and is required for tRNA binding and kinase activation. *EMBO J* **20**, 1425-38 (2001).

8. Padyana, A.K., Qiu, H., Roll-Mecak, A., Hinnebusch, A.G. & Burley, S.K. Structural basis for autoinhibition and mutational activation of eukaryotic initiation factor 2alpha protein kinase GCN2. *J Biol Chem* **280**, 29289-99 (2005).

9. Romano, P.R. et al. Autophosphorylation in the activation loop is required for full kinase activity in vivo of human and yeast eukaryotic initiation factor 2alpha kinases PKR and GCN2. *Mol Cell Biol* **18**, 2282-97 (1998).

10. Lageix, S., Rothenburg, S., Dever, T.E. & Hinnebusch, A.G. Enhanced interaction between pseudokinase and kinase domains in Gcn2 stimulates eIF2alpha phosphorylation in starved cells. *PLoS Genet* **10**, e1004326 (2014).

11. Garcia-Barrio, M., Dong, J., Ufano, S. & Hinnebusch, A.G. Association of GCN1-GCN20 regulatory complex with the N-terminus of eIF2alpha kinase GCN2 is required for GCN2 activation. *EMBO J* **19**, 1887-99 (2000).

12. Zhu, S. & Wek, R.C. Ribosome-binding domain of eukaryotic initiation factor-2 kinase GCN2 facilitates translation control. *J Biol Chem* **273**, 1808-14 (1998).

13. He, H. et al. Crystal structures of GCN2 protein kinase C-terminal domains suggest regulatory differences in yeast and mammals. *J Biol Chem* **289**, 15023-34 (2014).

14. Sood, R., Porter, A.C., Olsen, D.A., Cavener, D.R. & Wek, R.C. A mammalian homologue of GCN2 protein kinase important for translational control by phosphorylation of eukaryotic initiation factor-2alpha. *Genetics* **154**, 787-801 (2000).

15. Donnelly, N., Gorman, A.M., Gupta, S. & Samali, A. The eIF2alpha kinases: their structures and functions. *Cell Mol Life Sci* **70**, 3493-511 (2013).

16. Wek, R.C., Jiang, H.Y. & Anthony, T.G. Coping with stress: eIF2 kinases and translational control. *Biochem Soc Trans* **34**, 7-11 (2006).

17. Andreev, D.E. et al. Translation of 5' leaders is pervasive in genes resistant to eIF2 repression. *Elife* **4**, e03971 (2014).

18. Sonenberg, N. & Hinnebusch, A.G. Regulation of translation initiation in eukaryotes: mechanisms and biological targets. *Cell* **136**, 731-45 (2009).

19. Proud, C.G. eIF2 and the control of cell physiology. *Semin Cell Dev Biol* **16**, 3-12 (2005).

20. Buttgereit, F. & Brand, M.D. A hierarchy of ATP-consuming processes in mammalian cells. *Biochem J* **312 (Pt 1)**, 163-7 (1995).

21. Rolfe, D.F. & Brown, G.C. Cellular energy utilization and molecular origin of standard metabolic rate in mammals. *Physiol Rev* **77**, 731-58 (1997).

22. Vattem, K.M. & Wek, R.C. Reinitiation involving upstream ORFs regulates ATF4 mRNA translation in mammalian cells. *Proc Natl Acad Sci U S A* **101**, 11269-74 (2004).

23. Lu, P.D., Harding, H.P. & Ron, D. Translation reinitiation at alternative open reading frames regulates gene expression in an integrated stress response. *J Cell Biol* **167**, 27-33 (2004).

24. Lee, Y.Y., Cevallos, R.C. & Jan, E. An upstream open reading frame regulates translation of GADD34 during cellular stresses that induce eIF2alpha phosphorylation. *J Biol Chem* **284**, 6661-73 (2009).

25. Zhou, D. et al. Phosphorylation of eIF2 directs ATF5 translational control in response to diverse stress conditions. *J Biol Chem* **283**, 7064-73 (2008).

26. Harding, H.P. et al. An integrated stress response regulates amino acid metabolism and resistance to oxidative stress. *Mol Cell* **11**, 619-33 (2003).

27. Jiang, H.Y. et al. Activating transcription factor 3 is integral to the eukaryotic initiation factor 2 kinase stress response. *Mol Cell Biol* **24**, 1365-77 (2004).

28. Averous, J. et al. Induction of CHOP expression by amino acid limitation requires both ATF4 expression and ATF2 phosphorylation. *J Biol Chem* **279**, 5288-97 (2004).

29. Ma, Y. & Hendershot, L.M. Delineation of a negative feedback regulatory loop that controls protein translation during endoplasmic reticulum stress. *J Biol Chem* **278**, 34864-73 (2003).

30. Harding, H.P. et al. Regulated translation initiation controls stress-induced gene expression in mammalian cells. *Mol Cell* **6**, 1099-108 (2000).

31. Chaveroux, C. et al. Identification of GCN2 as new redox regulator for oxidative stress prevention in vivo. *Biochem Biophys Res Commun* **415**, 120-4 (2011).

32. Kalinina, E.V., Chernov, N.N. & Novichkova, M.D. Role of glutathione, glutathione transferase, and glutaredoxin in regulation of redox-dependent processes. *Biochemistry (Mosc)* **79**, 1562-83 (2014).

33. Awan, M.U. & Deng, Y. Role of autophagy and its significance in cellular homeostasis. *Appl Microbiol Biotechnol* **98**, 5319-28 (2014).

34. B'Chir, W. et al. The eIF2alpha/ATF4 pathway is essential for stress-induced autophagy gene expression. *Nucleic Acids Res* **41**, 7683-99 (2013).

35. Malumbres, M. & Barbacid, M. Cell cycle, CDKs and cancer: a changing paradigm. *Nat Rev Cancer* **9**, 153-66 (2009).

36. Asghar, U., Witkiewicz, A.K., Turner, N.C. & Knudsen, E.S. The history and future of targeting cyclin-dependent kinases in cancer therapy. *Nat Rev Drug Discov* **14**, 130-46 (2015).

37. Hamanaka, R.B., Bennett, B.S., Cullinan, S.B. & Diehl, J.A. PERK and GCN2 contribute to eIF2alpha phosphorylation and cell cycle arrest after activation of the unfolded protein response pathway. *Mol Biol Cell* **16**, 5493-501 (2005).

38. Bourougaa, K. et al. Endoplasmic reticulum stress induces G2 cell-cycle arrest via mRNA translation of the p53 isoform p53/47. *Mol Cell* **38**, 78-88 (2010).

39. Rodriguez, P.C., Quiceno, D.G. & Ochoa, A.C. L-arginine availability regulates T-lymphocyte cell-cycle progression. *Blood* **109**, 1568-73 (2007).

40. Martin, R., Berlanga, J.J. & de Haro, C. New roles of the fission yeast eIF2alpha kinases Hri1 and Gcn2 in response to nutritional stress. *J Cell Sci* **126**, 3010-20 (2013).

41. Tvegård, T. et al. A novel checkpoint mechanism regulating the G1/S transition. *Genes & Development* **21**, 649-654 (2007).

42. Jones, R.G. et al. AMP-activated protein kinase induces a p53-dependent metabolic checkpoint. *Mol Cell* **18**, 283-93 (2005).

43. Leung-Pineda, V., Pan, Y., Chen, H. & Kilberg, M.S. Induction of p21 and p27 expression by amino acid deprivation of HepG2 human hepatoma cells involves mRNA stabilization. *Biochem J* **379**, 79-88 (2004).

44. Anthony, T.G. et al. Preservation of liver protein synthesis during dietary leucine deprivation occurs at the expense of skeletal muscle mass in mice deleted for eIF2 kinase GCN2. *J Biol Chem* **279**, 36553-61 (2004).

45. Guo, F. & Cavener, D.R. The GCN2 eIF2alpha kinase regulates fatty-acid homeostasis in the liver during deprivation of an essential amino acid. *Cell Metab* **5**, 103-14 (2007).

46. Xu, X., Hu, J., McGrath, B.C. & Cavener, D.R. GCN2 regulates the CCAAT enhancer binding protein beta and hepatic gluconeogenesis. *Am J Physiol Endocrinol Metab* **305**, E1007-17 (2013).

47. Maurin, A.C. et al. The GCN2 kinase biases feeding behavior to maintain amino acid homeostasis in omnivores. *Cell Metab* **1**, 273-7 (2005).

48. Peng, W. et al. Surgical stress resistance induced by single amino acid deprivation requires Gcn2 in mice. *Sci Transl Med* **4**, 118ra11 (2012).

49. Costa-Mattioli, M. et al. Translational control of hippocampal synaptic plasticity and memory by the eIF2alpha kinase GCN2. *Nature* **436**, 1166-73 (2005).

50. Berlanga, J.J. et al. Antiviral effect of the mammalian translation initiation factor 2alpha kinase GCN2 against RNA viruses. *EMBO J* **25**, 1730-40 (2006).

51. Won, S. et al. Increased susceptibility to DNA virus infection in mice with a GCN2 mutation. *J Virol* **86**, 1802-8 (2012).

52. del Pino, J. et al. GCN2 has inhibitory effect on human immunodeficiency virus-1 protein synthesis and is cleaved upon viral infection. *PLoS One* **7**, e47272 (2012).

53. Uyttenhove, C. et al. Evidence for a tumoral immune resistance mechanism based on tryptophan degradation by indoleamine 2,3-dioxygenase. *Nat Med* **9**, 1269-74 (2003).

54. Munn, D.H. et al. Expression of indoleamine 2,3-dioxygenase by plasmacytoid dendritic cells in tumor-draining lymph nodes. *J Clin Invest* **114**, 280-90 (2004).

55. Munn, D.H. et al. GCN2 kinase in T cells mediates proliferative arrest and anergy induction in response to indoleamine 2,3-dioxygenase. *Immunity* **22**, 633-42 (2005).

56. Sharma, M.D. et al. Plasmacytoid dendritic cells from mouse tumor-draining lymph nodes directly activate mature Tregs via indoleamine 2,3-dioxygenase. *J Clin Invest* **117**, 2570-82 (2007).

57. DeBerardinis, R.J., Lum, J.J., Hatzivassiliou, G. & Thompson, C.B. The biology of cancer: metabolic reprogramming fuels cell growth and proliferation. *Cell Metab* **7**, 11-20 (2008).

58. Ye, J. et al. The GCN2-ATF4 pathway is critical for tumour cell survival and proliferation in response to nutrient deprivation. *EMBO J* **29**, 2082-2096 (2010).

59. Koumenis, C. et al. Regulation of protein synthesis by hypoxia via activation of the endoplasmic reticulum kinase PERK and phosphorylation of the translation initiation factor eIF2alpha. *Mol Cell Biol* **22**, 7405-16 (2002).

60. Kaufman, R.J. et al. The unfolded protein response in nutrient sensing and differentiation. *Nat Rev Mol Cell Biol* **3**, 411-21 (2002).

61. Cullinan, S.B. et al. Nrf2 is a direct PERK substrate and effector of PERK-dependent cell survival. *Mol Cell Biol* **23**, 7198-209 (2003).

62. Bobrovnikova-Marjon, E. et al. PERK utilizes intrinsic lipid kinase activity to generate phosphatidic acid, mediate Akt activation, and promote adipocyte differentiation. *Mol Cell Biol* **32**, 2268-78 (2012).

63. Bi, M. et al. ER stress-regulated translation increases tolerance to extreme hypoxia and promotes tumor growth. *EMBO J* **24**, 3470-81 (2005).

64. Bobrovnikova-Marjon, E. et al. PERK promotes cancer cell proliferation and tumor growth by limiting oxidative DNA damage. *Oncogene* **29**, 3881-95 (2010).

65. Gupta, S., McGrath, B. & Cavener, D.R. PERK regulates the proliferation and development of insulin-secreting beta-cell tumors in the endocrine pancreas of mice. *PLoS One* **4**, e8008 (2009).

66. Ameri, K. et al. Anoxic induction of ATF-4 through HIF-1–independent pathways of protein stabilization in human cancer cells. *Blood* **103**, 1876-1882 (2004).

67. Tang, X. et al. Functional interaction between responses to lactic acidosis and hypoxia regulates genomic transcriptional outputs. *Cancer Res* **72**, 491-502 (2012).

68. Galluzzi, L. et al. Autophagy in malignant transformation and cancer progression. *EMBO J* (2015).

69. Wang, Y. et al. Amino acid deprivation promotes tumor angiogenesis through the GCN2/ATF4 pathway. *Neoplasia* **15**, 989-97 (2013).

70. Shackelford, R.E., Kaufmann, W.K. & Paules, R.S. Cell cycle control, checkpoint mechanisms, and genotoxic stress. *Environ Health Perspect* **107 Suppl 1**, 5-24 (1999).

71. Jung, Y.S., Qian, Y. & Chen, X. Examination of the expanding pathways for the regulation of p21 expression and activity. *Cell Signal* **22**, 1003-12 (2010).

72. El-Deiry, W.S. et al. WAF1, a potential mediator of p53 tumor suppression. *Cell* **75**, 817-825 (1993).

73. El-Deiry, W.S. et al. WAF1/CIP1 is induced in p53-mediated G1 arrest and apoptosis. *Cancer Res* **54**, 1169-74 (1994).

74. Kivinen, L. et al. Ras induces p21Cip1/Waf1 cyclin kinase inhibitor transcriptionally through Sp1-binding sites. *Oncogene* **18**, 6252-61 (1999).

75. Huang, L., Sowa, Y., Sakai, T. & Pardee, A.B. Activation of the p21WAF1/CIP1 promoter independent of p53 by the histone deacetylase inhibitor suberoylanilide hydroxamic acid (SAHA) through the Sp1 sites. *Oncogene* **19**, 5712-9 (2000).

76. Joseph, B., Orlian, M. & Furneaux, H. p21(waf1) mRNA contains a conserved element in its 3'-untranslated region that is bound by the Elav-like mRNA-stabilizing proteins. *J Biol Chem* **273**, 20511-6 (1998).

77. Wang, W. et al. HuR regulates p21 mRNA stabilization by UV light. *Mol Cell Biol* **20**, 760-9 (2000).

78. Lu, Z. & Hunter, T. Ubiquitylation and proteasomal degradation of the p21(Cip1), p27(Kip1) and p57(Kip2) CDK inhibitors. *Cell Cycle* **9**, 2342-52 (2010).

79. Child, E.S. & Mann, D.J. The intricacies of p21 phosphorylation: protein/protein interactions, subcellular localization and stability. *Cell Cycle* **5**, 1313-9 (2006).

80. Gartel, A.L., Radhakrishnan, S.K., Serfas, M.S., Kwon, Y.H. & Tyner, A.L. A novel p21WAF1/CIP1 transcript is highly dependent on p53 for its basal expression in mouse tissues. *Oncogene* **23**, 8154-7 (2004).

81. Radhakrishnan, S.K., Gierut, J. & Gartel, A.L. Multiple alternate p21 transcripts are regulated by p53 in human cells. *Oncogene* **25**, 1812-5 (2006).

82. Maalouf, M. et al. Different mechanisms of cell death in radiosensitive and radioresistant p53 mutated head and neck squamous cell carcinoma cell lines exposed to carbon ions and x-rays. *Int J Radiat Oncol Biol Phys* **74**, 200-9 (2009).

83. Koritzinsky, M. et al. Gene expression during acute and prolonged hypoxia is regulated by distinct mechanisms of translational control. *The EMBO Journal* **25**, 1114-1125 (2006).

84. Kaul, G., Pattan, G. & Rafeequi, T. Eukaryotic elongation factor-2 (eEF2): its regulation and peptide chain elongation. *Cell Biochem Funct* **29**, 227-34 (2011).

85. Barrios-Rodiles, M. et al. High-throughput mapping of a dynamic signaling network in mammalian cells. *Science* **307**, 1621-5 (2005).

86. Datto, M.B. et al. Transforming growth factor beta induces the cyclin-dependent kinase inhibitor p21 through a p53-independent mechanism. *Proc Natl Acad Sci U S A* **92**, 5545-9 (1995).

87. Brewer, J.W. & Diehl, J.A. PERK mediates cell-cycle exit during the mammalian unfolded protein response. *Proc Natl Acad Sci U S A* **97**, 12625-30 (2000).

88. Braun, F., Bertin-Ciftci, J., Gallouet, A.S., Millour, J. & Juin, P. Serum-nutrient starvation induces cell death mediated by Bax and Puma that is counteracted by p21 and unmasked by Bcl-x(L) inhibition. *PLoS One* **6**, e23577 (2011).

89. Han, J. et al. ER-stress-induced transcriptional regulation increases protein synthesis leading to cell death. *Nat Cell Biol* **15**, 481-90 (2013).

90. Palam, L.R., Baird, T.D. & Wek, R.C. Phosphorylation of eIF2 facilitates ribosomal bypass of an inhibitory upstream ORF to enhance CHOP translation. *J Biol Chem* **286**, 10939-49 (2011).

91. Baird, T.D. et al. Selective mRNA translation during eIF2 phosphorylation induces expression of IBTKalpha. *Mol Biol Cell* **25**, 1686-97 (2014).

92. Raveh-Amit, H. et al. Translational control of protein kinase Ceta by two upstream open reading frames. *Mol Cell Biol* **29**, 6140-8 (2009).

93. Grewe, M., Gansauge, F., Schmid, R.M., Adler, G. & Seufferlein, T. Regulation of cell growth and cyclin D1 expression by the constitutively active FRAP-p70s6K pathway in human pancreatic cancer cells. *Cancer Res* **59**, 3581-7 (1999).

94. Hashemolhosseini, S. et al. Rapamycin inhibition of the G1 to S transition is mediated by effects on cyclin D1 mRNA and protein stability. *J Biol Chem* **273**, 14424-9 (1998).

95. Kawamata, S., Sakaida, H., Hori, T., Maeda, M. & Uchiyama, T. The upregulation of p27Kip1 by rapamycin results in G1 arrest in exponentially growing T-cell lines. *Blood* **91**, 561-9 (1998).

96. Abbas, T. & Dutta, A. p21 in cancer: intricate networks and multiple activities. *Nat Rev Cancer* **9**, 400-14 (2009).

97. Hart, L.S. et al. ER stress-mediated autophagy promotes Myc-dependent transformation and tumor growth. *J Clin Invest* **122**, 4621-34 (2012).

98. Blais, J.D. et al. Perk-dependent translational regulation promotes tumor cell adaptation and angiogenesis in response to hypoxic stress. *Mol Cell Biol* **26**, 9517-32 (2006).

99. Frese, K.K. & Tuveson, D.A. Maximizing mouse cancer models. *Nat Rev Cancer* **7**, 645-58 (2007).

100. Kirsch, D.G. et al. A spatially and temporally restricted mouse model of soft tissue sarcoma. *Nat Med* **13**, 992-7 (2007).

101. Devi, L. & Ohno, M. Deletion of the eIF2alpha Kinase GCN2 fails to rescue the memory decline associated with Alzheimer's disease. *PLoS One* **8**, e77335 (2013).

102. Detwiller, K.Y. et al. Analysis of hypoxia-related gene expression in sarcomas and effect of hypoxia on RNA interference of vascular endothelial cell growth factor A. *Cancer Res* **65**, 5881-9 (2005).

103. Mito, J.K. et al. Cross species genomic analysis identifies a mouse model as undifferentiated pleomorphic sarcoma/malignant fibrous histiocytoma. *PLoS One* **4**, e8075 (2009).

104. Young, N.P., Crowley, D. & Jacks, T. Uncoupling cancer mutations reveals critical timing of p53 loss in sarcomagenesis. *Cancer Res* **71**, 4040-7 (2011).

105. Schonhuber, N. et al. A next-generation dual-recombinase system for time- and host-specific targeting of pancreatic cancer. *Nat Med* **20**, 1340-7 (2014).

106. Axten, J.M. et al. Discovery of 7-methyl-5-(1-{[3-(trifluoromethyl)phenyl]acetyl}-2,3-dihydro-1H-indol-5-yl)-7H-p yrrolo[2,3-d]pyrimidin-4-amine (GSK2606414), a potent and selective first-in-class inhibitor of protein kinase R (PKR)-like endoplasmic reticulum kinase (PERK). *J Med Chem* **55**, 7193-207 (2012).

107. Axten, J.M. et al. Discovery of GSK2656157: An Optimized PERK Inhibitor Selected for Preclinical Development. *ACS Med Chem Lett* **4**, 964-8 (2013).

108. Pytel, D. et al. Enzymatic Characterization of ER Stress-Dependent Kinase, PERK, and Development of a High-Throughput Assay for Identification of PERK Inhibitors. *J Biomol Screen* **19**, 1024-1034 (2014).

109. Robert, F. et al. Blocking UV-induced eIF2alpha phosphorylation with small molecule inhibitors of GCN2. *Chem Biol Drug Des* **74**, 57-67 (2009).

110. Atkins, C. et al. Characterization of a novel PERK kinase inhibitor with antitumor and antiangiogenic activity. *Cancer Res* **73**, 1993-2002 (2013).

111. Thomas, J.D. & Johannes, G.J. Identification of mRNAs that continue to associate with polysomes during hypoxia. *RNA* **13**, 1116-31 (2007).

112. Ingolia, N.T., Ghaemmaghami, S., Newman, J.R. & Weissman, J.S. Genome-wide analysis in vivo of translation with nucleotide resolution using ribosome profiling. *Science* **324**, 218-23 (2009).

113. Ingolia, N.T. Ribosome profiling: new views of translation, from single codons to genome scale. *Nat Rev Genet* **15**, 205-13 (2014).

114. Daga, R.R., Bolanos, P. & Moreno, S. Regulated mRNA stability of the Cdk inhibitor Rum1 links nutrient status to cell cycle progression. *Curr Biol* **13**, 2015-24 (2003).

115. O'Keefe, M.C. & Post, M.D. Pulmonary capillary hemangiomatosis: a rare cause of pulmonary hypertension. *Arch Pathol Lab Med* **139**, 274-7 (2015).

116. Best, D.H. et al. EIF2AK4 mutations in pulmonary capillary hemangiomatosis. *Chest* **145**, 231-6 (2014).

117. Scheuner, D. et al. Translational control is required for the unfolded protein response and in vivo glucose homeostasis. *Mol Cell* **7**, 1165-76 (2001).

118. Lassot, I. et al. ATF4 degradation relies on a phosphorylation-dependent interaction with the SCF(betaTrCP) ubiquitin ligase. *Mol Cell Biol* **21**, 2192-202 (2001).

119. Koditz, J. et al. Oxygen-dependent ATF-4 stability is mediated by the PHD3 oxygen sensor. *Blood* **110**, 3610-7 (2007).

120. Lassot, I. et al. p300 modulates ATF4 stability and transcriptional activity independently of its acetyltransferase domain. *J Biol Chem* **280**, 41537-45 (2005).

121. Linch, M., Miah, A.B., Thway, K., Judson, I.R. & Benson, C. Systemic treatment of soft-tissue sarcoma-gold standard and novel therapies. *Nat Rev Clin Oncol* **11**, 187-202 (2014).

122. Wang, D. & Abrams, R.A. Radiotherapy for soft tissue sarcoma: 50 years of change and improvement. *Am Soc Clin Oncol Educ Book*, 244-51 (2014).

123. van der Graaf, W.T. et al. Pazopanib for metastatic soft-tissue sarcoma (PALETTE): a randomised, double-blind, placebo-controlled phase 3 trial. *Lancet* **379**, 1879-86 (2012).

124. Messeguer, X. et al. PROMO: detection of known transcription regulatory elements using species-tailored searches. *Bioinformatics* **18**, 333-4 (2002).

125. Farre, D. et al. Identification of patterns in biological sequences at the ALGGEN server: PROMO and MALGEN. *Nucleic Acids Res* **31**, 3651-3 (2003).

126. Bonavida, B. & Kaufhold, S. Prognostic significance of YY1 protein expression and mRNA levels by bioinformatics analysis in human cancers: A therapeutic target. *Pharmacol Ther* (2015).

127. Jackson, E.L. et al. The differential effects of mutant p53 alleles on advanced murine lung cancer. *Cancer Res* **65**, 10280-8 (2005).

128. Rhim, A.D. et al. EMT and dissemination precede pancreatic tumor formation. *Cell* **148**, 349-61 (2012).

129. Bunpo, P. et al. The eIF2 kinase GCN2 is essential for the murine immune system to adapt to amino acid deprivation by asparaginase. *J Nutr* **140**, 2020-7 (2010).

130. Donehower, L.A. The p53-deficient mouse: a model for basic and applied cancer studies. *Semin Cancer Biol* **7**, 269-78 (1996).

131. Martin-Caballero, J., Flores, J.M., Garcia-Palencia, P. & Serrano, M. Tumor susceptibility of p21(Waf1/Cip1)-deficient mice. *Cancer Res* **61**, 6234-8 (2001).

132. Shiohara, M. et al. Absence of WAF1 mutations in a variety of human malignancies. *Blood* **84**, 3781-4 (1994).

133. Roninson, I.B. Oncogenic functions of tumour suppressor p21(Waf1/Cip1/Sdi1): association with cell senescence and tumour-promoting activities of stromal fibroblasts. *Cancer Lett* **179**, 1-14 (2002).

134. Ohata, M., Nakamura, S., Fujita, H. & Isemura, M. Prognostic implications of p21 (Waf1/Cip1) immunolocalization in multiple myeloma. *Biomed Res* **26**, 91-8 (2005).

135. Pindzola, J.A., Palazzo, J.P., Kovatich, A.J., Tuma, B. & Nobel, M. Expression of p21WAF1/CIP1 in soft tissue sarcomas: a comparative immunohistochemical study with p53 and Ki-67. *Pathol Res Pract* **194**, 685-91 (1998).

136. Johannes, G. & Sarnow, P. Cap-independent polysomal association of natural mRNAs encoding c-myc, BiP, and eIF4G conferred by internal ribosome entry sites. *RNA* **4**, 1500-1513 (1998).

137. Jackson, E.L. et al. Analysis of lung tumor initiation and progression using conditional expression of oncogenic K-ras. *Genes Dev* **15**, 3243-8 (2001).

138. Jonkers, J. et al. Synergistic tumor suppressor activity of BRCA2 and p53 in a conditional mouse model for breast cancer. *Nat Genet* **29**, 418-25 (2001).